Weighted Delta-Tracking with Scattering implemented in the Serpent 2 Monte Carlo Code

by

J.S. Rehak

A thesis submitted in partial satisfaction of the

requirements for the degree of

Masters of Science

in

Engineering – Nuclear Engineering

in the

Graduate Division

of the

University of California, Berkeley

Committee in charge:

Professor Rachael Slaybaugh, Chair
Professor Massimiliano Fratoni
Professor Leslie Kerby

Spring 2017

The thesis of J.S. Rehak, titled Weighted Delta-Tracking with Scattering implemented in the Serpent 2 Monte Carlo Code, is approved:

Chair _____ Date _____

_____ Date _____

_____ Date _____

University of California, Berkeley

Weighted Delta-Tracking with Scattering implemented in the Serpent 2 Monte Carlo Code

Contents

List of Figures

List of Tables

Chapter 1

Introduction

Nuclear energy continues to be an important source of carbon-free baseload power in countries around the world. Unlike many other baseload power sources, nuclear reactors do not rely on carbon-releasing fuels, but harness the energy released by the natural splitting of very heavy atoms, such as Uranium and Plutonium. This event, called fission, relies on the nucleus absorbing a free neutral particle, called a neutron. The splitting then releases more neutrons, resulting in further events. Early nuclear scientists realized that, given enough material in the correct physical layout, the reaction could be self-sustaining: a chain reaction.

This nuclear chain reaction is harnessed by modern nuclear reactors to generate large amounts of energy. Neutrons are the key to starting and maintaining the chain reaction, so understanding their energy and spatial distribution is central to the study of reactors. Many methods have been developed to understand this problem, one of which is the Monte Carlo method. This method using stochastic sampling to simulate the propagation and interactions of neutrons within the reactor.

The Idaho National Lab (INL) has begun a program to restart a test reactor, the Transient Reactor Test Facility (TREAT) to assess the viability of advanced nuclear fuels. Experiments performed by this reactor will support the development and deployment of the next generation of nuclear reactors by testing transient and accident conditions [3].

INL has developed advanced deterministic multi-group codes within the MOOSE framework [2] to model the neutron distribution in this reactor. These codes rely on Monte Carlo codes, such as Serpent 2, to calculate the cross-sections used by the multi-group solver [12]. The fuel elements in the TREAT reactor contain a large amount of graphite, leading to a highly scattering environment. Because it can be quite difficult to accurately represent relatively large amounts of scattering, calculation of scattering cross-sections is of vital importance. One of the methods proposed to improve this cross-section generation is weighted delta-tracking (WDT).

In this manuscript, we will discuss the background of Monte Carlo codes and neutron propagation methods. We will then discuss the new method, WDT, and describe an extension of the method to include scattering. Finally, we will assess the results of three test-cases, to

evaluate the usefulness of the WDT method and refine the parameters of its use.

Chapter 2

Background

Monte Carlo codes are vital tools in a diverse number of fields. Based in simple random number generators, these tools harness the power of statistics to predict and describe a wide variety of behaviors. In nuclear engineering, there is a long history of Monte Carlo methods used to simulate neutral particle propagation. These methods enjoy a wide variety of applications within the field, from fuel cell development to full core analysis. A vital part of the simulation is the propagation and interaction of neutral particles, neutrons. In this chapter we will describe the history and mathematics of these neutral particle propagation methods.

2.1 The Monte Carlo Method

The history of Monte Carlo methods begins with nuclear science and engineering. Nicholas Metropolis and S. Ulam [11] at Los Alamos National Laboratory developed the method to support the Manhattan Project. Today, Monte Carlo methods have found diverse applications across the hard and social sciences. In nuclear engineering, we still use Monte Carlo for its original purpose, the propagation of neutral particles. Now, its use has expanded from weapons research to assessing the viability and properties of nuclear reactors.

When used for particle transport, the Monte Carlo method uses a random number generator to simulate a particle's history. As the simulation runs, various parameters are calculated and recorded. This will continue for a finite number of histories, N, after which the mean value of the parameters of interest are calculated:

$$\bar{x} = \frac{1}{N} \sum_{n=1}^{N} x_n \, ,$$

where x_n is the value from the n-th history[1]. The process for sampling will be described in general here, and then extended to particle propagation methods in Sec. 2.2.

As described by Lewis and Miller [1], we first must consider a random variable, x. We define the probability that x will have a value between a and b: $P\{a \leq x \leq b\}$. We are

interested in the probability that our random variable will have one specific value. Therefore, we define the probability that our variable will fall within a differential distance to a given value x in the limit that the differential distance goes to zero. This is the probability density function (PDF), the probability that x' will be between x and $x + \Delta x$:

$$f(x)\Delta x = \lim_{\Delta x \to 0} P\{x \leq x' \leq x + \Delta x\} \,. \tag{2.1}$$

Integrating the PDF gives the overall probability for the range:

$$\int_a^b f(x)dx = P\{a \leq x \leq b\} \,. \tag{2.2}$$

If we integrate the PDF over the entire range of possible values of x, it must equal unity; there is a 100% chance that its value is in the range. Therefore, we must normalize the PDF:

$$\int_{-\infty}^{\infty} f(x)dx = 1, \quad x \in (-\infty, \infty) \,.$$

We then may define a cumulative distribution function (CDF):

$$F(x) = P\{x' \leq x\} = \int_{-\infty}^{x} f(x')dx' \,. \tag{2.3}$$

In the limit where $x \to \infty$, $F(x) \to 1$ and as $x \to -\infty$, $F(x) \to 0$ from the normalization of the PDF. The CDF is uniformly distributed from zero to unity [1], with each value corresponding to a single value of x. We therefore have a means to generate values of x using a random number generator uniformly distributed from zero unity. To do so, we set:

$$F(x) = \xi \,,$$

where $\xi \in [0, 1)$ is a random number. For each random number sampled, we sample a single value of x. This is determined by inverting the CDF:

$$F^{-1}(\xi) = x \,. \tag{2.4}$$

We now have a direct way of using a random number generator to generate a randomly distributed variable x. We will now apply this to particle propagation. There are methods available when the CDF is not invertible. Each CDF used for particle propagation is invertible, so these methods are outside the scope of discussion.

2.2 Particle Propagation Methods

As a particle moves through a medium, multiple forces and events will affect its trajectory. We will consider neutral elementary particles, neutrons, so that the effects of gravitational

and electromagnetic force are negligible. It is therefore a good assumption that a neutron will travel in a straight line until a physical collision with another particle. Despite the large number of neutrons present in our simulation, we will ignore improbable collisions between neutrons themselves. Neutron collisions with atoms result in an array of effects, including absorption and scattering. The relative probability of a collision occurring and the resulting type of collision are dependent on the atom that the neutron collides with and the energy of the neutron. Modeling the propagation of neutrons is accomplished through a variety of algorithms, some of which we described in this section.

Ray Tracing

The basic algorithm for simulating particle transport using Monte Carlo is ray tracing. This method follows a particle from collision to collision, assuming that it travels in a straight, statistically-sampled path. Material properties determine the distance between collisions, and therefore material boundaries must be considered explicitly.

Particles propagating through a material have an interaction probability characterized by the material's experimentally-determined total cross section, a function of position and the incident neutron energy, $\Sigma_t(\mathbf{r}, E)$. The probability of an interaction occurring in a differential distance ds is related to the macroscopic cross-section:

$$\frac{dP}{ds} = \Sigma_t(\mathbf{r}, E) \, . \tag{2.5}$$

We assume that each interaction will remove the neutron from the incident flux, as it is absorbed or deflected out of the original path in position, energy, or both. The medium therefore attenuates an incident mono-energetic neutron flux ϕ_0 as a function of distance:

$$\phi(s) = \phi_0 e^{-s\Sigma_t(\mathbf{r})} \, . \tag{2.6}$$

The probability that a neutron has its first interaction in differential distance ds after traveling a distance s is found by dividing the flux at that position $\phi(s)$ by the total flux:

$$f(s)ds = \frac{\phi(s)}{\int_0^\infty \phi(s)ds} ds \, . \tag{2.7}$$

The basis of Eq. (2.7) is clarified by an example: if the flux after a distance s is half the total flux, then half of the neutrons have undergone an interaction.

We consider the cross-section in a single material region, where we assume that the material is homogeneous. In this case, the cross-section is no longer a function of position. Using Eqs. (2.6) and (2.7), and assuming that the total cross-section is constant over $\mathbf{r}$[9]:

$$f(s)ds = \Sigma_t e^{-s\Sigma_t} ds \, . \tag{2.8}$$

This is the PDF of the distance traveled before the first collision, s. As the distance a neutron travels increases, the value of $f(s)$ decreases; it is less probable that a neutron will

travel further without collision. The PDF gives us the probability at a point s that a neutron undergoes a collision exactly there; integrating over the distance s provides us the probably that a neutron undergoes a collision between 0 and s. This is the CDF:

$$F(s) = \int_0^s f(s')ds' = 1 - e^{-s\Sigma_t} \,. \tag{2.9}$$

As expected, increasing s causes the probability of any interaction, $F(s)$, to approach unity. Plots illustrating the behavior of the PDF and CDF are shown in Fig. 2.1.

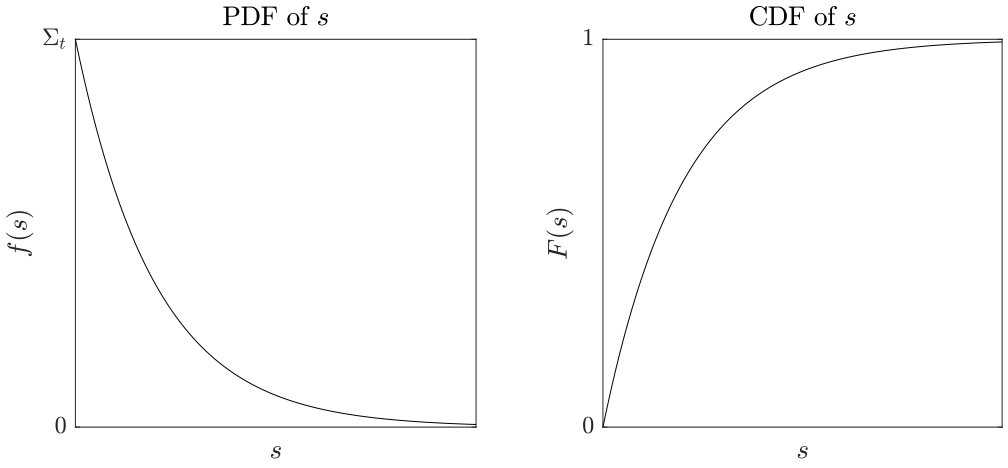

Figure 2.1: Plots of the CDF and PDF for collision probability per distance travelled s.

As the CDF ranges from zero to unity, we can sample its value by a uniformly distributed random variable $\xi \in [0, 1)$. The distance traveled, s, referred to as the path length, can then be expressed as a function of this sampled random variable:

$$\begin{aligned} F(s) = 1 - e^{-s\Sigma_t} &= \xi \,, \\ \ln(e^{-s\Sigma_t}) &= \ln(1-\xi) \,, \\ -\Sigma_t s &= \ln(\xi) \,, \\ s(\xi) &= \frac{1}{\Sigma_t} \ln(\xi) \,. \end{aligned}$$

After sampling the path length of the neutron, its position is updated based on its original position and direction. We assumed that the cross-section Σ_t was constant in a material region, so the sampled path length is only valid as long as the neutron remains in that region. If the neutron reaches the boundary between two material regions, a new path length must be sampled using the cross-section of the region it is entering. Each time a path length is sampled, the distance to the nearest boundary in the direction of motion is determined, and the neutron is moved to the boundary and path length is resampled if appropriate. This can become computationally expensive in complicated geometries and when the probability of crossing boundaries with each sample path length is high.

2.3 Woodcock Delta-tracking

As discussed in Section 2.2, the value of Σ_t at a given position depends on the material at that point. Therefore, $\Sigma_t(\mathbf{r})$ is a piece-wise discontinuous function that varies arbitrarily with position and the geometry of the problem [6]. Using the ray tracing method, neutrons must stop at boundaries to sample a new path length in a new material region. To avoid the computational inefficiency that arises in geometrically-complicated regions, a rejection sampling technique known as Woodcock delta-tracking was developed [15].

Woodcock delta-tracking introduces the concept of the majorant cross-section, chosen to be the maximum of all material total cross-sections in the region of interest:

$$\Sigma_{\text{maj}} \equiv \max_{\mathbf{r}\in\mathbb{V}}\{\Sigma_t(\mathbf{r})\}\,, \tag{2.10}$$

where $\mathbb{V}$ is the volume of interest. The majorant concept is shown in a one-dimensional region in Fig. 2.2.

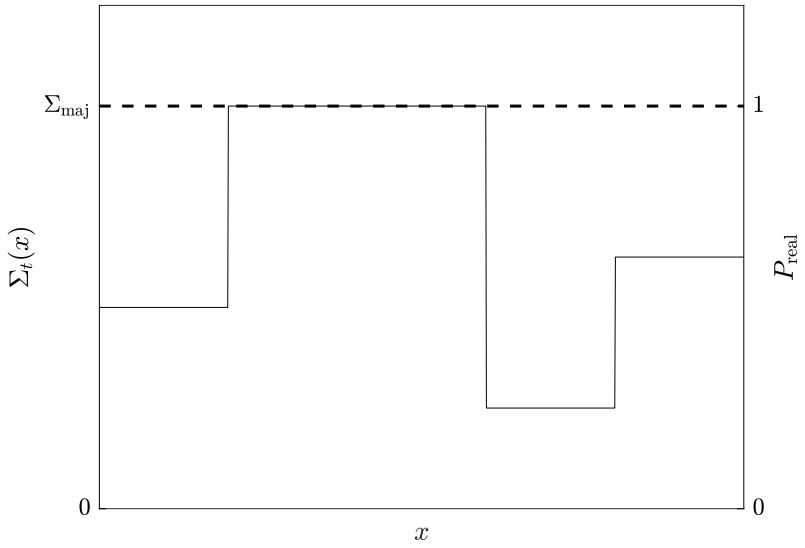

Figure 2.2: Total cross-section as a function of position in one dimension. The majorant cross-section is the largest value in the region of interest and determines the probability of a real collision.

The majorant cross-section can also be represented as the summation of the total cross-section and a delta cross-section:

$$\Sigma_{\text{maj}} = \Sigma_\delta(\mathbf{r}) + \Sigma_t(\mathbf{r}), \quad \forall \mathbf{r} \in \mathbb{V}\,. \tag{2.11}$$

Following from the definition of Σ_{maj} in Eq. (2.10), the function $\Sigma_\delta(\mathbf{r})$ is chosen such that Σ_{maj} is constant for the entire region of interest. At the position $\mathbf{r}$ where the maximum value of $\Sigma_t(\mathbf{r})$ occurs, the delta cross-section is zero.

The majorant cross-section is constant throughout the entire region of interest, so we can treat it as a single material. Following the same derivation in Section 2.2, the PDF of the first collision occurring after s in the region of interest using the majorant cross-section is given by:

$$f_{\text{maj}}(s) = \Sigma_{\text{maj}} e^{-\Sigma_{\text{maj}} s} \tag{2.12}$$

$$= (\Sigma_\delta(\mathbf{r}) + \Sigma_t(\mathbf{r})) e^{-\Sigma_{\text{maj}} s} \, . \tag{2.13}$$

In most of the region of interest, the majorant cross-section is not the real cross-section. To accurately preserve physics, we must use a technique called rejection sampling to simulate sampling the real $\Sigma_t(\mathbf{r})$ while actually sampling using Σ_{maj}.

Rejection Sampling

As described by Lux and Koblinger [9], rejection sampling requires a PDF of interest, $f(x)$, and a second PDF $g(x)$ for which:

$$f(x) \leq M \cdot g(x), \quad \forall x \, , \tag{2.14}$$

where $M \in \mathbb{R}$ is a constant. Sampling from $M \cdot g(x)$ and accepting these samples with probability:

$$P = \frac{f(x)}{M \cdot g(x)} \tag{2.15}$$

replicates sampling directly from $f(x)$.

For example, consider a PDF of interest $f(x) = x^2$ on the interval $x \in (0, 1]$ as shown in Fig. 2.3. As described in the previous section, we could sample $f(x)$ using the $F(x)$ found by integrating and then inverting. Instead, we can sample from a different PDF that is always majorant of $f(x)$, as defined in Eq. (2.14). We can choose $g(x) = M = 1$, as $f(x) \leq 1$ on the interval of interest. The CDF of $g(x)$ is easy to determine, because it is a constant value, and is just $G(x) = x$. Therefore, we can sample $g(x)$ by simply sampling a random value $\xi \in (0, 1]$ and taking this as the value of x. To replicate sampling from $f(x)$, we then sample another random value $\xi_2 \in (0, 1]$ and accept our value of x using the probability defined in Eq. (2.15):

$$\xi_2 \leq \frac{f(x)}{M \cdot g(x)} = x^2 \, .$$

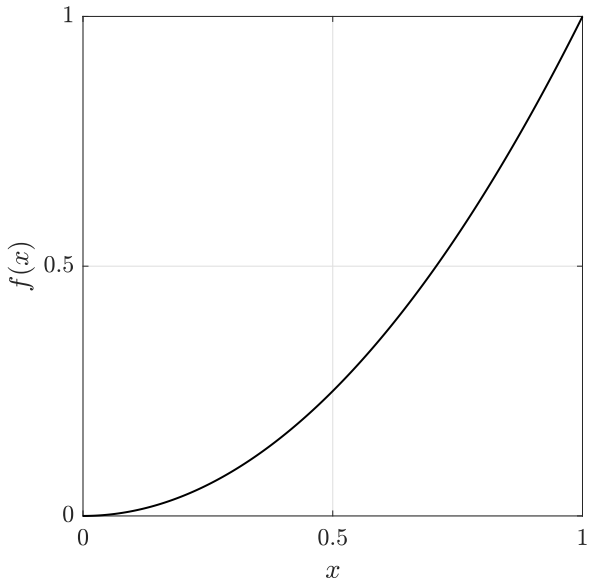

Figure 2.3: Example PDF function $f(x) = x^2$.

The following Matlab script replicates this procedure and generates the histogram shown in Fig. 2.4.

```
a = [];                          % Accepted samples
for i = 1:1000
    x = rand;                    % Sample g(x)
    y = rand;                    % Gen random number xi2
    if y <= x.^2                 % If xi2 <= f(x)/g(x)
        a(end+1) = x;            % Accept sample
    end
end
```

As expected, the procedure has reproduced the desired PDF of $f(x) = x^2$. Although this requires sampling two random variables, it can be advantageous if $F(x)$ is difficult or impossible to invert.

Application to Delta-tracking

As we saw in Fig. 2.2, the total cross-section Σ_t is a piecewise discontinuous function that depends on the geometry of our problem. Therefore, each region has a different CDF for sampling path length, and described in Section 2.2. Using rejection sampling, we can sample the real collision PDF, using a different, simpler PDF. In Woodcock delta tracking, the second PDF, $g(x)$, is chosen to be the majorant PDF, Eq. (2.13). This is beneficial because the majorant cross-section is constant over the entire region.

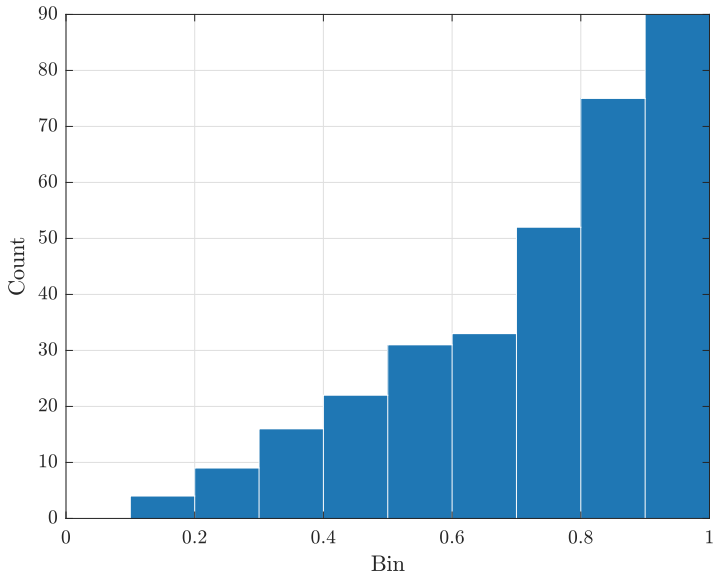

Figure 2.4: Histogram of results from sampling and applying the rejection sampling algorithm.

These functions are both maximized at $x = 0$, where the inequality of Eq. (2.14) is satisfied by setting $M = 1$:

$$\Sigma_t(\mathbf{r}) \leq \Sigma_{\text{maj}}(\mathbf{r}), \forall \mathbf{r} \in \mathbb{V} \,. \tag{2.16}$$

We sample path length using the constant majorant cross-section:

$$s_{\text{maj}}(\xi) = -\frac{1}{\Sigma_{\text{maj}}} \ln(\xi) \,, \tag{2.17}$$

which samples the PDF defined in Eq.(2.13). We can see that this PDF is the sum of two different ones: one representing actual collisions based on the real total cross-section Σ_t and one representing the non-physical collisions based on Σ_δ. We call these non-physical collisions "virtual" collisions, and these should be eliminated by our rejection sampling. To apply rejection sampling, we therefore pick the PDF we want to sample, $f(x)$, and the PDF we will actually sample, $g(x)$, as such:

$$f(x) = \Sigma_t(\mathbf{r}) e^{-\Sigma_{\text{maj}} s} \,,$$
$$g(x) = \Sigma_{\text{maj}} e^{-\Sigma_{\text{maj}} s} \,.$$

The equation $g(x)$ is always majorant to $f(x)$, by the definition of Σ_{maj}, so we set $M = 1$. We will therefore accept samples with the probability given in Eq. (2.15):

$$P_{\text{real}}(\mathbf{r}) = \frac{f(x)}{M \cdot g(x)} = \frac{\Sigma_t(\mathbf{r}) e^{-\Sigma_{\text{maj}} s}}{\Sigma_{\text{maj}} e^{-\Sigma_{\text{maj}} s}} = \frac{\Sigma_t(\mathbf{r})}{\Sigma_{\text{maj}}} \,. \tag{2.18}$$

We will refer to this as the probability of a "real" collision, P_{real}, to differentiate these physical collisions from the non-physical virtual collisions. It is important to note that the probability is independent of path length s, but is dependent on position $\mathbf{r}$. At each collision, the material region at the neutron position must be determined, but we do not need to explicitly track boundaries nor calculate their distance each time a path length is sampled. The algorithm for delta-tracking is shown in Fig. 2.5.

Now, the path length can be sampled across multiple material regions of varying Σ_t without explicitly stopping the neutron at a given boundary. This allows us to avoid determining the distance to the nearest boundary after each path length sampling. Delta-tracking is also much more efficient in regions where the geometry is complex or material region thicknesses are on the same order as the path length.This method can become computationally inefficient in regions where the total cross-section is much less than the majorant cross-section, leading to oversampling of virtual collisions. This is seen in geometries that include localized absorbers, such as control rods.

2.4 The Serpent 2 Monte Carlo Code

The Serpent Monte Carlo code was developed at VTT Technical Research Centre of Finland (VTT) as a PhD thesis project [4]. A second iteration of the code, Serpent 2, is currently under development. Both versions of Serpent use a combination of surface tracking, Woodcock delta-tracking, and rejection sampling for non-uniform density distributions. Serpent 2 selects between surface tracking and delta-tracking by examining the ratio of total cross-section to majorant cross-section [5]. In regions where many virtual collisions would occur, the code preferentially switches to ray tracing. This is to avoid the computational inefficiency of processing virtual collisions that provide no statistics. This selection is determined by a constant c and the inequality in Eq. (2.19).

$$\frac{\Sigma_t(\mathbf{r})}{\Sigma_{\text{maj}}} > 1 - c \tag{2.19}$$

If this inequality is true, delta-tracking is used, otherwise ray-tracing (referred to as surface-tracking in Serpent 2) is used. By default, the value of c is 0.9, as this was determined to produce the best improvement in run time [5]. We note that this inequality is identical to the value of P_{real}. Prior to sampling path length, the code tests this ratio for the current neutron position and determines if surface tracking or delta-tracking should be used. If delta-tracking is used, the code then determines if the collision is virtual or real. The value of c can be set in the input file using `set dt`.

Algorithm 1 Delta-tracking

1: **Sample** path length
2: **Look up** location to get $\Sigma_t(\mathbf{r})$
3: $P_{\text{real}} \leftarrow \frac{\Sigma_t(\mathbf{r})}{\Sigma_{\text{maj}}}$
4: **Sample** random number $\xi \in [0, 1)$
5: **if** $\xi < P_{\text{real}}$ **then** ▷ Collision is real
6: **Execute** real collision
7: **else** ▷ Collision is virtual
8: **Execute** virtual collision
9: **end if**

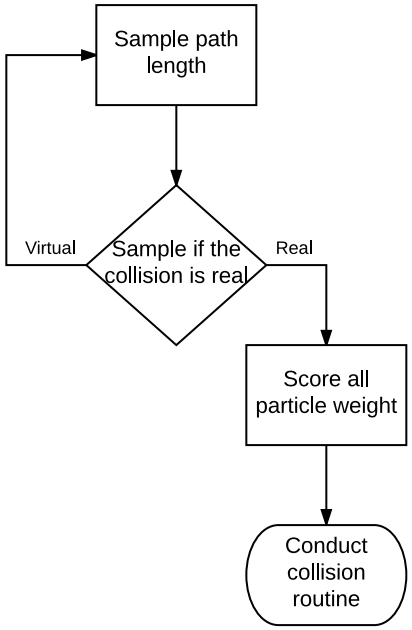

Figure 2.5: Delta-tracking algorithm and flow chart.

Chapter 3

Method

The Serpent 2 Monte Carlo code uses a combination of ray tracing and delta-tracking to simulate the propagation of particles. The WDT method modifies delta-tracking for an absorbing medium, replacing virtual collisions with a weight reduction. In this chapter, we will discuss the WDT routine for absorption events, and extend the method to include scattering. We will then define the WDT threshold, a key parameter for its implementation in Serpent 2.

3.1 Weighted delta-tracking

Morgan and Kotlyar [10] introduced a method to improve the inefficiencies of Woodcock delta-tracking in the presence of large absorbers. The method, WDT, replaces the rejection sampling algorithm of delta-tracking with a weight reduction algorithm. This process is similar to survival biasing, or implicit capture.

Implicit Statistical Events

We consider a process that can result in multiple outcomes, each with their own probability. One approach is to sample a random variable and determine which outcome actually occurred. If the event occurs many times, we can instead replace the statistical process by using the expected value of the random process [9]. The expected value of a random variable x that can take values $x_1 \dots x_n$ with probabilities $p_1 \dots p_n$, respectively, is given by:

$$E[x] = x_1 p_1 + x_2 p_2 \dots + x_n p_n \,. \tag{3.1}$$

For example, imagine we have a bag with four coins, three worth \$0.25 and one worth \$0.10. The values and their probabilities are:

$$x_1 = 0.25, \quad p_1 = \frac{3}{4} = 0.75\,;$$
$$x_2 = 0.10, \quad p_2 = \frac{1}{4} = 0.25\,.$$

For a given draw, we could sample a random value and use the probabilities p_1 and p_2 to determine the coin drawn. Or, we can describe the expected value of the drawn coin:

$$\begin{aligned} E[x] &= x_1 p_1 + x_2 p_2 \\ &= (0.25 \times 0.75) + (0.10 \times 0.25) \\ &= 0.2125 \end{aligned}$$

This value represents the average value of a coin drawn, if we perform many draws. The following Matlab code replicates this procedure:

```
v = 0;
n = 1000;
for i = 1:n
    xi = rand;
    v = v + (xi < 0.25)*0.1 + (xi >= 0.25)*0.25;
end
```

Although the exact values will vary due to the small sample size, `v/n` ≈ 0.2125, as we expected.

This framework is often applied to neutron propagation in a process called "survival biasing" [1]. At each collision location, the type of interaction is sampled and the appropriate action taken. In the case of a capture event, the neutron is "killed" (removed from the simulation). While this accurately reflects the physical reality, it does not produce good statistics. Assuming we are using a collision estimator, the neutron's contribution to our simulation is the history of collisions. Each of these provide a score to that particular collision, contributing to the overall simulation statistics. Capture events that kill neutrons, therefore, are removing the very particles we need to generate better statistics, resulting in the need for many more particles. Mitigating this issue is the goal of survival biasing.

Survival biasing avoids killing neutrons by replacing capture events with an expected outcome. As described above, we do not need to track the outcome of every single event, but can rely on the expected value. This will give us, on average, the outcome of our many events. To eliminate our explicit consideration of capture events, we therefore have two possible event types: capture events, and scattering events. The probabilities p will be given by the ratios of the cross-sections:

$$\begin{aligned} p_c &= \frac{\Sigma_c}{\Sigma_t}\,, \\ p_s &= \frac{\Sigma_s}{\Sigma_t}\,, \end{aligned}$$

where Σ_c and Σ_s are the macroscopic cross-sections for capture and scattering, respectively.

In the coin example, each had a different monetary value, giving us an expected value when we drew many times. We must introduce something similar for neutrons. It is convention to call this intrinsic value "weight", which represents the importance of the neutron.

All neutrons are born with the same weight, usually unity, and are killed when they have zero weight. At each point of interaction, the incoming neutron has an initial weight based on the neutron's history w_i, and a final weight w_f that depends on the type of interaction. A capture event that kills a neutron immediately forces the final weight of the neutron to zero $w_{f,c} = 0$. We can then calculate the expected value of the interaction of a neutron with initial weight w_i:

$$\begin{aligned} E[w_f] &= w_{f,s}p_{\mathrm{s}} + w_{f,c}p_{\mathrm{c}} \\ &= w_{f,s}p_{\mathrm{s}} \end{aligned}$$

A scattering event merely changes the location of the neutron in energy and angle phase space, leaving its importance unchanged. Therefore, $w_{f,s} = w_i$ and:

$$E[w_f] = w_i p_s \, .$$

With implicit capture every collision is considered to be a non-capture event. The neutron continues with a lower weight, proportional to the probability that the event was scattering. The weight lost in the collision is scored as capture:

$$\begin{aligned} S_c &= E[w_i - w_f] \\ &= E[w_i] - E[w_f] \\ &= w_i - w_i p_s \\ &= w_i(1 - p_s) \, , \end{aligned}$$

where S_c is the score for capture. A similar method will be used by weighted delta-tracking.

Russian Rouletting

When the survival biasing routine described in Sec. 3.1 is used, the loss of neutrons is entirely reliant on leakage from the problem or fission events. Neutrons will continue to undergo collisions and subsequent weight reduction until they have a very low weight. These particles will only contribute small amounts to our statistics, so tracking them is computationally inefficient. To mitigate this, a lower cutoff for the weight is introduced. Once neutrons are below this weight, they have a chance of being killed by a Russian Rouletting routine.

The general algorithm is shown in Algorithm 2. Following a collision, if the weight of the colliding particle is below a defined weight threshold, a random number is sampled. If this number is below a defined rouletting probability, the particle is killed. If the particle survives rouletting, its weight is increased proportionaly to the rouletting probability. By either killing low weight particles or increasing their weight, the inefficiency of tracking low-weight particles can be reduced.

Algorithm 2 Rouletting Routine

```
if weight < weight threshold then
    ξ ← random number ∈ [0, 1)
    if ξ < roulette probability then
        Kill particle
    else
        w_f ← w_i/(roulette probability)
    end if
end if
```

Weighted delta-tracking

Morgan and Kotlyar [10] introduced a method to improve the inefficiencies of Woodcock delta-tracking in the presence of large absorbers. The method, WDT, replaces the rejection sampling of delta-tracking with a weight reduction. This is similar to the process of implicit capture discussed in Section 3.1.

The WDT method samples the particle path length in the same fashion as Woodcock delta-tracking. As described in Section 2.3, after each path length is sampled, the delta-tracking method accepts the collision as real with the probability shown in Eq. 2.15. The WDT method bypasses this rejection sampling by accepting all collisions as real with a subsequent reduction in weight. As discussed in Section 3.1, replacing a statistical event requires calculation of the expectated value. In this case, the two events are a real collision and a virtual collision:

$$E[w_f] = w_{f,\text{real}} P_{\text{real}} + w_{f,\text{virt}} P_{\text{virt}} \, . \tag{3.2}$$

Morgan and Kotlyar examine a 1D test case with absorption. As an absorption event removes the particle, the resulting final weight of a real collision is zero. A virtual collision is rejected, and therefore leaves the weight unchanged. Inserting the appropriate values into Eq. (3.2) gives the expected value of the final weight for an absorption event:

$$\begin{aligned} E[w_f] &= w_{f,\text{real}} P_{\text{real}} + w_{f,\text{virt}} P_{\text{virt}} \\ &= 0 + w_i P_{\text{virt}} \\ &= w_i (1 - P_{\text{real}}) \\ &= w_i \left(1 - \frac{\Sigma_t}{\Sigma_{\text{maj}}} \right) \, . \end{aligned}$$

The particle that is left following the collision continues propagating as if it underwent a virtual collision. In this case, the absorption is then scored using the expectation value of

the score.

$$\begin{aligned} S_{\text{absorption}} &= E[w_i - w_f] \\ &= E[w_i] - E[w_f] \\ &= w_i \left(\frac{\Sigma_t}{\Sigma_{\text{maj}}} \right) \end{aligned}$$

This algorithm is implemented by Kotlyar and Morgan in a 1D problem and the results are verified with an analytical solution. The authors point out that a rouletting routine should be implemented when WDT is used, to prevent the tracking of low-weight neutrons.

3.2 Weighted delta-tracking with scattering

In a scattering event, the weight of the incident particle does not change. Therefore, application of the expectation value as in Section 3.1 results in an expected value of the final weight equal to the initial weight:

$$\begin{aligned} E[w_f] &= w_{f,\text{real}} P_{\text{real}} + w_{f,\text{virt}} P_{\text{virt}} \\ &= w_i P_{\text{real}} + w_i P_{\text{virt}} \\ &= w_i (P_{\text{real}} + 1 - P_{\text{real}}) \\ &= w_i \, . \end{aligned}$$

This doesn't model what we expect. We can view WDT as splitting the weighted neutron into two particles. One carries the real portion of the weight and experiences the collision. The other carries the virtual portion of the weight and continues propagating as if no collision occurred. This works fine for absorption, where the portion that experiences the collision does not propagate: it is immediately killed and scored. But, when the neutron is split into a scattering portion and a virtual portion, no weight is lost because neither of those events change the weight.

Therefore, extension of this methodology to scattering requires duplication of the particle at the point of collsion. The virtual portion of the weight is carried away by a particle that propagates as if no collision has occured, and the real portion is carried away by a particle that undergoes scattering. In problems with scattering, this results in a rapid multiplication of neutrons. When implemented into Serpent 2, this multiplication very quickly filled any available neutron buffer in simulations of a boiling water reactor (BWR), ending the simulation. We therefore expanded the WDT method with a novel approach to handling scattering. This approach combines the WDT methodology with the standard delta-tracking rejection sampling in a way that has not been done before.

Scattering Rejection Sampling

As described in the last section, the WDT method may result in an intractable simulation when applied to scattering. This occurred because the WDT method splits the incoming

weight in two: one portion for a real collision, one portion for a virtual collision. We developed a new methodology that avoids splitting the neutron when scattering, while keeping the splitting otherwise. To accomplish this, the original delta-tracking rejection sampling was moved into the scattering subroutine. The algorithm is shown in Alg. 3 and a flow chart of the routine is shown in Fig. 3.1

Note that there are two separate scoring events in each collision subroutine: scoring of the actual collision type for calculating specific reaction rates, and scoring of collision itself used by the collision flux estimator. In addition, scoring the fission reaction also encompasses generation of fission neutrons.

In the original delta-tracking routine, the rejection sampling takes place prior to collision type sampling, and collision scoring can occur between the two. This is the routine that Serpent 2 used, prior to modification for the above scheme. By moving the rejection sampling after the collision type sampling, the collision score is no longer agnostic to the type of collision that will occur. Therefore, in the implementation of this routine in Serpent 2, the collision scoring was moved after the collision type sampling.

3.3 Implementation in Serpent 2

The WDT algorithm is implemented to work alongside the current implementation of ray tracing and delta-tracking, as described in Sec. 2.4. WDT is designed to improve the effectiveness of delta-tracking when the change of a virtual collision is high. We can hypothesize that the algorithm will benefit in the regime where P_{real} is low. At high values of P_{real}, a majority of the weight of the incoming particle is scored. This leaves the particle that undergoes a virtual collision with a very low weight, relying on the rouletting routine to prevent computational inefficiency. These two situations imply that there is a region between low and high values of P_{real} where WDT may provide benefit.

This region is defined by two values, summarized in Fig. 3.2. On the lower end, the value of $(1 - c)$ defines the threshold below which surface tracking is used. On the upper end, a new parameter t_{wdt} defines the threshold below which WDT will be used instead of normal delta-tracking. This provides the user with the ability to exactly define the region where WDT will be used.

Algorithm 3 Weighted delta-tracking with scattering

Sample path length
Sample collision type
if collision type == (capture or fission) **then**
    Score capture or fission $\leftarrow w_i P_{\text{real}}$
    Score collision $\leftarrow w_i P_{\text{real}}$
    $w_f \leftarrow w_i(1 - P_{\text{real}})$
    Execute virtual collision
else
    Sample random number $\xi \in [0, 1)$
    if $\xi < P_{\text{real}}$ **then** ▷ Collision is real
        Score scattering $\leftarrow w_i$
        Score collision $\leftarrow w_i$
        Execute scattering collision
    else ▷ Collision is virtual
        Execute virtual collision
    end if
end if

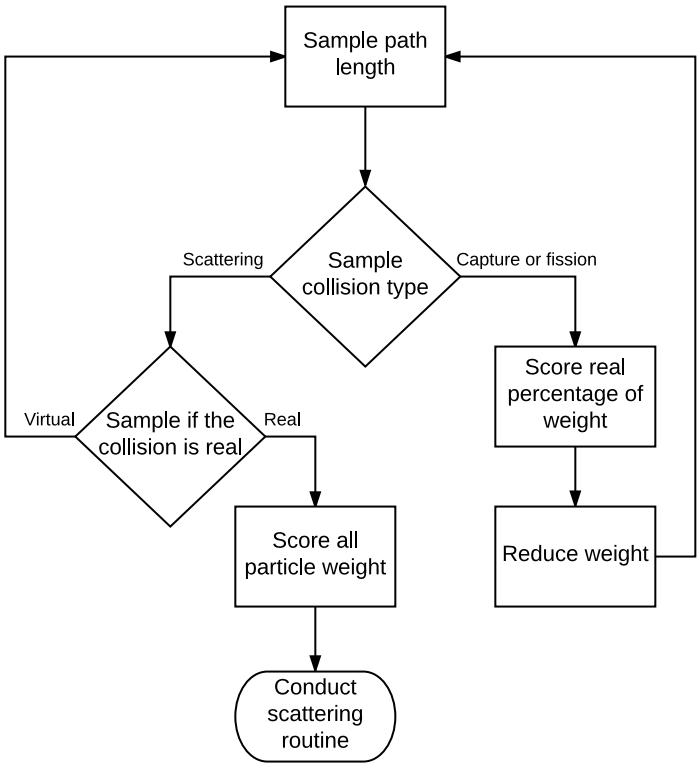

Figure 3.1: Weighted delta-tracking with scattering rejection sampling.

$$\text{Mode} = \begin{cases} \text{Raytracing}, & P_{\text{real}} < 1 - c \\ \text{WDT}, & 1 - c \leq P_{\text{real}} < t_{\text{wdt}} \\ \text{Delta} - \text{tracking}, & P_{\text{real}} \geq t_{\text{wdt}} \end{cases}$$

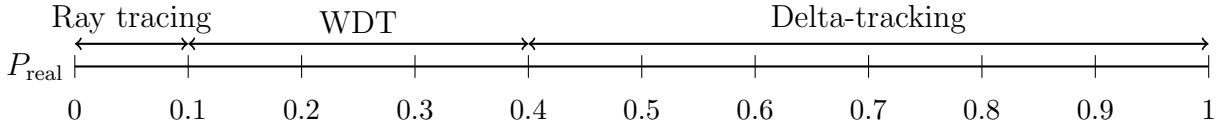

Figure 3.2: Implemented selection scheme for ray-tracing, weighted, and normal delta-tracking. Shown using the values of $(1 - c) = 0.1$ and $t_{\text{wdt}} = 0.4$.

Chapter 4

Results

We expect that the WDT method will improve the statistics of Serpent 2 calculations. With normal delta-tracking, virtual collisions provide no statistical benefit, and are therefore an inefficient use of computational resources. Virtual collisions that result in absorption events do contribute to statistics when using WDT. Therefore, we expect an improvement in the results of a Serpent 2 simulation. In this section, we will describe how performance in Serpent 2 is quantified, describe the three test cases, and the results of those test cases.

4.1 Performance metrics

Figure of Merit

Monte Carlo codes such as Serpent 2 run many iterations of a single simulation, calculating the mean of values of interest $\hat{x}$ across many runs. All calculations done in this study were criticality source calculations. For these types of calculations in Serpent 2, source neutrons are run in cycles. Each cycle contains the same number of source neutrons, and the source distribution is determined by the previous cycle [7]. By the central limit theorem, we know that the means across these many simulations will form a normal distribution with variance $\sigma^2(\hat{x})$. We are interested in reducing the variance of the final value, which will provide more confidence in the simulation results. In general, running the simulation more times with more particle histories will reduce this variance at the cost of requiring more computation time. The variance depends on the number of particle histories, which is proportional to the number of cycles n:

$$\sigma^2(\hat{x}) \propto \frac{1}{n}\,. \tag{4.1}$$

Cycles will be used in this report in the place of particle histories because this value is easily drawn from the Serpent 2 output files.

Serpent 2 reports the standard deviation of the mean, $\sigma(\hat{x})$, which is proportional to $n^{-1/2}$. The standard deviation plotted against cycles is shown in Fig. 4.1 on a log-log plot. As expected, we see a linear evolution with a slope of 1/2 once enough cycles have been

executed to give good statistical calculations. Per the central limit theorem and Eq. (4.1),

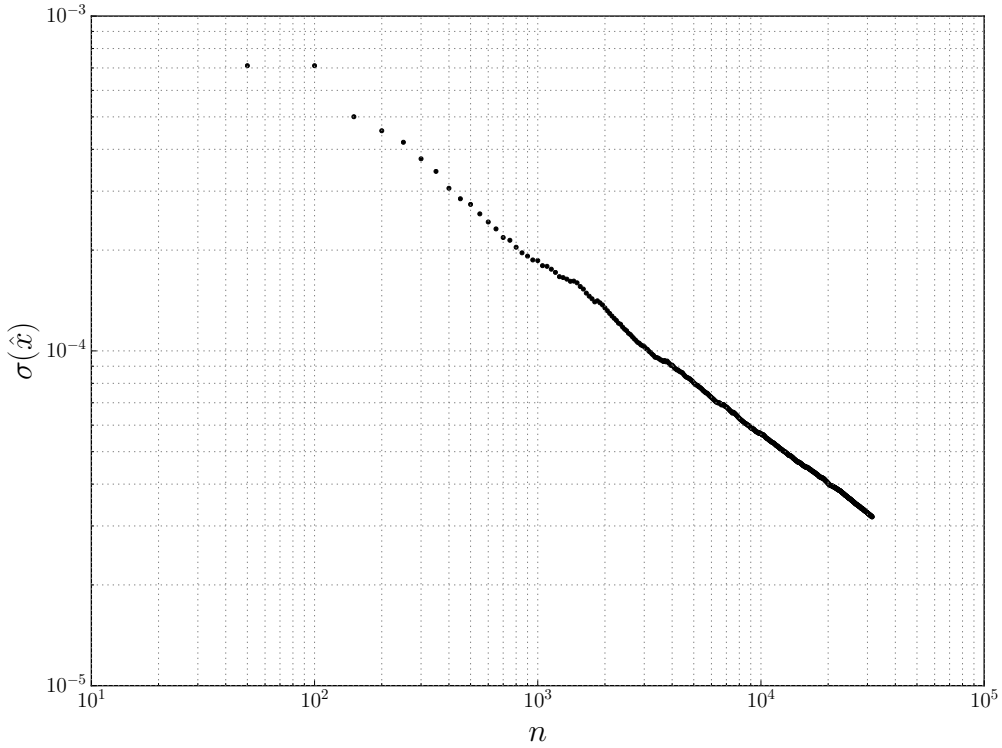

Figure 4.1: Variance in the infinite flux ϕ_∞ for the fast-neutron group as a function of Serpent 2 cycle, with WDT threshold of 0.2.

we can always continue running more cycles to improve the variance. A more efficient simulation should provide better statistics, resulting in a lower variance in less time. The variance is therefore dependent on two things: the number of cycles we run, and the efficiency of our algorithm.

For this study, we are interested in the efficiency of the WDT algorithm. We therefore need to establish a standard measuring device, a figure of merit (FOM), that is independent of the number of cycles, n. This will then allow us to utilize the variance to directly measure of the efficiency of our algorithm. The standard FOM used by most simulations, described by Lewis and Miller [1], is shown in Eq. (4.2):

$$\text{FOM} = \frac{1}{\sigma(\hat{x})^2 T}\,, \tag{4.2}$$

where T is the runtime of the simulation and is proportional to the number of cycles $T \propto n$. Plugging this and Eq. (4.1) into Eq. (4.2) yields:

$$\text{FOM} = \frac{1}{\sigma(\hat{x})^2 T} = \frac{n}{C_1} \cdot \frac{1}{C_2 \cdot n} = C_3\,,$$

where C_1, C_2, C_3 are constants.

As we can see, we expect the FOM to be a constant value, independent of the number of cycles n. A higher FOM indicates higher accuracy per computation time, and therefore a more efficient algorithm. Serpent 2 collects scores for each cycle (or batch of cycles) and outputs the sample mean and standard deviation [13]. This enables comparison of Serpent 2 running with and without WDT to determine the efficiency of the algorithm.

Convergence

As discussed in the previous section, the FOM should be independent of cycle number n. In reality, it takes enough cycles for good statistics to develop for the FOM to converge to its final value. As seen in Fig. 4.2, the FOM begins to converge around 1×10^4 cycles in this example. It may take many cycles for the FOM to converge to a single value. Therefore, we calculate an average value using a selected number of the final data points.

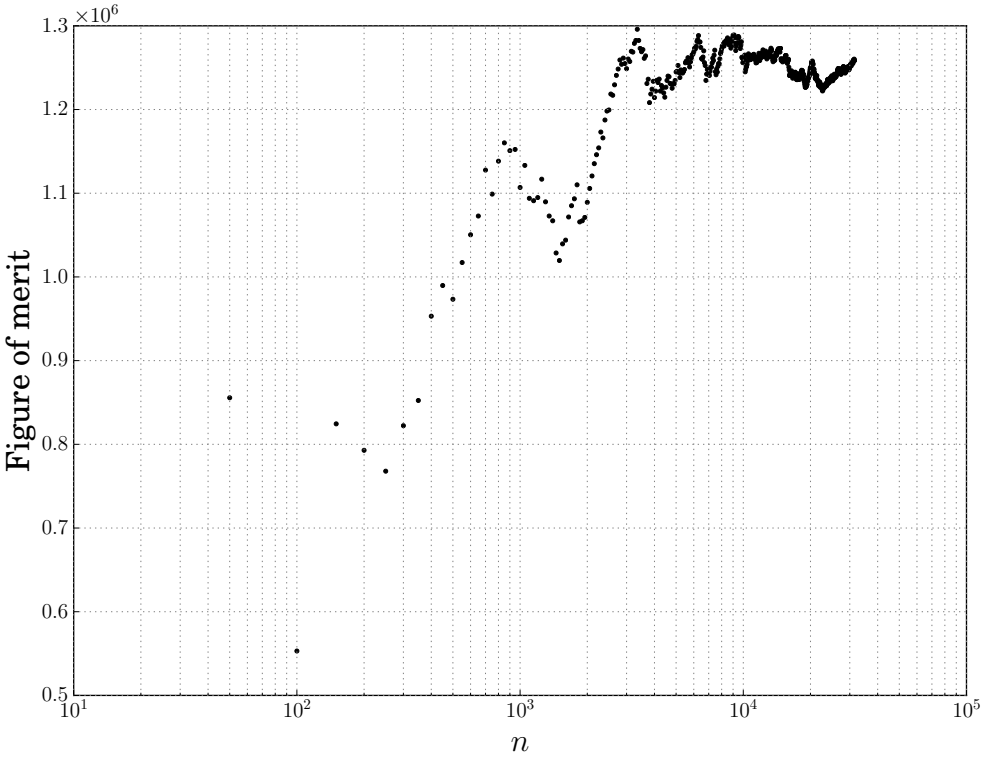

Figure 4.2: Figure of merit in ϕ_∞ for the fast-neutron group as a function of Serpent 2 cycle, with WDT threshold of 0.2.

4.2 Analysis Tools

Serpent 2 generates a single output file as the simulation runs. The parameters of interest are overwritten as their mean value and standard deviation are updated. This is sufficient to calculate the final value of the FOM, which gives an indication of the quality of the simulation. In addition to this, figures such as those shown in Sec. 4.1 are useful to verify that the FOM has in fact converged, and that the variance is reducing as expecting. Therefore, in addition to changing the Serpent 2 source code to include the WDT method, it was modified to generate uniquely named output files at the end of each batch. Processing these files enables us to generate variance and FOM convergence graphs.

As seen in Fig. 4.2, the final FOM is not a single value, but may oscillate for a large number of cycles. Therefore, we calculated an average FOM value for each run, to allow comparison of runs without requiring a visual inspection of each graph. To support processing the large amount of data, we developed a python package, `WDT_Analysis`.

The `WDT_Analysis` package

As described above, we modified the Serpent 2 source code to generate uniquely named output files at various cycle values. The `WDT_Analysis` package[1] leverages python's object oriented programming structure to enable easy analysis of the data. We utilize a module, `fom`, to analyze the convergence of FOM across many Serpent 2 output files. A summary of each of the major objects used by the `fom` module are outlined in Table. 4.1. Detailed use of

Table 4.1: Object structure of the `WDT_Analysis` package.

Object	Description
`DataFile`	Contains all the data from a single Serpent 2 output file.
`Analyzer`	Contains all the `DataFile` objects from a run of Serpent 2.
`Comparator`	Compares the FOM convergence for one or more `Analyzer` objects.

the package is provided in the package documentation. Use of the package makes analysis of the FOM convergence simple:

1. Run desired Serpent 2 simulations.
2. Place all output files from each desired run in separate directories
3. Initialize a `Comparator` object, providing the directories and names for the datasets. While initializing, the `Comparator` will:
    a) Create a `DataFile` object for each serpent output file.

[1] Available on GitHub `https://github.com/jsrehak/WDT_Analysis`

b) Collect the `DataFile` objects from a single run into a single `Analyzer`.

c) Collect these `Analyzer` objects into the `Comparator`.

4. Use the `compare` and `plot` functions of the `Comparator` object to observe the FOM convergence.

We used this process to compare the FOM convergence for different values of the WDT threshold for three test cases.

4.3 Parameters of Study

Each Serpent 2 simulation generates hundreds of output parameters that describe all processes that occur during particle propagation. Finding values where the WDT method improves the FOM is a daunting task. To focus our search, we identified three quantities that will be the focus of this research study. Further study into other parameters may reveal further benefit or issues with the WDT method. The three parameters we selected are flux, total cross-section, and the scattering matrices for the zeroth scattering moment. Each of the three test-cases have reflective boundary conditions, so we will examine the infinite values for these parameters.

The neutron flux quantifies the total distance traveled by all neutrons in a volume per unit time. This is an important quantity, as it is representative of the neutron population. A low variance is desired in neutron flux, as it indicates that the uncertainty in the neutron population in each energy group is well understood.

The total cross-section quantifies the total interaction probability for neutrons of that energy range. The zeroth scattering moment is a matrix that quantifies scattering between the energy groups in the problem, both upscattering and downscattering. A low variance is desired in these parameters, as the goal of implementing this method is to improve cross-section development for a highly scattering medium, TREAT.

A Serpent 2 simulation was run for each of the three test cases using values of the WDT threshold (t_{wdt}) from 0.1 to unity in increments of 0.1, maintaining a value of $(1 - c) = 0.1$, as described in Fig. 3.2. To determine the effectiveness of WDT, we compared the final average FOM for each value of t_{wdt} to the final average FOM with no WDT:

$$R(t_{\text{wdt}}) = \frac{\overline{\text{FOM}}(t_{\text{wdt}})}{\overline{\text{FOM}}_0} ,$$

where $\overline{\text{FOM}}_0 = \overline{\text{FOM}}(0.1)$ is the average FOM with no WDT. Increasing values of t_{wdt} leads to increasing amount of WDT over regular delta-tracking. The parameters for the rouletting scheme are kept constant, with a weight cutoff of $w = 0.1$ and probability of rouletting $P_{\text{kill}} = 0.5$.

Test Cases

Three test cases were selected to test the FOM values for the WDT method. These are a pressurized water reactor (PWR) pin cell, a fast reactor pin cell, and a homogenous fuel element based on the composition of the TREAT fuel elements at the INL. All test cases were run on the Abacus server at UC Berkeley, the specifications of the server are shown in Tab. 4.2.

Table 4.2: Abacus server specifications

Parameter	Specification
Processor	2 x TenCore Intel Xeon Processor E52687W v3 3.10GHz 25MB Cache
RAM	16 x 16GB PC417000 2133MHz DDR4
Hard drive	2 x 800GB Intel SATA 6.0Gb/s Solid State Drive

4.4 Pressurized water reactor pin cell

The PWR pin cell was chosen from the Serpent 2 validation input files provided on the VTT Serpent webpage [14]. The geometry and physical parameters are shown in Fig. 4.3. The fuel is a 2.68 w/o enriched UO_2 mixture, with Zircalloy cladding, light water moderation, and reflective boundary conditions. We ran the simulation with two energy groups with the group boundary at 0.625 eV.

Infinite Flux

A summary of the FOM ratio and $\overline{\text{FOM}}(t_{\text{wdt}})$, for the PWR pin cell for infinite flux (ϕ_∞) is shown in Tab. 4.3 and shown graphically in Fig. 4.4. These ratios were calculated using the final 20 data points for each series, then compared to the base case. For the fast group, WDT threshold values of 0.6 and higher return a consistently higher FOM ratio. This behavior is not observed in the thermal group FOM ratio.

Infinite Total Cross-section

A summary of the FOM ratio and $\overline{\text{FOM}}(t_{\text{wdt}})$, for the PWR pin cell for infinite total cross-section ($\Sigma_{t,\infty}$) is shown in Tab. 4.4 and shown graphically in Fig. 4.5. The FOM ratio for the fast group when using WDT is always less than unity. The FOM ratio behavior for this quantity is inverted compared to the fast group infinite flux FOM ratio. The thermal group shows consistent improvement with increased WDT, but with no meaningful trend. The peak improvement occurs with full WDT, $t_{\text{wdt}} = 1.0$, as with the infinite flux.

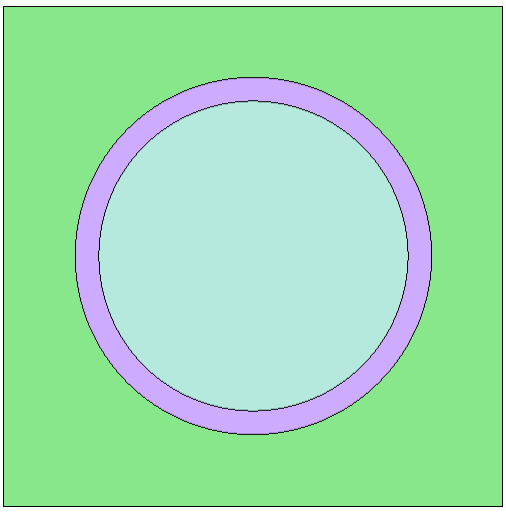

Parameter	**Value (cm)**
Fuel radius	0.412
Cladding radius	0.475
Pitch	1.33

Figure 4.3: Pressurized water reactor geometry and physical parameters. The fuel is shown in light blue, the cladding in purple and the coolant is green.

Table 4.3: $\overline{\text{FOM}}$ as a function of t_{wdt} and the ratio of values to the base case for the PWR pin cell *infinite flux*.

Fast group ($E > 0.0625$)			Thermal group		
t_{wdt}	$\overline{\text{FOM}}$	Ratio	t_{wdt}	$\overline{\text{FOM}}$	Ratio
0.1	1.240281×10^6	1.000000	0.1	1.283594×10^6	1.000000
0.2	1.257046×10^6	1.013517	0.2	1.305878×10^6	1.017360
0.3	1.262320×10^6	1.017769	0.3	1.335006×10^6	1.040053
0.4	1.302585×10^6	1.050233	0.4	1.309221×10^6	1.019965
0.5	1.268738×10^6	1.022944	0.5	1.322382×10^6	1.030218
0.6	1.304854×10^6	1.052063	0.6	1.321435×10^6	1.029481
0.7	1.311428×10^6	1.057364	0.7	1.283419×10^6	0.999863
0.8	1.296513×10^6	1.045338	0.8	1.304767×10^6	1.016495
0.9	1.306470×10^6	1.053366	0.9	1.339323×10^6	1.043416
1.0	1.302047×10^6	1.049800	1.0	1.360193×10^6	1.059675

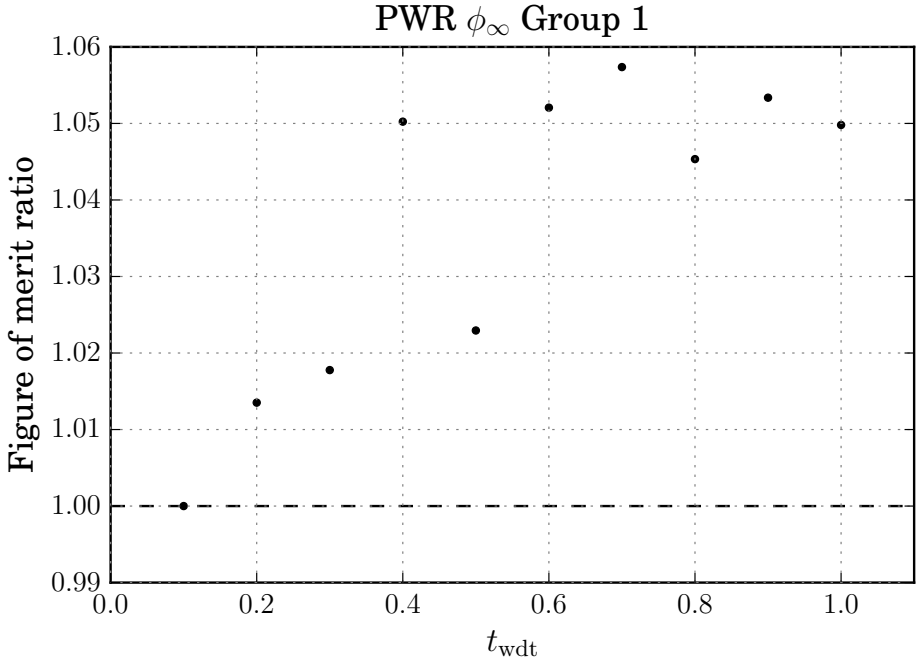

(a) Group 1

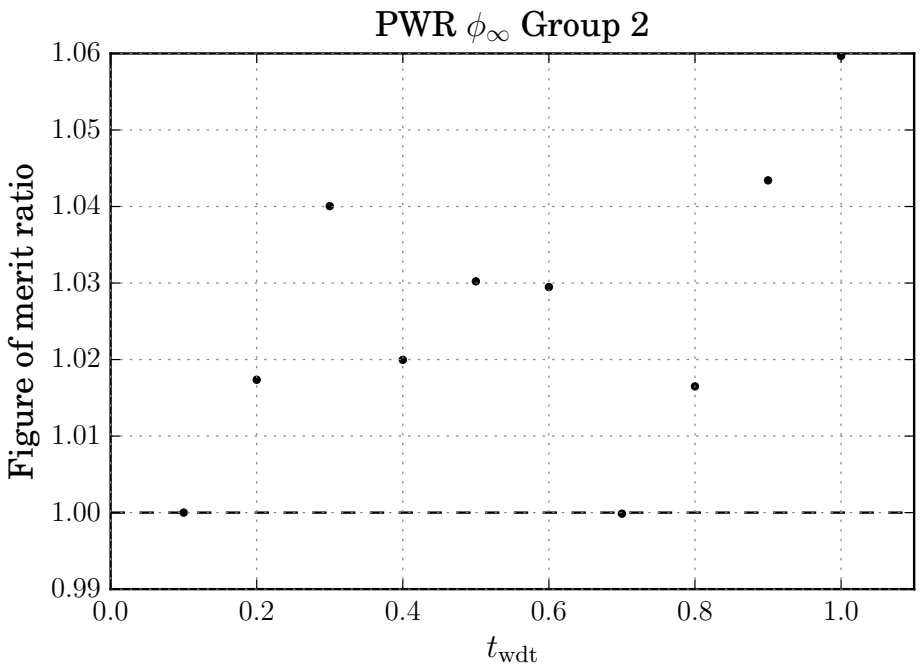

(b) Group 2

Figure 4.4: Figure of merit ratio of the *infinite flux* for the PWR vs the WDT threshold for the (a) fast and (b) thermal energy groups. The group boundary is at 0.0625 eV. FOM is calculated using the last 20 data points.

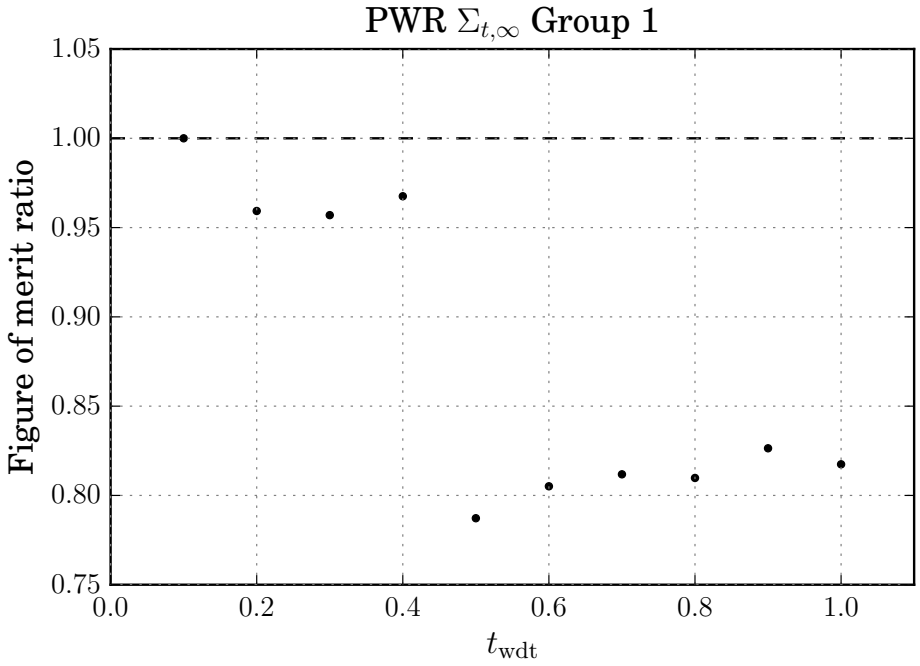

(a)

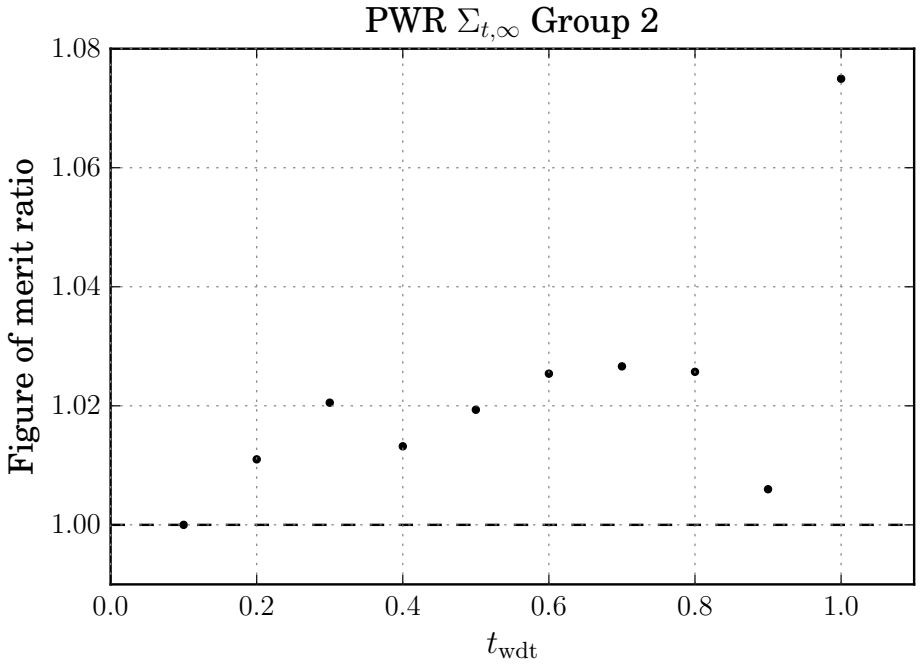

(b)

Figure 4.5: Figure of merit ratio of the *infinite total cross-section* for the PWR vs the WDT threshold for the (a) fast and (b) thermal energy groups. The group boundary is at 0.0625 eV. FOM is calculated using the last 20 data points.

Table 4.4: $\overline{\text{FOM}}$ as a function of t_{wdt} and the ratio of values to the base case for the PWR pin cell *infinite total cross-section*.

Fast group ($E > 0.0625$)			thermal group		
t_{wdt}	$\overline{\text{FOM}}$	Ratio	t_{wdt}	$\overline{\text{FOM}}$	Ratio
0.1	1.467242×10^7	1.000000	0.1	8.065829×10^6	1.000000
0.2	1.407526×10^7	0.959300	0.2	8.154616×10^6	1.011008
0.3	1.404113×10^7	0.956974	0.3	8.231395×10^6	1.020527
0.4	1.419632×10^7	0.967552	0.4	8.172302×10^6	1.013200
0.5	1.155054×10^7	0.787228	0.5	8.221818×10^6	1.019339
0.6	1.181301×10^7	0.805117	0.6	8.270724×10^6	1.025403
0.7	1.191133×10^7	0.811818	0.7	8.280600×10^6	1.026627
0.8	1.188149×10^7	0.809784	0.8	8.273215×10^6	1.025712
0.9	1.212526×10^7	0.826398	0.9	8.114104×10^6	1.005985
1.0	1.199368×10^7	0.817430	1.0	8.670363×10^6	1.074950

Scattering Matrices

For the two-group case, the scattering matrices for the zeroth moment, S_0, is 2×2. A summary of the FOM ratio for S_0 is shown in Table 4.5. The tables are for the entry in row g and column g', which represents scattering from group g' into group g, indicated as $g' \rightarrow g$. The FOM ratios are shown graphically in Fig. 4.6.

The WDT method under-performs in most cases, except the inscattering cross-section for the thermal group.

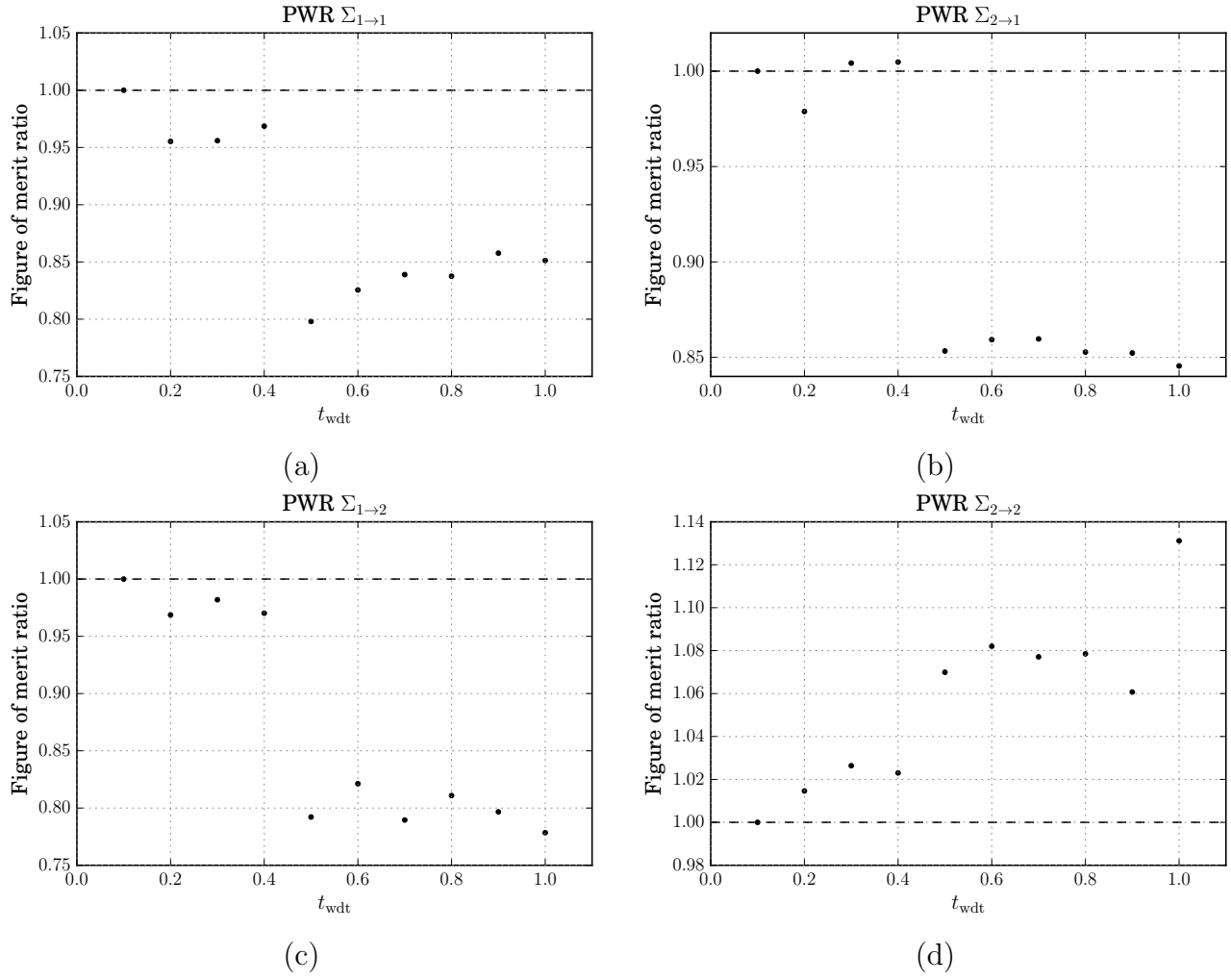

Figure 4.6: Figure of merit ratio of the *infinite zeroth-moment of the scattering cross-section* S_0 for the PWR vs the WDT threshold for the (a) $\Sigma_{1\to1}$, (b) $\Sigma_{2\to1}$, (c) $\Sigma_{1\to2}$ and (d) $\Sigma_{2\to2}$ entries. The group boundary is at 0.0625 eV. FOM is calculated using the last 20 data points.

Table 4.5: $\overline{\text{FOM}}$ as a function of t_{wdt} and the ratio of values to the base case for the PWR pin cell *infinite S_0 scattering matrix*

$\Sigma_{1\to1}$			$\Sigma_{2\to1}$		
t_{wdt}	$\overline{\text{FOM}}$	Ratio	t_{wdt}	$\overline{\text{FOM}}$	Ratio
0.1	1.422641×10^{7}	1.000000	0.1	1.395679×10^{6}	1.000000
0.2	1.358990×10^{7}	0.955258	0.2	1.366134×10^{6}	0.978831
0.3	1.359954×10^{7}	0.955936	0.3	1.401562×10^{6}	1.004215
0.4	1.378010×10^{7}	0.968628	0.4	1.402313×10^{6}	1.004753
0.5	1.135270×10^{7}	0.798002	0.5	1.190960×10^{6}	0.853319
0.6	1.174407×10^{7}	0.825511	0.6	1.199284×10^{6}	0.859284
0.7	1.193568×10^{7}	0.838981	0.7	1.199826×10^{6}	0.859672
0.8	1.191534×10^{7}	0.837551	0.8	1.190166×10^{6}	0.852750
0.9	1.220204×10^{7}	0.857703	0.9	1.189501×10^{6}	0.852274
1.0	1.211019×10^{7}	0.851247	1.0	1.180054×10^{6}	0.845505
$\Sigma_{1\to2}$			$\Sigma_{2\to2}$		
t_{wdt}	$\overline{\text{FOM}}$	Ratio	t_{wdt}	$\overline{\text{FOM}}$	Ratio
0.1	9.700866×10^{3}	1.000000	0.1	1.395679×10^{6}	1.000000
0.2	9.397108×10^{3}	0.968688	0.2	1.366134×10^{6}	0.978831
0.3	9.525420×10^{3}	0.981914	0.3	1.401562×10^{6}	1.004215
0.4	9.411723×10^{3}	0.970194	0.4	1.402313×10^{6}	1.004753
0.5	7.684674×10^{3}	0.792164	0.5	1.190960×10^{6}	0.853319
0.6	7.966642×10^{3}	0.821230	0.6	1.199284×10^{6}	0.859284
0.7	7.659128×10^{3}	0.789530	0.7	1.199826×10^{6}	0.859672
0.8	7.866229×10^{3}	0.810879	0.8	1.190166×10^{6}	0.852750
0.9	7.728249×10^{3}	0.796656	0.9	1.189501×10^{6}	0.852274
1.0	7.551567×10^{3}	0.778443	1.0	1.180054×10^{6}	0.845505

Discussion

There is no clear value of the WDT threshold that improves FOM for all cases. Depending on the desired output parameters of the simulation, using WDT may be beneficial. We observe an improvement or parity in infinite flux for both groups across all values of t_{wdt}. Therefore, we should look to other parameters to determine a useful value of t_{wdt}.

The infinite total cross-section for the thermal group shows a similar improvement to the infinite flux but the fast group data show a consistent under performance as shown in Fig. 4.5 and Tab. 4.4. Values of $t_{\text{wdt}} \geq 0.5$ result in the largest reduction, these values have a mean FOM ratio of 0.81. Lower values $0.1 \leq t_{\text{wdt}} \leq 0.4$ have a mean FOM ratio of 0.92.

We see a similar pattern in the entries in the scattering matrix, as shown in Fig. 4.6 and Tab. 4.5. The thermal-group inscattering cross-section has a consistent improvement, while

the fast group underperforms. For the fast group scattering into either group, as with infinite total cross-section, there are two domains. When $0.1 \leq t_{\text{wdt}} \leq 0.4$, the ratio is between 0.95 and unity, and is much lower otherwise. These data, therefore, suggest the same range of WDT threshold as the infinite total cross-section. For the upscattering cross-section $\Sigma_{2\to1}$, two values within this range return an improvement in FOM ratio, $t_{\text{wdt}} = 0.3, 0.4$.

Overall, the ratio data indicate that a WDT threshold of $t_{\text{wdt}} = 0.3$ or $t_{\text{wdt}} = 0.4$ provides an improvement in the statistics for thermal neutrons, without much loss of statistics elsewhere. The final FOM ratios for these values are summarized in Tab. 4.6. If the thermal group infinite parameters discussed here for a PWR are desired with high accuracy, the WDT method provides a means to improve these statistics without causing a significant impact on the fast group.

Table 4.6: Summary of FOM ratios for the PWR for select cases of WDT threshold.

$t_{\text{wdt}} = 0.3$		$t_{\text{wdt}} = 0.4$	
Parameter	**$\overline{\text{FOM}}$ Ratio**	**Parameter**	**$\overline{\text{FOM}}$ Ratio**
$\phi_{1,\infty}$	1.017769	$\phi_{1,\infty}$	1.050233
$\phi_{2,\infty}$	1.040053	$\phi_{2,\infty}$	1.019965
$\Sigma_{1,t}$	0.956974	$\Sigma_{1,t}$	0.967552
$\Sigma_{2,t}$	1.020527	$\Sigma_{2,t}$	1.013200
$\Sigma_{1\to1}$	0.955936	$\Sigma_{1\to1}$	0.968628
$\Sigma_{2\to1}$	1.004215	$\Sigma_{2\to1}$	1.004753
$\Sigma_{1\to2}$	0.981914	$\Sigma_{1\to2}$	0.970194
$\Sigma_{2\to2}$	1.004215	$\Sigma_{2\to2}$	1.004753

4.5 Fast reactor pin cell

We adapted the fast reactor pin cell from another example provided in the Serpent validation files [14]. This is a lead cooled pin cell with Mixed Oxide (MOX) fuel containing uranium, plutonium and a small amount of americium. The relative isotope amounts are shown in Tab. 4.7. The cladding is stainless steel. The lattice is hexagonal and has reflective boundary conditions. As with the PWR pin cell, we ran the simulation with two energy groups with the group boundary at 0.625 eV.

Table 4.7: Relative atomic density of the fast reactor pin cell MOX fuel.

Isotope	Relative Atomic Density
^{238}U	1.00
^{239}Pu	0.16
^{240}Pu	7.40×10^{-2}
^{242}Pu	2.09×10^{-2}
^{238}Pu	6.45×10^{-3}
^{235}U	4.11×10^{-3}
^{241}Am	3.57×10^{-3}
^{236}U	1.00×10^{-4}
^{234}U	3.01×10^{-5}

Infinite flux

A summary of the FOM ratio and $\overline{\text{FOM}}(t_{\text{wdt}})$, for the fast reactor pin cell for infinite flux (ϕ_∞) is shown in Tab. 4.8 and shown graphically in Fig. 4.8. The FOM ratio for group 1 is consistently higher; for group 2 the FOM values are very low. Although there appears to be a high ratio (3.140) at the threshold value $t_{\text{wdt}} = 0.4$, this merely reflects the poor statistics. As seen in Fig. 4.9, the FOM is not converging to a single value. We expect the thermal group to be underpopulated in a fast reactor, resulting in poor statistics. The WDT method does not improve this, but the statistics of the thermal group is of minimal interest in a fast reactor.

Infinite total cross-section

A summary of the FOM ratio and $\overline{\text{FOM}}(t_{\text{wdt}})$, for the fast reactor pin cell for infinite total cross-section ($\Sigma_{t,\infty}$) is shown in Tab. 4.9 and shown graphically in Fig. 4.10. The FOM ratio for group 1 is higher for all values of t_{wdt}, with the exception of 0.2. For group 2, as seen in Sec. 4.5, the FOM values are very low, and one ratio is artificially inflated when $t_{\text{wdt}} = 0.6$ due to the lack of convergence. This case is shown in Fig. 4.11; there are not

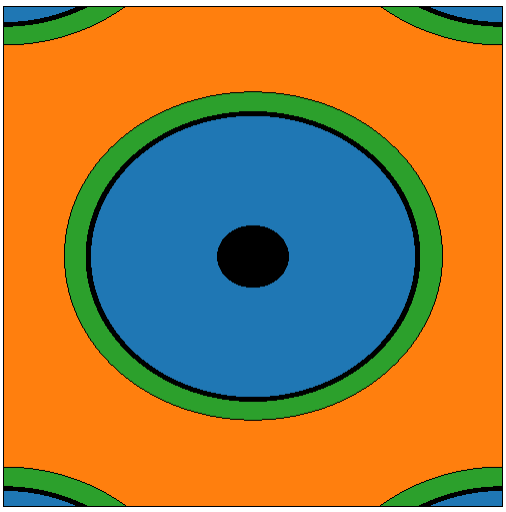

Parameter	Value (cm)
Void radius	0.1
Pellet radius	0.45
Inner cladding radius	0.465
Outer cladding radius	0.525
Pitch	1.789

Figure 4.7: Fast pin cell geometry and physical parameters. The pellet is shown in blue, the cladding green, and the coolant orange. Black regions are voids.

Table 4.8: $\overline{\text{FOM}}$ as a function of t_{wdt} and the ratio of values to the base case for the fast pin cell *infinite flux*.

Group 1 ($E > 0.0625$)			Group 2		
t_{wdt}	$\overline{\text{FOM}}$	Ratio	t_{wdt}	$\overline{\text{FOM}}$	Ratio
0.1	1.398529×10^{6}	1.000000	0.1	5.027779×10^{-4}	1.000000
0.2	1.458968×10^{6}	1.043217	0.2	4.567251×10^{-4}	0.908403
0.3	1.639208×10^{6}	1.172095	0.3	2.867434×10^{-4}	0.570318
0.4	1.715773×10^{6}	1.226841	0.4	1.578718×10^{-3}	3.139990
0.5	1.688965×10^{6}	1.207673	0.5	4.364983×10^{-4}	0.868173
0.6	1.903000×10^{6}	1.360716	0.6	3.411268×10^{-4}	0.678484
0.7	1.858063×10^{6}	1.328584	0.7	3.863250×10^{-4}	0.768381
0.8	1.818223×10^{6}	1.300097	0.8	4.222281×10^{-4}	0.839790
0.9	1.758294×10^{6}	1.257245	0.9	0.000000×10^{0}	0.000000
1.0	1.581456×10^{6}	1.130800	1.0	2.816380×10^{-4}	0.560164

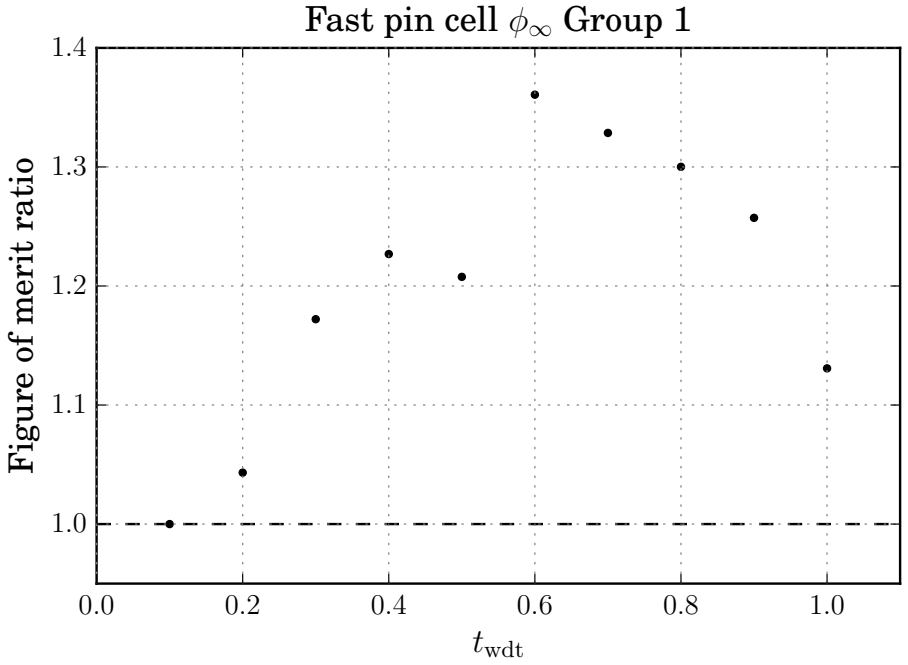

(a)

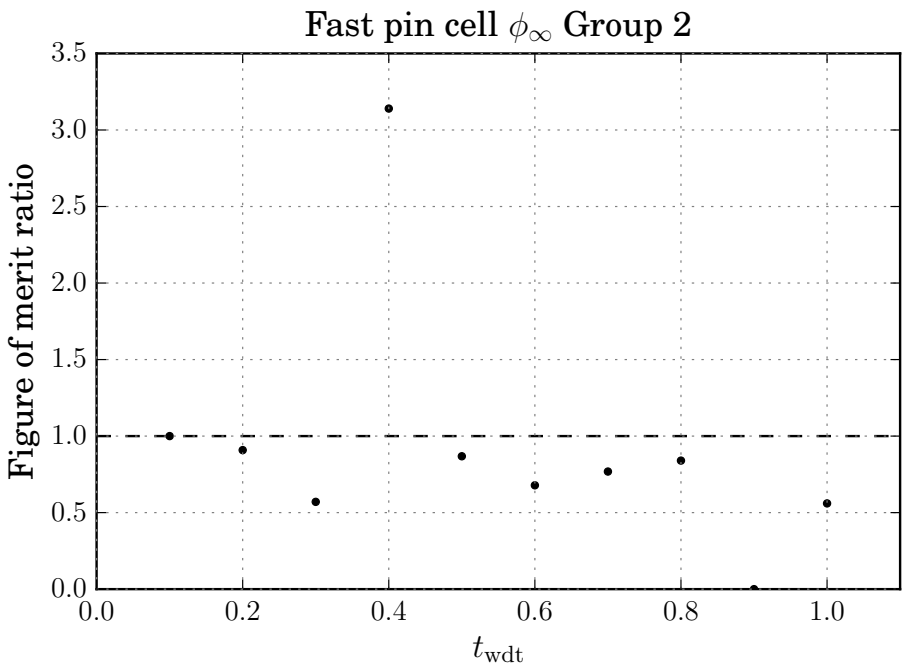

(b)

Figure 4.8: Figure of merit ratio of the *infinte flux* for the fast pin cell vs the WDT threshold for the (a) fast and (b) thermal energy groups. The group boundary is at 0.0625 eV. FOM is calculated using the last 20 data points.

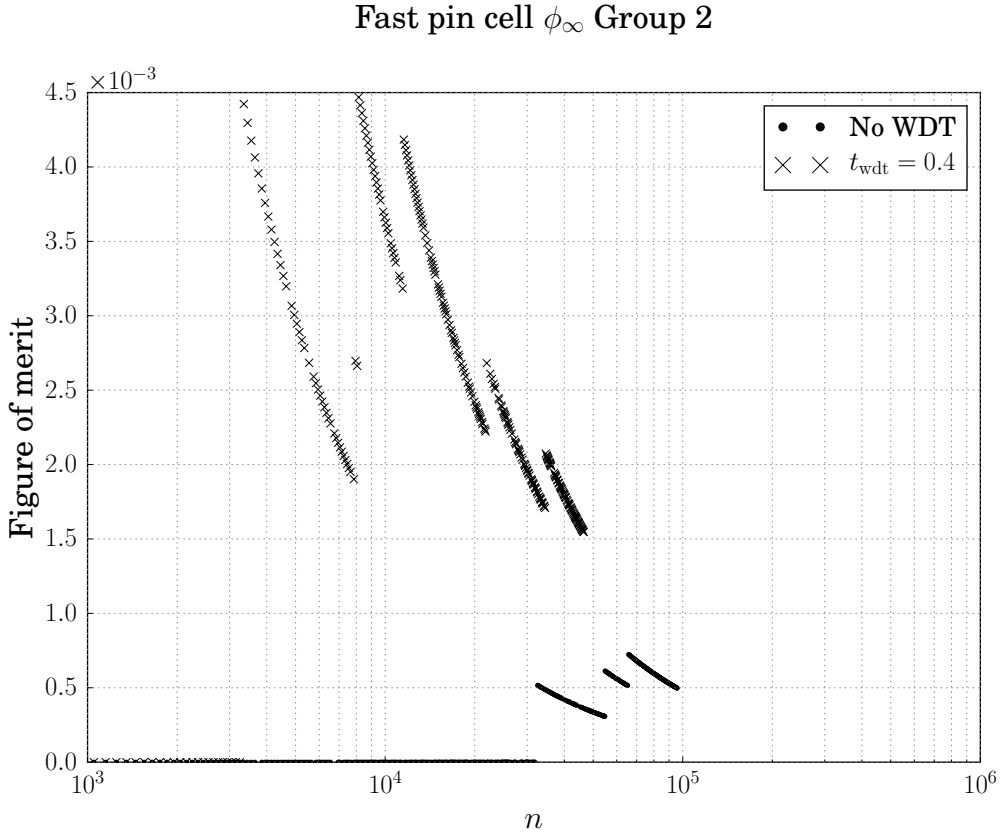

Figure 4.9: FOM convergence for *infinite flux* the base and $t_{\text{wdt}} = 0.4$ case for group 2 in the fast pin cell.

enough statistics for the low energy group to cause the FOM to converge to a high enough value to be significant.

Scattering Matrices

For the two-group case, the scattering matrices for S_0 is again 2×2. A summary of the FOM ratio for the zeroth moment S_0 is shown in Table 4.10. The tables are for the entry in row g and column g', which represents scattering from group g' into group g, indicated as $g' \to g$.

The group 1 inscattering matrix displays good statistics, the other three entries have an extremely low FOM, indicating that there are not enough statistics. The group 1 inscattering FOM ratio is plotted in Fig. 4.12. WDT returns a higher FOM for all values of $t_{\text{wdt}} \geq 0.3$, and close to parity for $t_{\text{wdt}} = 0.2$.

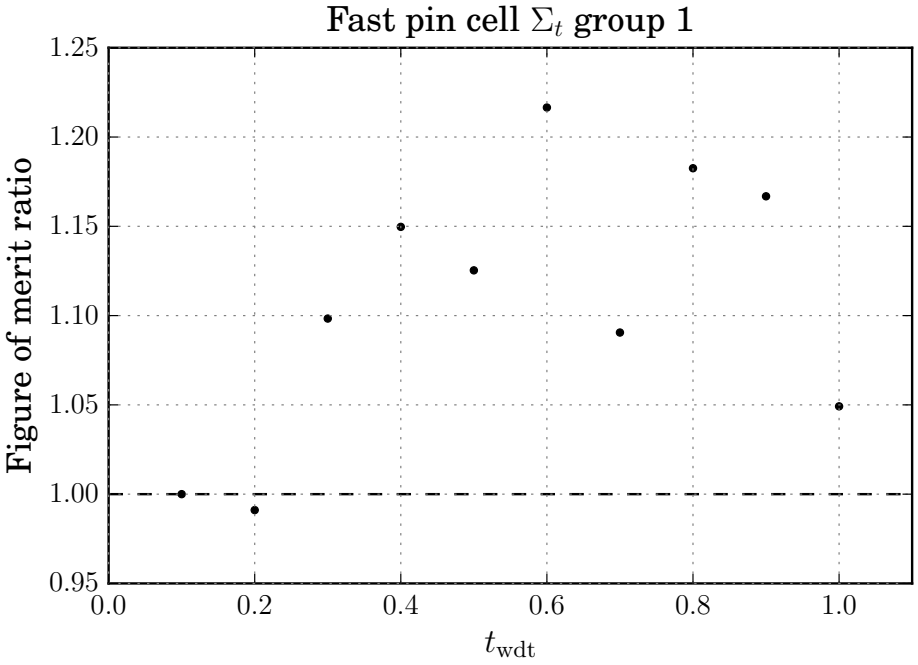

(a)

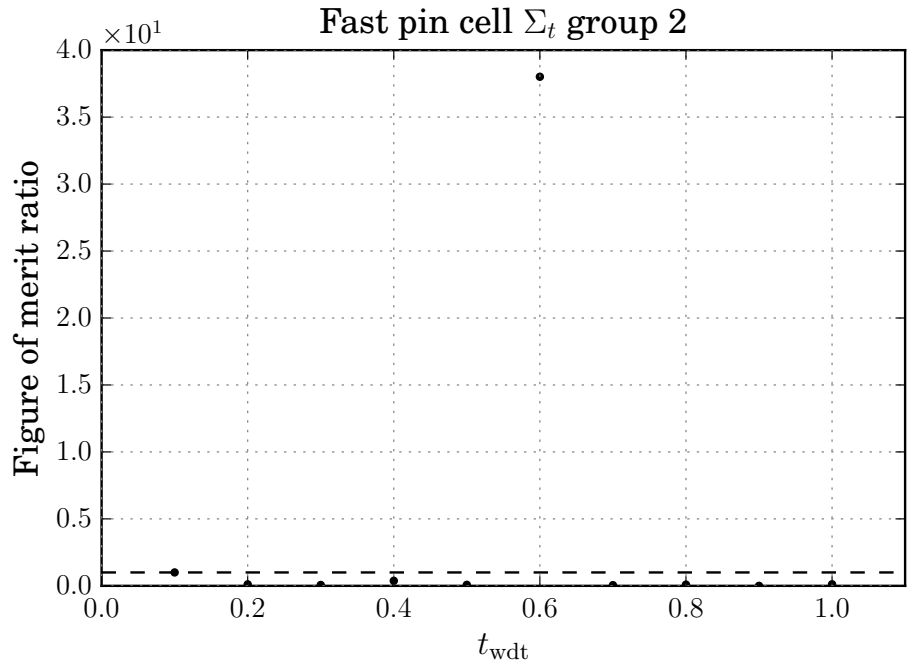

(b)

Figure 4.10: Figure of merit ratio of *infinite total cross-section* for the fast reactor pin cell vs the WDT threshold for (a) fast and (b) thermal groups. The group boundary is at 0.0625 eV. FOM is calculated using the last 20 data points.

Table 4.9: $\overline{\text{FOM}}$ as a function of t_{wdt} and the ratio of values to the base case for the fast reactor pin cell *infinite total cross-section*.

Group 1 ($E > 0.0625$)			Group 2		
t_{wdt}	$\overline{\text{FOM}}$	Ratio	t_{wdt}	$\overline{\text{FOM}}$	Ratio
0.1	1.136275×10^{7}	1.000000	0.1	8.481607×10^{-3}	1.000000
0.2	1.126136×10^{7}	0.991077	0.2	9.381356×10^{-4}	0.110608
0.3	1.248018×10^{7}	1.098342	0.3	5.493018×10^{-4}	0.064764
0.4	1.306365×10^{7}	1.149691	0.4	3.177720×10^{-3}	0.374660
0.5	1.278691×10^{7}	1.125336	0.5	6.372709×10^{-4}	0.075136
0.6	1.382315×10^{7}	1.216532	0.6	3.224228×10^{-1}	38.014350
0.7	1.239126×10^{7}	1.090516	0.7	4.215556×10^{-4}	0.049702
0.8	1.343677×10^{7}	1.182529	0.8	7.736467×10^{-4}	0.091215
0.9	1.325812×10^{7}	1.166806	0.9	0.000000×10^{0}	0.000000
1.0	1.192159×10^{7}	1.049182	1.0	9.794372×10^{-4}	0.115478

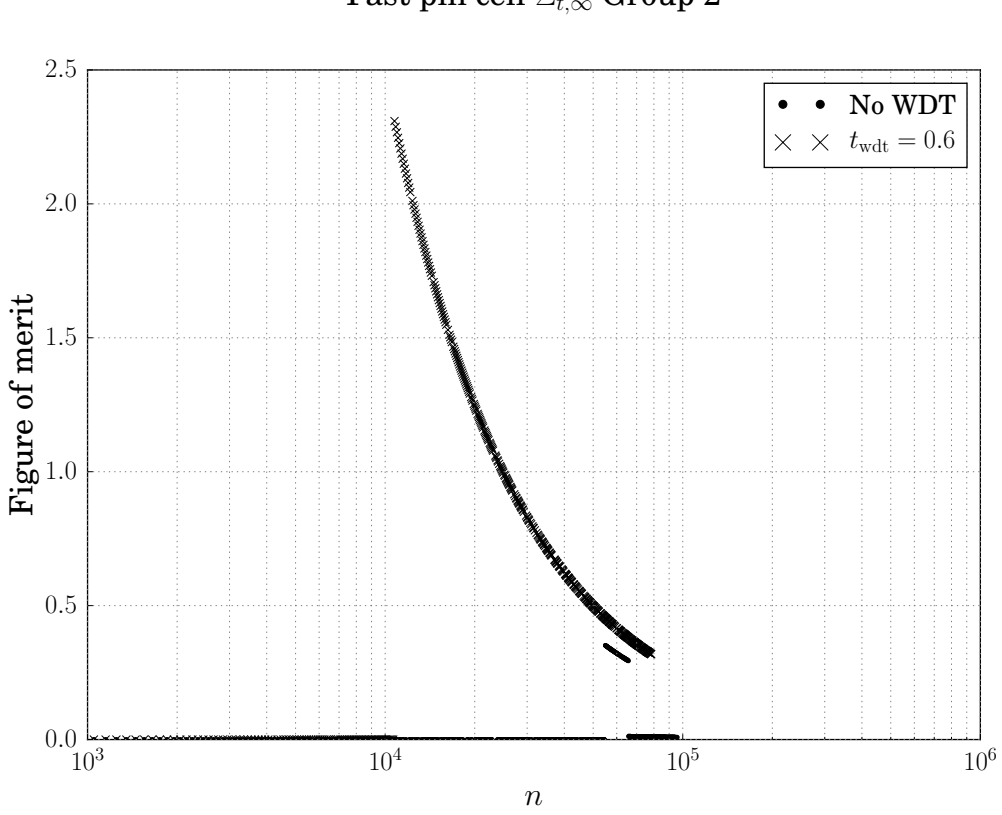

Figure 4.11: FOM convergence for *infinite total cross-section* the base and $t_{\text{wdt}} = 0.6$ case in the fast pin cell.

Table 4.10: $\overline{\text{FOM}}$ as a function of t_{wdt} and the ratio of values to the base case for the fast reactor pin cell *infinite zeroth-moment of the scattering matrix*

$\Sigma_{1\to1}$			$\Sigma_{2\to1}$		
t_{wdt}	$\overline{\text{FOM}}$	Ratio	t_{wdt}	$\overline{\text{FOM}}$	Ratio
0.1	1.025750×10^{7}	1.000000	0.1	0.000000×10^{0}	0.000000
0.2	1.026018×10^{7}	1.000262	0.2	3.461351×10^{-4}	0.000346
0.3	1.140244×10^{7}	1.111619	0.3	2.464090×10^{-4}	0.000246
0.4	1.203271×10^{7}	1.173064	0.4	1.541451×10^{-3}	0.001541
0.5	1.224380×10^{7}	1.193644	0.5	3.324048×10^{-4}	0.000332
0.6	1.375806×10^{7}	1.341268	0.6	0.000000×10^{0}	0.000000
0.7	1.246229×10^{7}	1.214944	0.7	7.124125×10^{-4}	0.000712
0.8	1.356487×10^{7}	1.322435	0.8	3.543062×10^{-4}	0.000354
0.9	1.334051×10^{7}	1.300561	0.9	0.000000×10^{0}	0.000000
1.0	1.221318×10^{7}	1.190659	1.0	6.957632×10^{-4}	0.000696
$\Sigma_{1\to2}$			$\Sigma_{2\to2}$		
t_{wdt}	$\overline{\text{FOM}}$	Ratio	t_{wdt}	$\overline{\text{FOM}}$	Ratio
0.1	0.000000×10^{0}	0.000000	0.1	0.000000×10^{0}	0.000000
0.2	0.000000×10^{0}	0.000000	0.2	6.991410×10^{-4}	0.000699
0.3	0.000000×10^{0}	0.000000	0.3	2.464090×10^{-4}	0.000246
0.4	0.000000×10^{0}	0.000000	0.4	3.295802×10^{-4}	0.000330
0.5	0.000000×10^{0}	0.000000	0.5	0.000000×10^{0}	0.000000
0.6	0.000000×10^{0}	0.000000	0.6	0.000000×10^{0}	0.000000
0.7	0.000000×10^{0}	0.000000	0.7	0.000000×10^{0}	0.000000
0.8	0.000000×10^{0}	0.000000	0.8	3.543062×10^{-4}	0.000354
0.9	0.000000×10^{0}	0.000000	0.9	0.000000×10^{0}	0.000000
1.0	0.000000×10^{0}	0.000000	1.0	2.317413×10^{-4}	0.000232

Discussion

There is very little thermal flux in a fast reactor. This results in poor statistics for that group, a fact that WDT does not remedy. As evidenced by the results presented in this section, all values of t_{wdt} continued to result in group 2 FOM orders of magnitude smaller than both group 1 for this problem, and either group for the PWR.

For the fast group, there is consistent improvement in the FOM for all values of t_{wdt}. The FOM ratio peaks at $t_{\text{wdt}} = 0.6$ for the infinite flux, total cross-section and group 1 inscattering cross-section. This value represents the highest improvement in group 1, and the values are summarized in Tab. 4.11. The values for group 2 are omitted as this value, like all others, did not result in meaningful improvement.

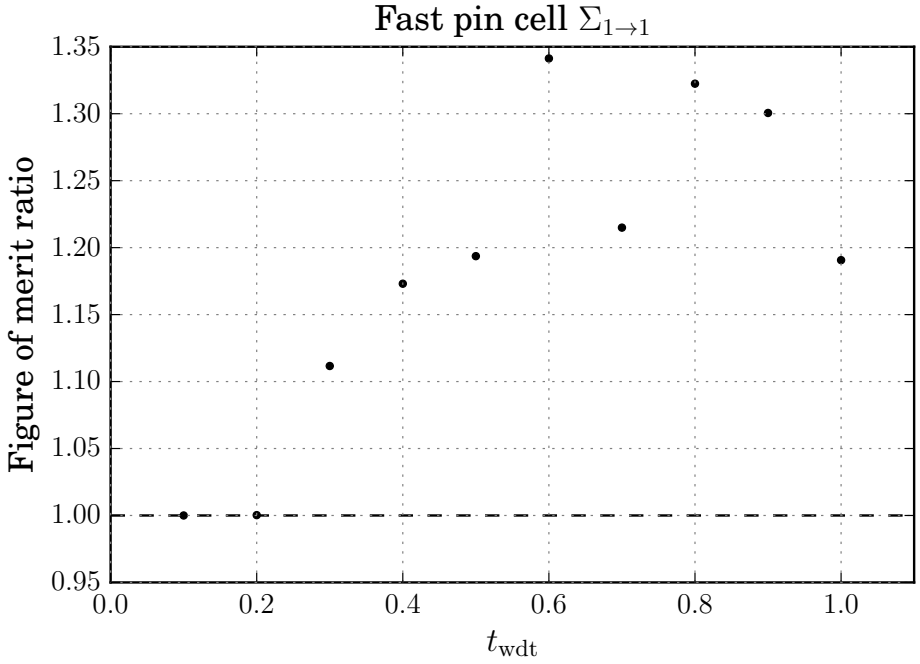

Figure 4.12: Figure of merit ratio of $\Sigma_{1\to1}$ for the fast reactor pin cell. The group boundary is at 0.0625 eV. FOM is calculated using the last 20 data points.

Table 4.11: Summary of FOM ratios for the fast reactor pin cell for $t_{\mathrm{wdt}} = 0.6$.

Parameter	$\overline{\mathbf{FOM}}$ **Ratio**
$\phi_{1,\infty}$	1.360716
$\Sigma_{1,t}$	1.216532
$\Sigma_{1\to1}$	1.341268

4.6 Homogenous fuel element

The third test case is derived from the TREAT reactor at INL. Work at INL focuses on using deterministic solvers to model the core; the Serpent 2 Monte Carlo code is used to generate the cross-sections for these solvers. We used a homogenized fuel element that replicates the material but not geometry of the TREAT fuel. The simulation uses eleven energy groups, which replicates the groups used by the deterministic solvers. This group structure is summarized in Table. 4.12.

To simplify the analysis, and to allow comparison between the other two test cases, these groups can be collapsed. The values we are considering, ϕ_∞, $\Sigma_{t,\infty}$, and the zeroth scattering matrix are all independent measurements with regard to energy. We can sum all the ϕ_∞ for each energy group to get a total ϕ_∞ for the entire energy range. As there is no covariance,

Table 4.12: Energy group structure for the homogenous fuel element.

Group	Upper energy limit (MeV)	Group	Upper energy limit (MeV)
1	20.0000	7	6.25000×10^{-7}
2	3.32870	8	2.09610×10^{-7}
3	1.15620×10^{-1}	9	7.64970×10^{-8}
4	3.48110×10^{-3}	10	4.73020×10^{-8}
5	1.32700×10^{-4}	11	2.00100×10^{-8}
6	8.10003×10^{-6}		

the variance of the sum will be the sum of the variance [8]. The variance for summing energy groups g to g' is therefore:

$$\mathrm{Var}\left(\sum_{j=g}^{g'} \phi_{g,\infty}\right) = \sum_{j=g}^{g'} \mathrm{Var}\left(\phi_{g,\infty}\right) \ .$$

This allows us to collapse groups one through six into a single group, hereafter denoted by an f for fast, and groups seven through eleven as a thermal group, t. The boundary of group seven aligns with the separation of the two groups in the previous test problems, so we can compare the results in a more natural fashion. Fig. 4.13 shows the FOM convergence for the combined fast group. As expected, the combined group shows the same convergence characteristic as the single groups.

Infinite flux

A summary of the FOM ratio and $\overline{\mathrm{FOM}}(t_{\mathrm{wdt}})$, for the homogenous fuel element for infinite flux (ϕ_∞) is shown in Tab. 4.13 and shown graphically in Fig. 4.14. The Tables for all eleven of the original energy groups are included in App. A.1.

As shown in both the table and plot, we observe an improvement in FOM for WDT threshold values $0.2 \leq t_{\mathrm{wdt}} \leq 0.6$ and $t_{\mathrm{wdt}} = 0.8, 1.0$ for the fast group. The improvement is moderate for this group, with a maximum improvement of 1.07 times the base case. The improvements are even slighter for the thermal group, where we observe a maximum of 1.014 times the base case for $0.4 \leq t_{\mathrm{wdt}} 0.6$ and $t_{\mathrm{wdt}} = 1.0$.

Infinite total cross-section

A summary of the FOM ratio and $\overline{\mathrm{FOM}}(t_{\mathrm{wdt}})$, for the homogeneous fuel element infinite total cross-section is shown in Tab. 4.14 and shown graphically in Fig. 4.15. The full data for all eleven groups is included in App. A.2.

For both groups, the WDT method underperforms the base case in all but a few select cases. Where it performs better, we observe a very moderate improvement in FOM, with the only shared improvement in both groups at $t_{\mathrm{wdt}} = 0.7$.

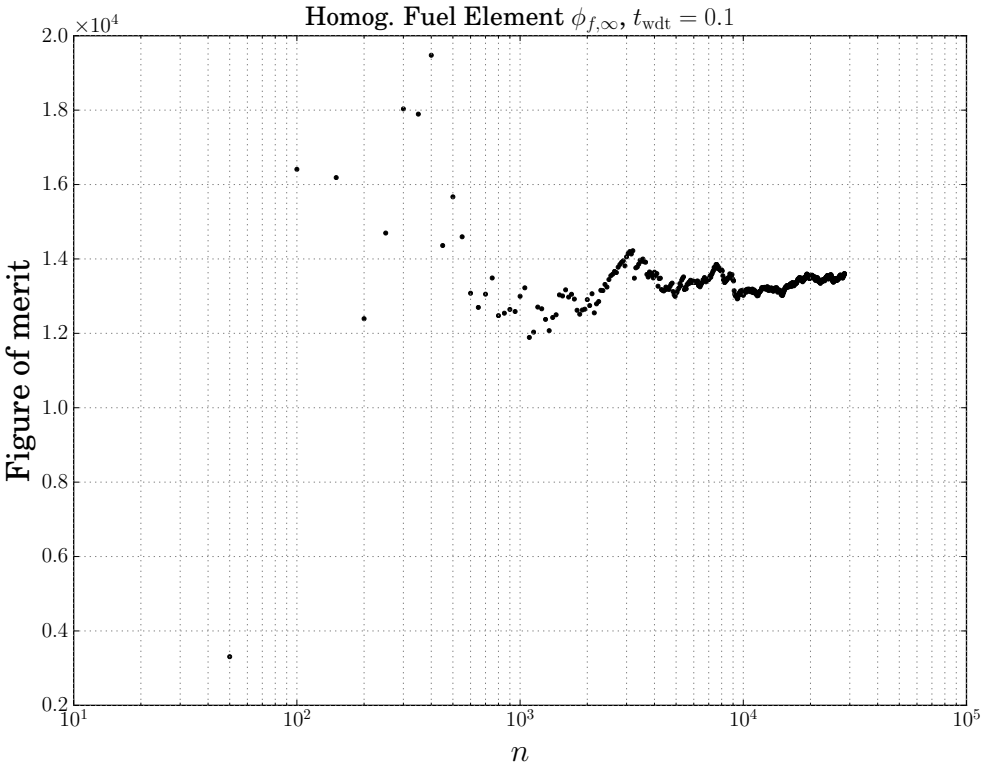

Figure 4.13: Convergence of *infinite flux* for the combined fast group for the homogenous fuel element for the base case $t_{\text{wdt}} = 0.1$.

Table 4.13: $\overline{\text{FOM}}$ as a function of t_{wdt} and the ratio of values to the base case for the homogenous fuel element *infinte flux*.

Fast Group ($E > 0.0625$)			Thermal Group		
t_{wdt}	$\overline{\text{FOM}}$	Ratio	t_{wdt}	$\overline{\text{FOM}}$	Ratio
0.1	1.354229×10^4	1.000000	0.1	3.309991×10^4	1.000000
0.2	1.373594×10^4	1.014299	0.2	3.189448×10^4	0.963582
0.3	1.409053×10^4	1.040483	0.3	3.189179×10^4	0.963501
0.4	1.444534×10^4	1.066684	0.4	3.338953×10^4	1.008750
0.5	1.398881×10^4	1.032972	0.5	3.355018×10^4	1.013604
0.6	1.372165×10^4	1.013244	0.6	3.338649×10^4	1.008658
0.7	1.341316×10^4	0.990465	0.7	3.271800×10^4	0.988462
0.8	1.359856×10^4	1.004155	0.8	3.202989×10^4	0.967673
0.9	1.347952×10^4	0.995365	0.9	3.283915×10^4	0.992122
1.0	1.433894×10^4	1.058826	1.0	3.332469×10^4	1.006791

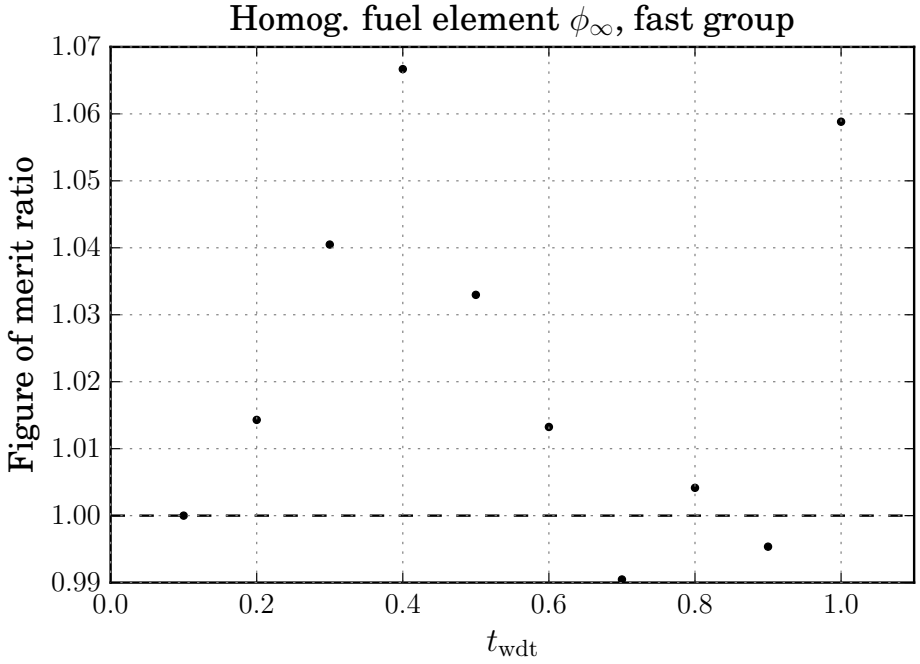

(a)

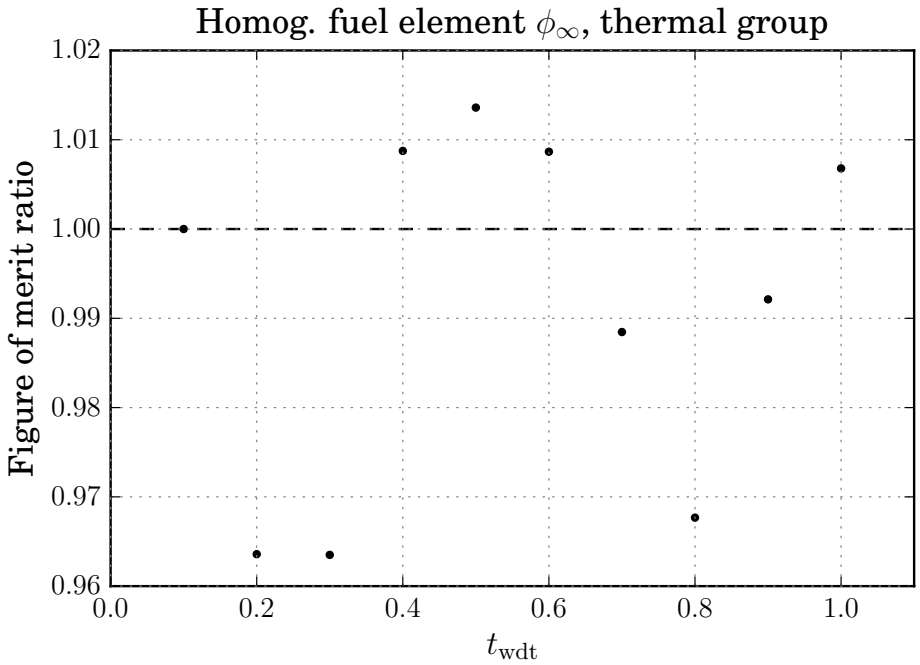

(b)

Figure 4.14: Figure of merit ratio of the *infinte flux* for the homogeneous fuel element vs the WDT threshold for the (a) fast and (b) thermal groups. The group boundary is at 0.0625 eV. FOM is calculated using the last 20 data points.

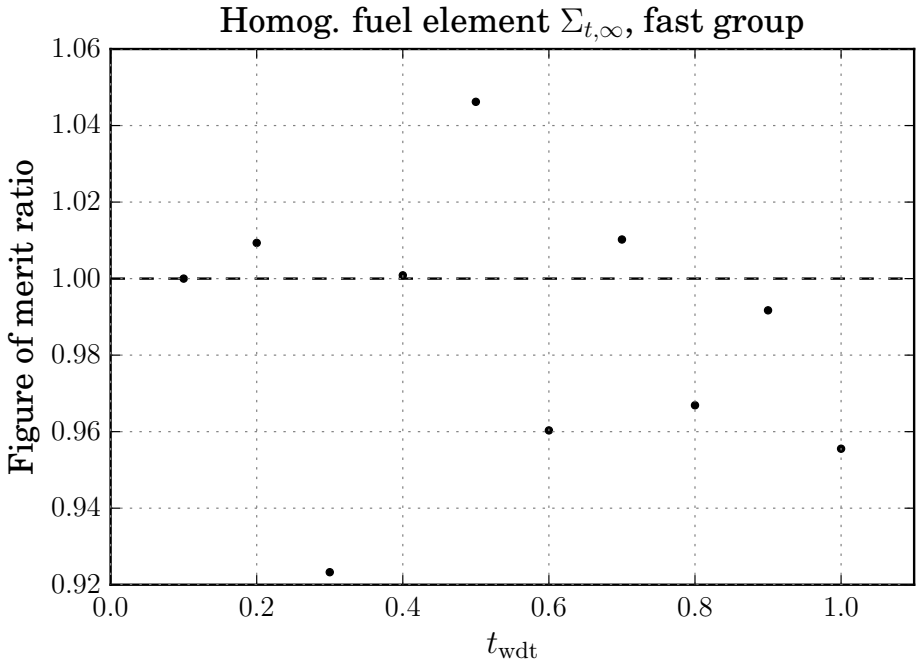

(a)

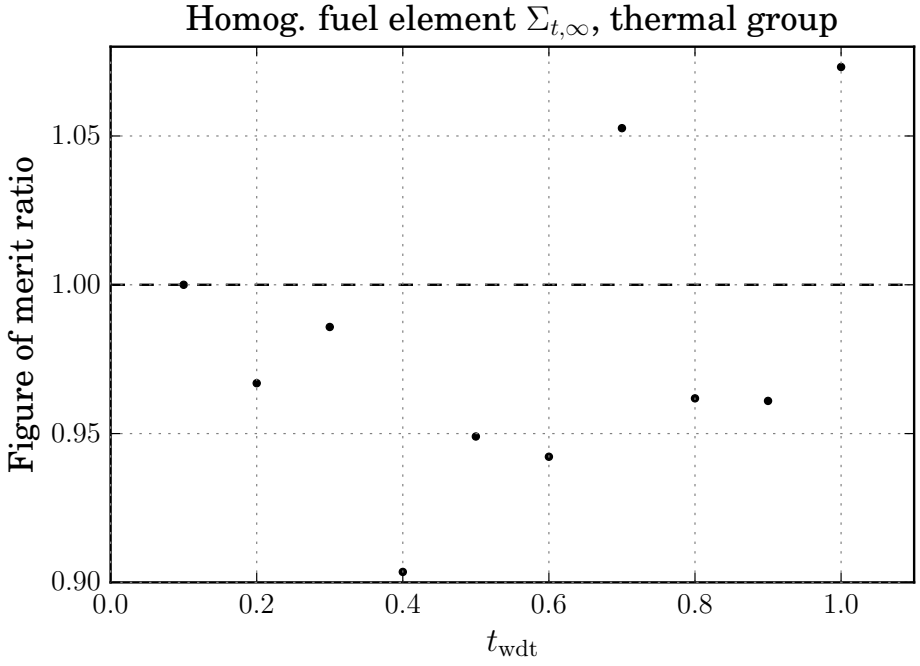

(b)

Figure 4.15: Figure of merit ratio of *infinite total cross-section* for the homogeneous fuel element vs the WDT threshold for (a) fast group and (b) thermal group. The group boundary is at 0.0625 eV. FOM is calculated using the last 20 data points.

Table 4.14: $\overline{\text{FOM}}$ as a function of t_{wdt} and the ratio of values to the base case for the homogeneous fuel element *infinite total cross-section*.

Fast group ($E > 0.0625$)			Thermal group		
t_{wdt}	$\overline{\text{FOM}}$	Ratio	t_{wdt}	$\overline{\text{FOM}}$	Ratio
0.1	4.126523×10^5	1.000000	0.1	2.319708×10^6	1.000000
0.2	4.165034×10^5	1.009333	0.2	2.242986×10^6	0.966926
0.3	3.809894×10^5	0.923270	0.3	2.286812×10^6	0.985819
0.4	4.130063×10^5	1.000858	0.4	2.095885×10^6	0.903513
0.5	4.317179×10^5	1.046202	0.5	2.201446×10^6	0.949019
0.6	3.962803×10^5	0.960325	0.6	2.185670×10^6	0.942218
0.7	4.168695×10^5	1.010220	0.7	2.441790×10^6	1.052628
0.8	3.989894×10^5	0.966890	0.8	2.231177×10^6	0.961836
0.9	4.092305×10^5	0.991708	0.9	2.229192×10^6	0.960980
1.0	3.943059×10^5	0.955540	1.0	2.489455×10^6	1.073176

Scattering Matrices

For the eleven-group case, the scattering matrices for the zeroth moment is 11×11. All the tables showing the FOM ratios for each value of the WDT threshold are shown in App. A.3. The tables are for the entry in row g and column g', which represents scattering from group g' into group g, indicated as $g' \to g$. Collapsing the groups for comparison can not be done in this case, as the FOM is so low in many of the matrix entries that it dominates the value of the FOM. Instead, we have created matrix maps that show the FOM ratios when WDT is used. These maps are included in App. A.3.

A characteristic map is shown in Fig. 4.16, for $t_{\text{wdt}} = 0.2$. The trend we observe in these images is a slight deviation from unity in most entries, indicating a moderate improvement or reduction in the FOM. In only three cases did the use of WDT populate an entry in the matrix where the base case did not. In each of these cases, the FOM remains very low, on the order of 10^{-4}. There is some improvement in the scattering entries for group five into higher energy groups, $\Sigma_{5\to1}, \Sigma_{5\to2}$, and $\Sigma_{5\to1}$. This improvement is higher in lower values of t_{wdt}.

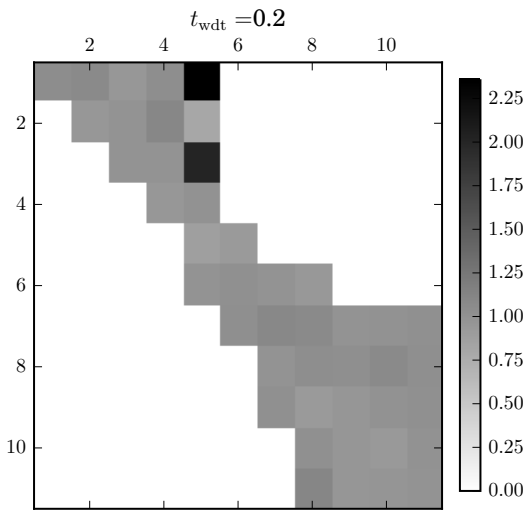

Figure 4.16: Matrix image for the *infinite zeroth-moment of the scattering cross-section* for the homogeneous fuel element for $t_{\mathrm{wdt}} = 0.2$.

Discussion

There is no clear WDT threshold value that creates an overall improvement in the parameters we studied. The results of the infinite flux show an improvement in most cases for the fast flux, and a moderate improvement for thermal flux, for $0.4 \leq t_{\mathrm{wdt}} \leq 0.6$ and unity. For the infinite total cross-section, improvement in the thermal group only occurs for two values, $t_{\mathrm{wdt}} = 0.7, 1.0$. We also observe improvement in the fast group total cross-section for $t_{\mathrm{wdt}} = 0.7$. The scattering matrices show similar patterns for all values of the WDT threshold. The original use of the homogeneous fuel element by INL is for the development of cross-sections. Based on this intent, a threshold value of $t_{\mathrm{wdt}} = 0.7$ will return improvements in both total cross-section and the zeroth order scattering matrix, and near parity with the FOM of the base case for flux. The ratios for this parameter are summarized in Fig. 4.17.

$t_{\text{wdt}} = 0.7$

Parameter	$\overline{\text{FOM}}$ Ratio
$\phi_{f,\infty}$	0.990465
$\phi_{s,\infty}$	0.988462
$\Sigma_{f,t}$	1.010220
$\Sigma_{s,t}$	1.052628

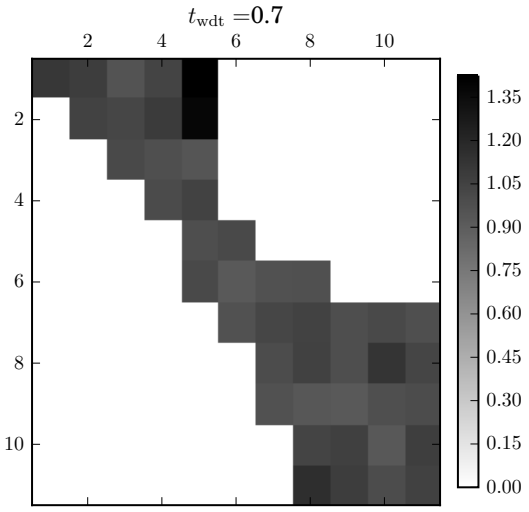

Figure 4.17: Summary of the data for the homogeneous fuel element for $t_{\text{wdt}} = 0.7$.

Chapter 5

Conclusions and Future Work

Monte Carlo codes are an invaluable tool when modeling neutron propagation. Our finite computing resources demand more efficient algorithms for more complex geometries and problems. One such algorithm with promising results is WDT. In this manuscript we have presented an extension of this method to include scattering. In this section, we will discuss the conclusions that can be drawn from the three test cases presented.

5.1 Summary of results

For each test case, we examined three parameters: the infinite flux, the total cross-section, and the scattering matrix for the zeroth scattering moment. For the PWR pin cell, we observed improvements in the FOM for the thermal group in all three parameters studied. A similar improvement was seen in the fast group for the fast reactor pin cell. There is no indication of a clear trend for the homogeneous fuel element.

Use of the WDT method improved the FOM for the PWR and fast reactor pin cells in the groups that experience the most absorption events. That is, the thermal group for the PWR and the fast group for the fast reactor. This is consistent with what we expect from using the WDT routine. With the original delta-tracking routine, collisions that may result in absorption may be discarded as virtual and therefore never scored. The WDT routine scores every collisions that results in absorption and reduces the weight as necessary. This is a more efficient routine in energy regions where absorption events are occurring at a high rate. The additional scoring of absorption events improves the FOM for the total cross-section; by not killing the neutrons at these events, the FOM for flux is improved by survival biasing.

In regions where a large amount of scattering occurs, the routine is slightly less efficient. Instead of rejecting virtual collisions outright, the rejection occurs after sampling the type of collision. We observe the impact of this inefficiency in energy regions where scattering dominates. The total cross-section and the scattering matrix entries for the PWR fast group both under perform standard delta-tracking. The large amount of graphite in the homogeneous fuel element makes it a highly scattering environment, which may explain the

under-performance in total cross-section of WDT in most cases.

We provide specific recommended values for the WDT threshold in the sections dedicated to the test cases. Overall, the method provides some improvement in the FOM in circumstances where there is a large amount of absorption, in line with what is expected of the method.

5.2 Future Work

There is still a large amount of work to assess the usefulness and performance of this method. Based on the results of this study, we should assess test cases that have geometrically small regions of high absorption, such as control rods. Also, test cases where delta-tracking does not perform well, such as Tristructural-isotropic (TRISO) particles, should be analyzed. In addition to more test cases, adjusting the upper boundary for ray tracing (see Fig. 3.2) should be analyzed. WDT may outperform ray tracing in some regions of very low real collision probability. An expanded parametric study of the WDT threshold should be performed to investigate if the general trend observed here holds. Such a study should include both a finer examination of the WDT threshold value, and examination of other output parameters of interest.

5.3 Conclusion

In this manuscript, we have sought to determine the usefulness of the WDT method. We discussed the background of the Monte Carlo simulation and how it is applied to neutral particle propagation. We introduced Woodcock delta-tracking as a method to improve the simulation in geometrically complex region. This algorithm was modified by a recently introduced method, weighted delta-tracking, which replaced some virtual collisions with a weight reduction. We then extended the method from considering only absorption events to include scattering events. Finally, we examined three parameters of interest from three test cases to assess the usefulness of WDT and determine a preferred threshold value for use of the algorithm. The FOM improvements are in line with what was expected of the WDT method. The suggested future work should improve our understanding of the impact of the method, and provide more robust recommendations for future simulations.

Bibliography

[1] E. E. Lewis and W.F. Miller, Jr. *Computational Methods of Neutron Transport*. American Nuclear Society, 1993.

[2] Derek Gaston, Chris Newman, Glen Hansen, and Damien Lebrun-Grandi. Moose: A parallel computational framework for coupled systems of nonlinear equations. *Nuclear Engineering and Design*, 239(10):1768 – 1778, 2009.

[3] Idaho National Laboratory. Transient Reactor Test Facility. `http://www4vip.inl.gov/research/transient-reactor-test-facility/`. Accessed: 2017 April 27.

[4] J. Leppänen. *Development of a New Monte Carlo Reactor Physics Code*. PhD thesis, Helsinki University of Technology, 2007.

[5] Jaakko Leppänen. Performance of Woodcock delta-tracking in lattice physics applications using the Serpent Monte Carlo reactor physics burnup calculation code. *Annals of Nuclear Energy*, 37:715–722, 2010.

[6] Jaakko Leppänen. Modeling of Nonuniform Density Distributions in the Serpent 2 Monte Carlo Code. *Nuclear Science and Engineering*, 174:318–325, 2013.

[7] Jaakko Leppänen. *Serpent – A Continuous-energy Monte Carlo Reactor Physics Burnup Calculation Code – User's Manual*, June 2015.

[8] John. R. Taylor. *An Introduction to Error Analysis*. University Science Books, Second edition, 1997.

[9] Iván Lux and László Koblinger. *Monte Carlo Particle Transport Methods: Neutron and Photon Calculations*. CRC Press, 1991.

[10] L.W.G. Morgan and D. Kotlyar. Weighted-delta-tracking for Monte Carlo particle transport. *Annals of Nuclear Energy*, 85:1184–1188, 2015.

[11] N. Metropolis and S. Ulam. The Monte Carlo Method. *Journal of the American Statistical Association*, 44(247):335–341, 1949.

[12] J. Ortensi et al. Updates to the Generation of Physics Data Inputs for MAMMOTH Simulations of the Transient Reactor Test Facility. Technical Report INL/EXT-16-39120, Idaho National Laboratory, June 2016.

[13] Toni Kaltiaisenaho. Statistical Tests and the Underestimation of Variance in Serpent 2. Technical Report VTT-R-00371-14, VTT Technical Research Centre of Finland, 2014.

[14] VTT Technical Research Centre of Finland. VTT Serpent. `http://montecarlo.vtt.fi/`. Accessed: 2017 April 18.

[15] E.R Woodcock et al. Techniques used in the GEM code for Monte Carlo neutronics calculations in reactors and other systems of complex geometry. *ANL-7050. Argonne National Laboratory.*, 1965.

Appendix A

Supplemental Data

The homogenous fuel element simulations used eleven energy groups. Printing all the data tables in the main body of the report is therefore unsuitable. The full data is presented here and available at the following link: `https://github.com/jsrehak/wdt_data/`

A.1 Infinite flux

Group 1

t_{wdt}	$\overline{\text{FOM}}$	Ratio
0.1	2.019388×10^{4}	1.000000
0.2	2.087831×10^{4}	1.033893
0.3	2.205485×10^{4}	1.092155
0.4	2.190425×10^{4}	1.084697
0.5	2.123522×10^{4}	1.051567
0.6	2.074022×10^{4}	1.027055
0.7	2.038235×10^{4}	1.009333
0.8	2.059303×10^{4}	1.019766
0.9	2.055086×10^{4}	1.017678
1.0	2.179478×10^{4}	1.079276

Group 2

t_{wdt}	$\overline{\text{FOM}}$	Ratio
0.1	1.774919×10^{5}	1.000000
0.2	1.765739×10^{5}	0.994828
0.3	1.740788×10^{5}	0.980770
0.4	1.843099×10^{5}	1.038413
0.5	1.775834×10^{5}	1.000516
0.6	1.775154×10^{5}	1.000132
0.7	1.726067×10^{5}	0.972476
0.8	1.751299×10^{5}	0.986692
0.9	1.691347×10^{5}	0.952915
1.0	1.879980×10^{5}	1.059192

Group 3

t_{wdt}	$\overline{\text{FOM}}$	Ratio
0.1	2.114826×10^{5}	1.000000
0.2	2.081977×10^{5}	0.984467
0.3	1.999475×10^{5}	0.945456
0.4	2.165336×10^{5}	1.023883
0.5	2.118403×10^{5}	1.001691
0.6	2.075683×10^{5}	0.981491
0.7	1.978024×10^{5}	0.935313
0.8	2.050604×10^{5}	0.969632
0.9	2.021991×10^{5}	0.956102
1.0	2.143964×10^{5}	1.013778

Group 4

t_{wdt}	$\overline{\text{FOM}}$	Ratio
0.1	2.097343×10^{5}	1.000000
0.2	2.066983×10^{5}	0.985525
0.3	2.000209×10^{5}	0.953687
0.4	2.176038×10^{5}	1.037522
0.5	2.117824×10^{5}	1.009766
0.6	2.061082×10^{5}	0.982711
0.7	2.037317×10^{5}	0.971380
0.8	2.084075×10^{5}	0.993674
0.9	2.057834×10^{5}	0.981162
1.0	2.109260×10^{5}	1.005682

Group 5

t_{wdt}	$\overline{\text{FOM}}$	Ratio
0.1	2.166128×10^{5}	1.000000
0.2	2.076210×10^{5}	0.958489
0.3	2.036029×10^{5}	0.939939
0.4	2.235133×10^{5}	1.031856
0.5	2.169855×10^{5}	1.001721
0.6	2.171284×10^{5}	1.002380
0.7	2.056187×10^{5}	0.949246
0.8	2.116409×10^{5}	0.977047
0.9	2.043084×10^{5}	0.943196
1.0	2.185315×10^{5}	1.008858

Group 6

t_{wdt}	$\overline{\text{FOM}}$	Ratio
0.1	2.185522×10^{5}	1.000000
0.2	2.090350×10^{5}	0.956453
0.3	2.012707×10^{5}	0.920927
0.4	2.242333×10^{5}	1.025994
0.5	2.122290×10^{5}	0.971068
0.6	2.103669×10^{5}	0.962547
0.7	2.053113×10^{5}	0.939415
0.8	2.054663×10^{5}	0.940125
0.9	2.034723×10^{5}	0.931001
1.0	2.195021×10^{5}	1.004346

Group 7

t_{wdt}	$\overline{\text{FOM}}$	Ratio
0.1	1.733678×10^{5}	1.000000
0.2	1.716411×10^{5}	0.990040
0.3	1.562465×10^{5}	0.901243
0.4	1.727754×10^{5}	0.996583
0.5	1.724759×10^{5}	0.994855
0.6	1.827056×10^{5}	1.053861
0.7	1.697682×10^{5}	0.979237
0.8	1.688477×10^{5}	0.973928
0.9	1.570857×10^{5}	0.906084
1.0	1.811281×10^{5}	1.044762

Group 8

t_{wdt}	$\overline{\text{FOM}}$	Ratio
0.1	2.533797×10^{5}	1.000000
0.2	2.415113×10^{5}	0.953160
0.3	2.493818×10^{5}	0.984222
0.4	2.646405×10^{5}	1.044443
0.5	2.550511×10^{5}	1.006596
0.6	2.652686×10^{5}	1.046921
0.7	2.548080×10^{5}	1.005637
0.8	2.368751×10^{5}	0.934862
0.9	2.634792×10^{5}	1.039859
1.0	2.545598×10^{5}	1.004658

Group 9

t_{wdt}	$\overline{\text{FOM}}$	Ratio
0.1	2.540478×10^{5}	1.000000
0.2	2.397671×10^{5}	0.943787
0.3	2.743308×10^{5}	1.079839
0.4	2.425684×10^{5}	0.954814
0.5	2.476198×10^{5}	0.974698
0.6	2.470087×10^{5}	0.972292
0.7	2.423236×10^{5}	0.953850
0.8	2.442812×10^{5}	0.961556
0.9	2.385152×10^{5}	0.938859
1.0	2.590934×10^{5}	1.019861

Group 10

t_{wdt}	$\overline{\text{FOM}}$	Ratio
0.1	2.930673×10^{5}	1.000000
0.2	2.772969×10^{5}	0.946188
0.3	2.843738×10^{5}	0.970336
0.4	2.808419×10^{5}	0.958284
0.5	3.066155×10^{5}	1.046229
0.6	2.868658×10^{5}	0.978839
0.7	2.876251×10^{5}	0.981430
0.8	2.806107×10^{5}	0.957496
0.9	2.897539×10^{5}	0.988694
1.0	2.878323×10^{5}	0.982137

Group 11

t_{wdt}	$\overline{\text{FOM}}$	Ratio
0.1	7.605590×10^{4}	1.000000
0.2	7.347728×10^{4}	0.966096
0.3	7.255308×10^{4}	0.953944
0.4	7.874324×10^{4}	1.035334
0.5	7.820177×10^{4}	1.028214
0.6	7.590409×10^{4}	0.998004
0.7	7.607182×10^{4}	1.000209
0.8	7.451932×10^{4}	0.979797
0.9	7.907545×10^{4}	1.039702
1.0	7.561979×10^{4}	0.994266

A.2 Infinite Total Cross-section

Group 1

t_{wdt}	$\overline{\text{FOM}}$	Ratio
0.1	4.245628×10^{5}	1.000000
0.2	4.291756×10^{5}	1.010865
0.3	3.916833×10^{5}	0.922557
0.4	4.259831×10^{5}	1.003345
0.5	4.448467×10^{5}	1.047776
0.6	4.074488×10^{5}	0.959690
0.7	4.285585×10^{5}	1.009411
0.8	4.105363×10^{5}	0.966962
0.9	4.214023×10^{5}	0.992556
1.0	4.047438×10^{5}	0.953319

Group 2

t_{wdt}	$\overline{\text{FOM}}$	Ratio
0.1	1.472014×10^{7}	1.000000
0.2	1.411534×10^{7}	0.958914
0.3	1.396493×10^{7}	0.948696
0.4	1.356688×10^{7}	0.921654
0.5	1.463783×10^{7}	0.994408
0.6	1.446779×10^{7}	0.982857
0.7	1.529469×10^{7}	1.039032
0.8	1.419543×10^{7}	0.964354
0.9	1.417871×10^{7}	0.963218
1.0	1.530251×10^{7}	1.039563

Group 3

t_{wdt}	$\overline{\text{FOM}}$	Ratio
0.1	2.198392×10^{10}	1.000000
0.2	2.283128×10^{10}	1.038545
0.3	2.195712×10^{10}	0.998781
0.4	2.146297×10^{10}	0.976303
0.5	2.338404×10^{10}	1.063688
0.6	2.240864×10^{10}	1.019320
0.7	2.345928×10^{10}	1.067111
0.8	2.192610×10^{10}	0.997370
0.9	2.078125×10^{10}	0.945293
1.0	2.309154×10^{10}	1.050383

Group 4

t_{wdt}	$\overline{\text{FOM}}$	Ratio
0.1	6.333824×10^{12}	1.000000
0.2	6.458797×10^{12}	1.019731
0.3	6.216834×10^{12}	0.981529
0.4	5.526360×10^{12}	0.872516
0.5	5.782943×10^{12}	0.913026
0.6	5.797261×10^{12}	0.915286
0.7	6.077155×10^{12}	0.959477
0.8	5.489190×10^{12}	0.866647
0.9	6.158502×10^{12}	0.972320
1.0	6.366220×10^{12}	1.005115

Group 5

t_{wdt}	$\overline{\text{FOM}}$	Ratio
0.1	4.652806×10^{11}	1.000000
0.2	4.630314×10^{11}	0.995166
0.3	4.305620×10^{11}	0.925381
0.4	4.280594×10^{11}	0.920003
0.5	4.544255×10^{11}	0.976670
0.6	4.376907×10^{11}	0.940703
0.7	4.192692×10^{11}	0.901111
0.8	4.273831×10^{11}	0.918549
0.9	4.652329×10^{11}	0.999897
1.0	4.652215×10^{11}	0.999873

Group 6

t_{wdt}	$\overline{\text{FOM}}$	Ratio
0.1	1.661085×10^{12}	1.000000
0.2	1.672770×10^{12}	1.007035
0.3	1.642196×10^{12}	0.988629
0.4	1.755438×10^{12}	1.056803
0.5	1.777644×10^{12}	1.070170
0.6	1.959100×10^{12}	1.179410
0.7	1.736168×10^{12}	1.045202
0.8	1.678525×10^{12}	1.010499
0.9	1.650555×10^{12}	0.993661
1.0	1.705421×10^{12}	1.026691

Group 7

t_{wdt}	$\overline{\text{FOM}}$	Ratio
0.1	1.618585×10^{11}	1.000000
0.2	1.546468×10^{11}	0.955445
0.3	1.529810×10^{11}	0.945153
0.4	1.482051×10^{11}	0.915647
0.5	1.562765×10^{11}	0.965513
0.6	1.503759×10^{11}	0.929058
0.7	1.642619×10^{11}	1.014849
0.8	1.465081×10^{11}	0.905162
0.9	1.633805×10^{11}	1.009404
1.0	1.599234×10^{11}	0.988045

Group 8

t_{wdt}	$\overline{\text{FOM}}$	Ratio
0.1	6.592099×10^{9}	1.000000
0.2	6.787996×10^{9}	1.029717
0.3	6.393179×10^{9}	0.969824
0.4	6.456111×10^{9}	0.979371
0.5	6.616259×10^{9}	1.003665
0.6	6.581349×10^{9}	0.998369
0.7	7.076784×10^{9}	1.073525
0.8	6.605516×10^{9}	1.002035
0.9	6.917757×10^{9}	1.049401
1.0	6.759434×10^{9}	1.025384

Group 9

t_{wdt}	$\overline{\text{FOM}}$	Ratio
0.1	6.735651×10^{8}	1.000000
0.2	6.500143×10^{8}	0.965036
0.3	6.422513×10^{8}	0.953510
0.4	6.533642×10^{8}	0.970009
0.5	6.615221×10^{8}	0.982120
0.6	6.693891×10^{8}	0.993800
0.7	6.922352×10^{8}	1.027718
0.8	6.658832×10^{8}	0.988595
0.9	7.225002×10^{8}	1.072651
1.0	6.866421×10^{8}	1.019414

Group 10

t_{wdt}	$\overline{\text{FOM}}$	Ratio
0.1	7.414966×10^{7}	1.000000
0.2	7.338848×10^{7}	0.989735
0.3	7.587417×10^{7}	1.023257
0.4	6.900917×10^{7}	0.930674
0.5	7.391399×10^{7}	0.996822
0.6	6.898857×10^{7}	0.930396
0.7	7.247328×10^{7}	0.977392
0.8	6.661034×10^{7}	0.898323
0.9	7.211591×10^{7}	0.972572
1.0	6.727716×10^{7}	0.907316

Group 11

t_{wdt}	$\overline{\text{FOM}}$	Ratio
0.1	2.404077×10^{6}	1.000000
0.2	2.322796×10^{6}	0.966190
0.3	2.367484×10^{6}	0.984779
0.4	2.169470×10^{6}	0.902413
0.5	2.277654×10^{6}	0.947413
0.6	2.265634×10^{6}	0.942413
0.7	2.537135×10^{6}	1.055347
0.8	2.317384×10^{6}	0.963939
0.9	2.308447×10^{6}	0.960221
1.0	2.595931×10^{6}	1.079803

A.3 Infinite zeroth scattering moment cross-section

Matrix images

Matrices include the ratio of the FOM for the shown WDT threshold parameter. Values in tables are shown when the FOM for the base case is zero.

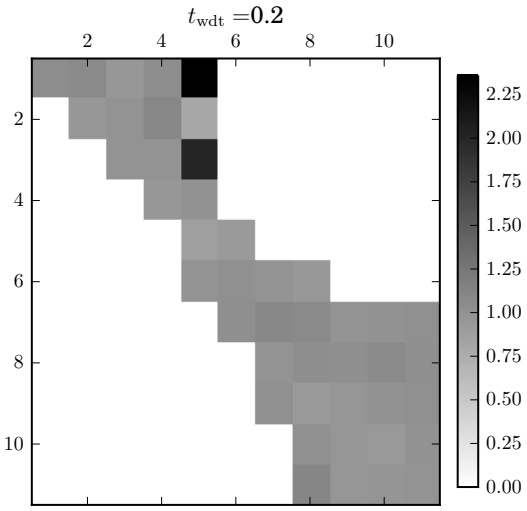

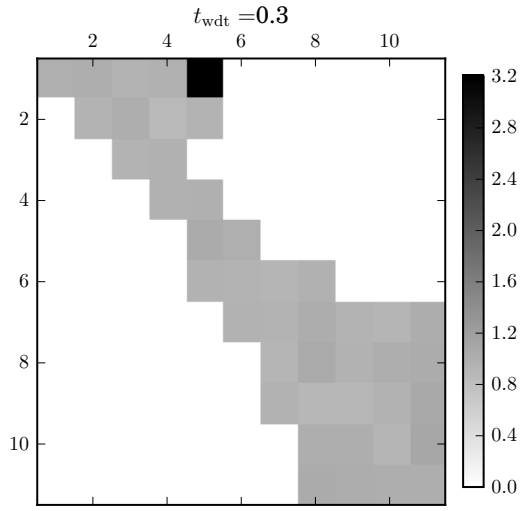

Entry	$\overline{\text{FOM}}$
(7→10)	2.541551×10^{-4}

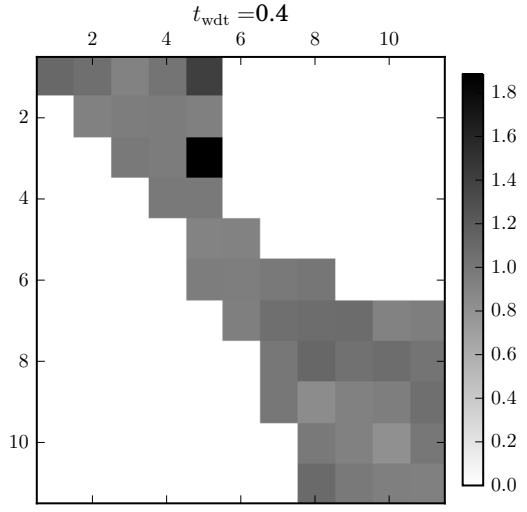

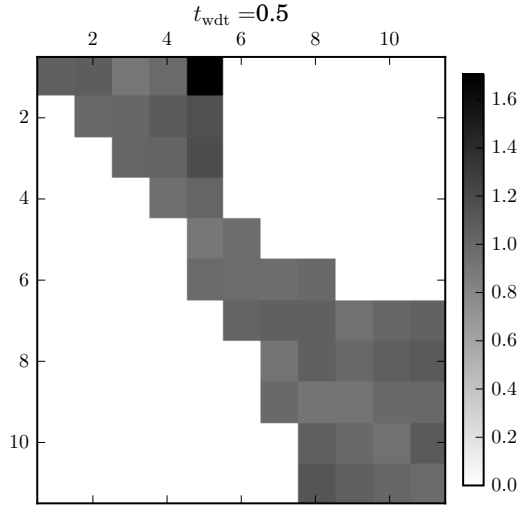

Entry	$\overline{\text{FOM}}$
(6→1)	3.679430×10^{-4}

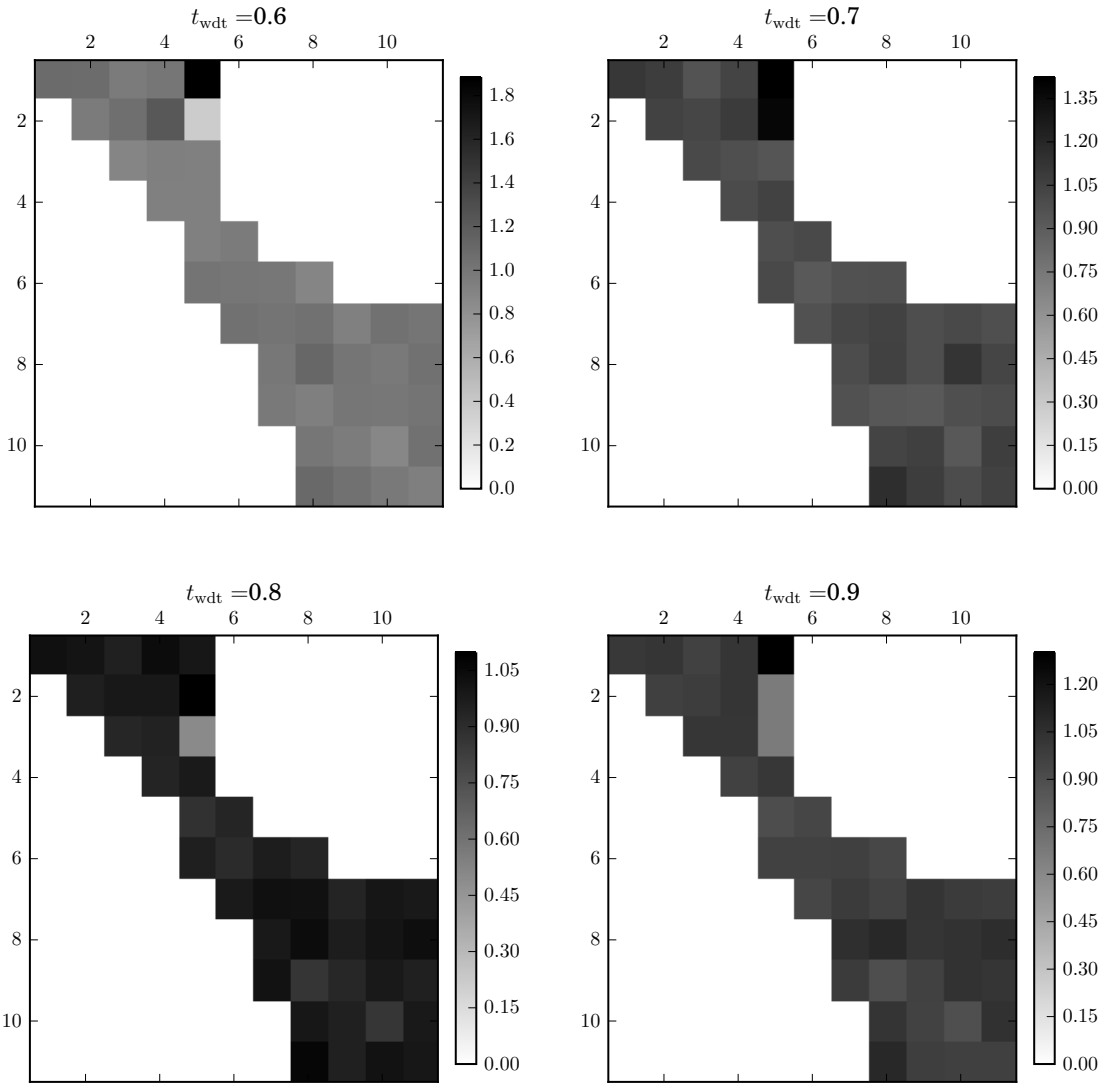

Entry	$\overline{\mathrm{FOM}}$
(7→10)	5.110467×10^{-4}

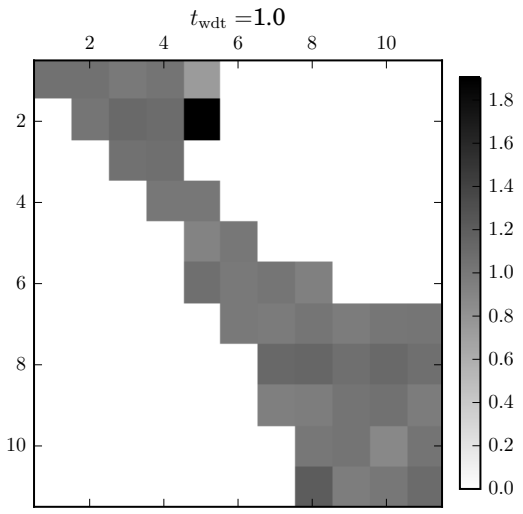
t_{wdt} =1.0
2
4
6
8
10
2
4
6
8
10
1.8
1.6
1.4
1.2
1.0
0.8
0.6
0.4
0.2
0.0

Data

$\Sigma_{1\to1}$

t_{wdt}	$\overline{\text{FOM}}$	Ratio
0.1	2.303773×10^{5}	1.000000
0.2	2.416892×10^{5}	1.049102
0.3	2.307097×10^{5}	1.001443
0.4	2.564921×10^{5}	1.113356
0.5	2.444285×10^{5}	1.060992
0.6	2.490984×10^{5}	1.081263
0.7	2.534176×10^{5}	1.100011
0.8	2.355754×10^{5}	1.022563
0.9	2.311391×10^{5}	1.003307
1.0	2.407415×10^{5}	1.044988

$\Sigma_{2\to1}$

t_{wdt}	$\overline{\text{FOM}}$	Ratio
0.1	4.683628×10^{4}	1.000000
0.2	5.021915×10^{4}	1.072228
0.3	4.771156×10^{4}	1.018688
0.4	4.989691×10^{4}	1.065348
0.5	5.067752×10^{4}	1.082014
0.6	5.026179×10^{4}	1.073138
0.7	5.050504×10^{4}	1.078332
0.8	4.699267×10^{4}	1.003339
0.9	4.816923×10^{4}	1.028460
1.0	4.888526×10^{4}	1.043748

$\Sigma_{3\to1}$

t_{wdt}	$\overline{\text{FOM}}$	Ratio
0.1	6.204512×10^{1}	1.000000
0.2	5.950573×10^{1}	0.959072
0.3	5.956541×10^{1}	0.960034
0.4	5.722592×10^{1}	0.922328
0.5	5.680238×10^{1}	0.915501
0.6	6.048370×10^{1}	0.974834
0.7	5.914001×10^{1}	0.953177
0.8	5.938799×10^{1}	0.957174
0.9	6.005187×10^{1}	0.967874
1.0	6.208868×10^{1}	1.000702

$\Sigma_{4\to1}$

t_{wdt}	$\overline{\text{FOM}}$	Ratio
0.1	1.805025×10^{-1}	1.000000
0.2	1.890662×10^{-1}	1.047443
0.3	1.766837×10^{-1}	0.978843
0.4	1.853607×10^{-1}	1.026915
0.5	1.785362×10^{-1}	0.989106
0.6	1.818917×10^{-1}	1.007696
0.7	1.876230×10^{-1}	1.039448
0.8	1.881331×10^{-1}	1.042274
0.9	1.854686×10^{-1}	1.027513
1.0	1.869678×10^{-1}	1.035818

$\Sigma_{6\to1}$

t_{wdt}	$\overline{\text{FOM}}$	Ratio
0.1	7.577997×10^{-4}	1.000000
0.2	1.784195×10^{-3}	2.354441
0.3	2.426759×10^{-3}	3.202375
0.4	1.070218×10^{-3}	1.412270
0.5	1.290321×10^{-3}	1.702721
0.6	1.424939×10^{-3}	1.880364
0.7	1.076956×10^{-3}	1.421162
0.8	7.544624×10^{-4}	0.995596
0.9	9.838320×10^{-4}	1.298275
1.0	5.670118×10^{-4}	0.748234

$\Sigma_{6\to1}$

t_{wdt}	$\overline{\text{FOM}}$	Ratio
0.1	0.000000×10^{0}	0.000000
0.2	0.000000×10^{0}	0.000000
0.3	0.000000×10^{0}	0.000000
0.4	0.000000×10^{0}	0.000000
0.5	3.679430×10^{-4}	0.000368
0.6	0.000000×10^{0}	0.000000
0.7	0.000000×10^{0}	0.000000
0.8	0.000000×10^{0}	0.000000
0.9	0.000000×10^{0}	0.000000
1.0	0.000000×10^{0}	0.000000

$\Sigma_{7\to1}$

t_{wdt}	$\overline{\text{FOM}}$	Ratio
0.1	0.000000×10^{0}	0.000000
0.2	0.000000×10^{0}	0.000000
0.3	0.000000×10^{0}	0.000000
0.4	0.000000×10^{0}	0.000000
0.5	0.000000×10^{0}	0.000000
0.6	0.000000×10^{0}	0.000000
0.7	0.000000×10^{0}	0.000000
0.8	0.000000×10^{0}	0.000000
0.9	0.000000×10^{0}	0.000000
1.0	0.000000×10^{0}	0.000000

$\Sigma_{8\to1}$

t_{wdt}	$\overline{\text{FOM}}$	Ratio
0.1	0.000000×10^{0}	0.000000
0.2	0.000000×10^{0}	0.000000
0.3	0.000000×10^{0}	0.000000
0.4	0.000000×10^{0}	0.000000
0.5	0.000000×10^{0}	0.000000
0.6	0.000000×10^{0}	0.000000
0.7	0.000000×10^{0}	0.000000
0.8	0.000000×10^{0}	0.000000
0.9	0.000000×10^{0}	0.000000
1.0	0.000000×10^{0}	0.000000

$\Sigma_{9\to1}$

t_{wdt}	$\overline{\text{FOM}}$	Ratio
0.1	0.000000×10^{0}	0.000000
0.2	0.000000×10^{0}	0.000000
0.3	0.000000×10^{0}	0.000000
0.4	0.000000×10^{0}	0.000000
0.5	0.000000×10^{0}	0.000000
0.6	0.000000×10^{0}	0.000000
0.7	0.000000×10^{0}	0.000000
0.8	0.000000×10^{0}	0.000000
0.9	0.000000×10^{0}	0.000000
1.0	0.000000×10^{0}	0.000000

$\Sigma_{10\to1}$

t_{wdt}	$\overline{\text{FOM}}$	Ratio
0.1	0.000000×10^{0}	0.000000
0.2	0.000000×10^{0}	0.000000
0.3	0.000000×10^{0}	0.000000
0.4	0.000000×10^{0}	0.000000
0.5	0.000000×10^{0}	0.000000
0.6	0.000000×10^{0}	0.000000
0.7	0.000000×10^{0}	0.000000
0.8	0.000000×10^{0}	0.000000
0.9	0.000000×10^{0}	0.000000
1.0	0.000000×10^{0}	0.000000

$\Sigma_{11\to1}$

t_{wdt}	$\overline{\text{FOM}}$	Ratio
0.1	0.000000×10^{0}	0.000000
0.2	0.000000×10^{0}	0.000000
0.3	0.000000×10^{0}	0.000000
0.4	0.000000×10^{0}	0.000000
0.5	0.000000×10^{0}	0.000000
0.6	0.000000×10^{0}	0.000000
0.7	0.000000×10^{0}	0.000000
0.8	0.000000×10^{0}	0.000000
0.9	0.000000×10^{0}	0.000000
1.0	0.000000×10^{0}	0.000000

$\Sigma_{1\to2}$

t_{wdt}	$\overline{\text{FOM}}$	Ratio
0.1	0.000000×10^{0}	0.000000
0.2	0.000000×10^{0}	0.000000
0.3	0.000000×10^{0}	0.000000
0.4	0.000000×10^{0}	0.000000
0.5	0.000000×10^{0}	0.000000
0.6	0.000000×10^{0}	0.000000
0.7	0.000000×10^{0}	0.000000
0.8	0.000000×10^{0}	0.000000
0.9	0.000000×10^{0}	0.000000
1.0	0.000000×10^{0}	0.000000

$\Sigma_{2\to2}$

t_{wdt}	$\overline{\text{FOM}}$	Ratio
0.1	1.816543×10^{7}	1.000000
0.2	1.742745×10^{7}	0.959374
0.3	1.737686×10^{7}	0.956589
0.4	1.683882×10^{7}	0.926971
0.5	1.812368×10^{7}	0.997701
0.6	1.771710×10^{7}	0.975320
0.7	1.898330×10^{7}	1.045023
0.8	1.748141×10^{7}	0.962345
0.9	1.762244×10^{7}	0.970109
1.0	1.863098×10^{7}	1.025628

$\Sigma_{3\to2}$

t_{wdt}	$\overline{\text{FOM}}$	Ratio
0.1	1.195780×10^{6}	1.000000
0.2	1.182143×10^{6}	0.988596
0.3	1.214955×10^{6}	1.016036
0.4	1.149282×10^{6}	0.961115
0.5	1.220434×10^{6}	1.020618
0.6	1.264691×10^{6}	1.057629
0.7	1.232960×10^{6}	1.031093
0.8	1.185685×10^{6}	0.991558
0.9	1.181820×10^{6}	0.988326
1.0	1.328150×10^{6}	1.110698

$\Sigma_{4\to2}$

t_{wdt}	$\overline{\text{FOM}}$	Ratio
0.1	6.724069×10^{-2}	1.000000
0.2	7.459400×10^{-2}	1.109358
0.3	5.924054×10^{-2}	0.881022
0.4	6.512928×10^{-2}	0.968599
0.5	7.338837×10^{-2}	1.091428
0.6	8.277739×10^{-2}	1.231061
0.7	7.345341×10^{-2}	1.092395
0.8	6.654432×10^{-2}	0.989644
0.9	6.900854×10^{-2}	1.026291
1.0	7.309238×10^{-2}	1.087026

$\Sigma_{6\to2}$

t_{wdt}	$\overline{\text{FOM}}$	Ratio
0.1	1.898731×10^{-3}	1.000000
0.2	1.528499×10^{-3}	0.805011
0.3	1.818228×10^{-3}	0.957602
0.4	1.786127×10^{-3}	0.940695
0.5	2.215810×10^{-3}	1.166995
0.6	7.114902×10^{-4}	0.374719
0.7	2.625849×10^{-3}	1.382950
0.8	2.080112×10^{-3}	1.095528
0.9	1.279446×10^{-3}	0.673843
1.0	3.608836×10^{-3}	1.900657

$\Sigma_{6\to2}$

t_{wdt}	$\overline{\text{FOM}}$	Ratio
0.1	0.000000×10^{0}	0.000000
0.2	0.000000×10^{0}	0.000000
0.3	0.000000×10^{0}	0.000000
0.4	0.000000×10^{0}	0.000000
0.5	0.000000×10^{0}	0.000000
0.6	0.000000×10^{0}	0.000000
0.7	0.000000×10^{0}	0.000000
0.8	0.000000×10^{0}	0.000000
0.9	0.000000×10^{0}	0.000000
1.0	0.000000×10^{0}	0.000000

$\Sigma_{7\to2}$

t_{wdt}	$\overline{\text{FOM}}$	Ratio
0.1	0.000000×10^{0}	0.000000
0.2	0.000000×10^{0}	0.000000
0.3	0.000000×10^{0}	0.000000
0.4	0.000000×10^{0}	0.000000
0.5	0.000000×10^{0}	0.000000
0.6	0.000000×10^{0}	0.000000
0.7	0.000000×10^{0}	0.000000
0.8	0.000000×10^{0}	0.000000
0.9	0.000000×10^{0}	0.000000
1.0	0.000000×10^{0}	0.000000

$\Sigma_{8\to2}$

t_{wdt}	$\overline{\text{FOM}}$	Ratio
0.1	0.000000×10^{0}	0.000000
0.2	0.000000×10^{0}	0.000000
0.3	0.000000×10^{0}	0.000000
0.4	0.000000×10^{0}	0.000000
0.5	0.000000×10^{0}	0.000000
0.6	0.000000×10^{0}	0.000000
0.7	0.000000×10^{0}	0.000000
0.8	0.000000×10^{0}	0.000000
0.9	0.000000×10^{0}	0.000000
1.0	0.000000×10^{0}	0.000000

$\Sigma_{9\to2}$

t_{wdt}	$\overline{\text{FOM}}$	Ratio
0.1	0.000000×10^{0}	0.000000
0.2	0.000000×10^{0}	0.000000
0.3	0.000000×10^{0}	0.000000
0.4	0.000000×10^{0}	0.000000
0.5	0.000000×10^{0}	0.000000
0.6	0.000000×10^{0}	0.000000
0.7	0.000000×10^{0}	0.000000
0.8	0.000000×10^{0}	0.000000
0.9	0.000000×10^{0}	0.000000
1.0	0.000000×10^{0}	0.000000

$\Sigma_{10\to2}$

t_{wdt}	$\overline{\text{FOM}}$	Ratio
0.1	0.000000×10^{0}	0.000000
0.2	0.000000×10^{0}	0.000000
0.3	0.000000×10^{0}	0.000000
0.4	0.000000×10^{0}	0.000000
0.5	0.000000×10^{0}	0.000000
0.6	0.000000×10^{0}	0.000000
0.7	0.000000×10^{0}	0.000000
0.8	0.000000×10^{0}	0.000000
0.9	0.000000×10^{0}	0.000000
1.0	0.000000×10^{0}	0.000000

$\Sigma_{11\to2}$

t_{wdt}	$\overline{\text{FOM}}$	Ratio
0.1	0.000000×10^{0}	0.000000
0.2	0.000000×10^{0}	0.000000
0.3	0.000000×10^{0}	0.000000
0.4	0.000000×10^{0}	0.000000
0.5	0.000000×10^{0}	0.000000
0.6	0.000000×10^{0}	0.000000
0.7	0.000000×10^{0}	0.000000
0.8	0.000000×10^{0}	0.000000
0.9	0.000000×10^{0}	0.000000
1.0	0.000000×10^{0}	0.000000

$\Sigma_{1\to3}$

t_{wdt}	$\overline{\text{FOM}}$	Ratio
0.1	0.000000×10^{0}	0.000000
0.2	0.000000×10^{0}	0.000000
0.3	0.000000×10^{0}	0.000000
0.4	0.000000×10^{0}	0.000000
0.5	0.000000×10^{0}	0.000000
0.6	0.000000×10^{0}	0.000000
0.7	0.000000×10^{0}	0.000000
0.8	0.000000×10^{0}	0.000000
0.9	0.000000×10^{0}	0.000000
1.0	0.000000×10^{0}	0.000000

$\Sigma_{2\to3}$

t_{wdt}	$\overline{\text{FOM}}$	Ratio
0.1	0.000000×10^{0}	0.000000
0.2	0.000000×10^{0}	0.000000
0.3	0.000000×10^{0}	0.000000
0.4	0.000000×10^{0}	0.000000
0.5	0.000000×10^{0}	0.000000
0.6	0.000000×10^{0}	0.000000
0.7	0.000000×10^{0}	0.000000
0.8	0.000000×10^{0}	0.000000
0.9	0.000000×10^{0}	0.000000
1.0	0.000000×10^{0}	0.000000

$\Sigma_{3\to3}$

t_{wdt}	$\overline{\text{FOM}}$	Ratio
0.1	4.335975×10^{9}	1.000000
0.2	4.296860×10^{9}	0.990979
0.3	4.113044×10^{9}	0.948586
0.4	4.253757×10^{9}	0.981038
0.5	4.464645×10^{9}	1.029675
0.6	3.908586×10^{9}	0.901432
0.7	4.363567×10^{9}	1.006364
0.8	4.040146×10^{9}	0.931773
0.9	4.419446×10^{9}	1.019251
1.0	4.507271×10^{9}	1.039506

$\Sigma_{4\to3}$

t_{wdt}	$\overline{\text{FOM}}$	Ratio
0.1	1.113999×10^{7}	1.000000
0.2	1.112852×10^{7}	0.998970
0.3	1.091167×10^{7}	0.979504
0.4	1.081007×10^{7}	0.970384
0.5	1.150492×10^{7}	1.032758
0.6	1.050764×10^{7}	0.943235
0.7	1.089186×10^{7}	0.977726
0.8	1.049502×10^{7}	0.942103
0.9	1.131167×10^{7}	1.015411
1.0	1.192004×10^{7}	1.070023

$\Sigma_{6\to3}$

t_{wdt}	$\overline{\text{FOM}}$	Ratio
0.1	3.786882×10^{-4}	1.000000
0.2	7.631421×10^{-4}	2.015225
0.3	0.000000×10^{0}	0.000000
0.4	7.130278×10^{-4}	1.882889
0.5	4.501173×10^{-4}	1.188622
0.6	3.555212×10^{-4}	0.938823
0.7	3.585387×10^{-4}	0.946791
0.8	1.884120×10^{-4}	0.497539
0.9	2.554126×10^{-4}	0.674467
1.0	0.000000×10^{0}	0.000000

$\Sigma_{6\to3}$

t_{wdt}	$\overline{\text{FOM}}$	Ratio
0.1	0.000000×10^{0}	0.000000
0.2	0.000000×10^{0}	0.000000
0.3	0.000000×10^{0}	0.000000
0.4	0.000000×10^{0}	0.000000
0.5	0.000000×10^{0}	0.000000
0.6	0.000000×10^{0}	0.000000
0.7	0.000000×10^{0}	0.000000
0.8	0.000000×10^{0}	0.000000
0.9	0.000000×10^{0}	0.000000
1.0	0.000000×10^{0}	0.000000

$\Sigma_{7\to3}$

t_{wdt}	$\overline{\text{FOM}}$	Ratio
0.1	0.000000×10^{0}	0.000000
0.2	0.000000×10^{0}	0.000000
0.3	0.000000×10^{0}	0.000000
0.4	0.000000×10^{0}	0.000000
0.5	0.000000×10^{0}	0.000000
0.6	0.000000×10^{0}	0.000000
0.7	0.000000×10^{0}	0.000000
0.8	0.000000×10^{0}	0.000000
0.9	0.000000×10^{0}	0.000000
1.0	0.000000×10^{0}	0.000000

$\Sigma_{8\to3}$

t_{wdt}	$\overline{\text{FOM}}$	Ratio
0.1	0.000000×10^{0}	0.000000
0.2	0.000000×10^{0}	0.000000
0.3	0.000000×10^{0}	0.000000
0.4	0.000000×10^{0}	0.000000
0.5	0.000000×10^{0}	0.000000
0.6	0.000000×10^{0}	0.000000
0.7	0.000000×10^{0}	0.000000
0.8	0.000000×10^{0}	0.000000
0.9	0.000000×10^{0}	0.000000
1.0	0.000000×10^{0}	0.000000

$\Sigma_{9\to3}$

t_{wdt}	$\overline{\text{FOM}}$	Ratio
0.1	0.000000×10^{0}	0.000000
0.2	0.000000×10^{0}	0.000000
0.3	0.000000×10^{0}	0.000000
0.4	0.000000×10^{0}	0.000000
0.5	0.000000×10^{0}	0.000000
0.6	0.000000×10^{0}	0.000000
0.7	0.000000×10^{0}	0.000000
0.8	0.000000×10^{0}	0.000000
0.9	0.000000×10^{0}	0.000000
1.0	0.000000×10^{0}	0.000000

$\Sigma_{10\to3}$

t_{wdt}	$\overline{\text{FOM}}$	Ratio
0.1	0.000000×10^{0}	0.000000
0.2	0.000000×10^{0}	0.000000
0.3	0.000000×10^{0}	0.000000
0.4	0.000000×10^{0}	0.000000
0.5	0.000000×10^{0}	0.000000
0.6	0.000000×10^{0}	0.000000
0.7	0.000000×10^{0}	0.000000
0.8	0.000000×10^{0}	0.000000
0.9	0.000000×10^{0}	0.000000
1.0	0.000000×10^{0}	0.000000

$\Sigma_{11\to3}$

t_{wdt}	$\overline{\text{FOM}}$	Ratio
0.1	0.000000×10^{0}	0.000000
0.2	0.000000×10^{0}	0.000000
0.3	0.000000×10^{0}	0.000000
0.4	0.000000×10^{0}	0.000000
0.5	0.000000×10^{0}	0.000000
0.6	0.000000×10^{0}	0.000000
0.7	0.000000×10^{0}	0.000000
0.8	0.000000×10^{0}	0.000000
0.9	0.000000×10^{0}	0.000000
1.0	0.000000×10^{0}	0.000000

$\Sigma_{1\to4}$

t_{wdt}	$\overline{\text{FOM}}$	Ratio
0.1	0.000000×10^{0}	0.000000
0.2	0.000000×10^{0}	0.000000
0.3	0.000000×10^{0}	0.000000
0.4	0.000000×10^{0}	0.000000
0.5	0.000000×10^{0}	0.000000
0.6	0.000000×10^{0}	0.000000
0.7	0.000000×10^{0}	0.000000
0.8	0.000000×10^{0}	0.000000
0.9	0.000000×10^{0}	0.000000
1.0	0.000000×10^{0}	0.000000

$\Sigma_{2\to4}$

t_{wdt}	$\overline{\text{FOM}}$	Ratio
0.1	0.000000×10^{0}	0.000000
0.2	0.000000×10^{0}	0.000000
0.3	0.000000×10^{0}	0.000000
0.4	0.000000×10^{0}	0.000000
0.5	0.000000×10^{0}	0.000000
0.6	0.000000×10^{0}	0.000000
0.7	0.000000×10^{0}	0.000000
0.8	0.000000×10^{0}	0.000000
0.9	0.000000×10^{0}	0.000000
1.0	0.000000×10^{0}	0.000000

$\Sigma_{3\to4}$

t_{wdt}	$\overline{\text{FOM}}$	Ratio
0.1	0.000000×10^{0}	0.000000
0.2	0.000000×10^{0}	0.000000
0.3	0.000000×10^{0}	0.000000
0.4	0.000000×10^{0}	0.000000
0.5	0.000000×10^{0}	0.000000
0.6	0.000000×10^{0}	0.000000
0.7	0.000000×10^{0}	0.000000
0.8	0.000000×10^{0}	0.000000
0.9	0.000000×10^{0}	0.000000
1.0	0.000000×10^{0}	0.000000

$\Sigma_{4\to4}$

t_{wdt}	$\overline{\text{FOM}}$	Ratio
0.1	4.050509×10^{9}	1.000000
0.2	3.882580×10^{9}	0.958541
0.3	3.983787×10^{9}	0.983528
0.4	4.016648×10^{9}	0.991640
0.5	3.900661×10^{9}	0.963005
0.6	3.792559×10^{9}	0.936317
0.7	4.062163×10^{9}	1.002877
0.8	3.812723×10^{9}	0.941295
0.9	3.915575×10^{9}	0.966687
1.0	4.087541×10^{9}	1.009143

$\Sigma_{6\to4}$

t_{wdt}	$\overline{\text{FOM}}$	Ratio
0.1	9.074242×10^{6}	1.000000
0.2	9.164401×10^{6}	1.009936
0.3	8.978538×10^{6}	0.989453
0.4	9.002886×10^{6}	0.992136
0.5	9.352286×10^{6}	1.030641
0.6	8.471827×10^{6}	0.933613
0.7	9.488225×10^{6}	1.045622
0.8	8.862906×10^{6}	0.976710
0.9	9.167852×10^{6}	1.010316
1.0	9.217577×10^{6}	1.015796

$\Sigma_{6\to4}$

t_{wdt}	$\overline{\text{FOM}}$	Ratio
0.1	0.000000×10^{0}	0.000000
0.2	0.000000×10^{0}	0.000000
0.3	0.000000×10^{0}	0.000000
0.4	0.000000×10^{0}	0.000000
0.5	0.000000×10^{0}	0.000000
0.6	0.000000×10^{0}	0.000000
0.7	0.000000×10^{0}	0.000000
0.8	0.000000×10^{0}	0.000000
0.9	0.000000×10^{0}	0.000000
1.0	0.000000×10^{0}	0.000000

$\Sigma_{7\to4}$

t_{wdt}	$\overline{\text{FOM}}$	Ratio
0.1	0.000000×10^{0}	0.000000
0.2	0.000000×10^{0}	0.000000
0.3	0.000000×10^{0}	0.000000
0.4	0.000000×10^{0}	0.000000
0.5	0.000000×10^{0}	0.000000
0.6	0.000000×10^{0}	0.000000
0.7	0.000000×10^{0}	0.000000
0.8	0.000000×10^{0}	0.000000
0.9	0.000000×10^{0}	0.000000
1.0	0.000000×10^{0}	0.000000

$\Sigma_{8\to4}$

t_{wdt}	$\overline{\text{FOM}}$	Ratio
0.1	0.000000×10^{0}	0.000000
0.2	0.000000×10^{0}	0.000000
0.3	0.000000×10^{0}	0.000000
0.4	0.000000×10^{0}	0.000000
0.5	0.000000×10^{0}	0.000000
0.6	0.000000×10^{0}	0.000000
0.7	0.000000×10^{0}	0.000000
0.8	0.000000×10^{0}	0.000000
0.9	0.000000×10^{0}	0.000000
1.0	0.000000×10^{0}	0.000000

$\Sigma_{9\to4}$

t_{wdt}	$\overline{\text{FOM}}$	Ratio
0.1	0.000000×10^{0}	0.000000
0.2	0.000000×10^{0}	0.000000
0.3	0.000000×10^{0}	0.000000
0.4	0.000000×10^{0}	0.000000
0.5	0.000000×10^{0}	0.000000
0.6	0.000000×10^{0}	0.000000
0.7	0.000000×10^{0}	0.000000
0.8	0.000000×10^{0}	0.000000
0.9	0.000000×10^{0}	0.000000
1.0	0.000000×10^{0}	0.000000

$\Sigma_{10\to4}$

t_{wdt}	$\overline{\text{FOM}}$	Ratio
0.1	0.000000×10^{0}	0.000000
0.2	0.000000×10^{0}	0.000000
0.3	0.000000×10^{0}	0.000000
0.4	0.000000×10^{0}	0.000000
0.5	0.000000×10^{0}	0.000000
0.6	0.000000×10^{0}	0.000000
0.7	0.000000×10^{0}	0.000000
0.8	0.000000×10^{0}	0.000000
0.9	0.000000×10^{0}	0.000000
1.0	0.000000×10^{0}	0.000000

$\Sigma_{11\to4}$

t_{wdt}	$\overline{\text{FOM}}$	Ratio
0.1	0.000000×10^{0}	0.000000
0.2	0.000000×10^{0}	0.000000
0.3	0.000000×10^{0}	0.000000
0.4	0.000000×10^{0}	0.000000
0.5	0.000000×10^{0}	0.000000
0.6	0.000000×10^{0}	0.000000
0.7	0.000000×10^{0}	0.000000
0.8	0.000000×10^{0}	0.000000
0.9	0.000000×10^{0}	0.000000
1.0	0.000000×10^{0}	0.000000

$\Sigma_{1\to5}$

t_{wdt}	$\overline{\text{FOM}}$	Ratio
0.1	0.000000×10^{0}	0.000000
0.2	0.000000×10^{0}	0.000000
0.3	0.000000×10^{0}	0.000000
0.4	0.000000×10^{0}	0.000000
0.5	0.000000×10^{0}	0.000000
0.6	0.000000×10^{0}	0.000000
0.7	0.000000×10^{0}	0.000000
0.8	0.000000×10^{0}	0.000000
0.9	0.000000×10^{0}	0.000000
1.0	0.000000×10^{0}	0.000000

$\Sigma_{2\to5}$

t_{wdt}	$\overline{\text{FOM}}$	Ratio
0.1	0.000000×10^{0}	0.000000
0.2	0.000000×10^{0}	0.000000
0.3	0.000000×10^{0}	0.000000
0.4	0.000000×10^{0}	0.000000
0.5	0.000000×10^{0}	0.000000
0.6	0.000000×10^{0}	0.000000
0.7	0.000000×10^{0}	0.000000
0.8	0.000000×10^{0}	0.000000
0.9	0.000000×10^{0}	0.000000
1.0	0.000000×10^{0}	0.000000

$\Sigma_{3\to5}$

t_{wdt}	$\overline{\text{FOM}}$	Ratio
0.1	0.000000×10^{0}	0.000000
0.2	0.000000×10^{0}	0.000000
0.3	0.000000×10^{0}	0.000000
0.4	0.000000×10^{0}	0.000000
0.5	0.000000×10^{0}	0.000000
0.6	0.000000×10^{0}	0.000000
0.7	0.000000×10^{0}	0.000000
0.8	0.000000×10^{0}	0.000000
0.9	0.000000×10^{0}	0.000000
1.0	0.000000×10^{0}	0.000000

$\Sigma_{4\to5}$

t_{wdt}	$\overline{\text{FOM}}$	Ratio
0.1	0.000000×10^{0}	0.000000
0.2	0.000000×10^{0}	0.000000
0.3	0.000000×10^{0}	0.000000
0.4	0.000000×10^{0}	0.000000
0.5	0.000000×10^{0}	0.000000
0.6	0.000000×10^{0}	0.000000
0.7	0.000000×10^{0}	0.000000
0.8	0.000000×10^{0}	0.000000
0.9	0.000000×10^{0}	0.000000
1.0	0.000000×10^{0}	0.000000

$\Sigma_{6\to5}$

t_{wdt}	$\overline{\text{FOM}}$	Ratio
0.1	2.107107×10^{9}	1.000000
0.2	1.874331×10^{9}	0.889528
0.3	2.216045×10^{9}	1.051700
0.4	1.910656×10^{9}	0.906768
0.5	1.916729×10^{9}	0.909650
0.6	1.979116×10^{9}	0.939258
0.7	2.074456×10^{9}	0.984505
0.8	1.856900×10^{9}	0.881256
0.9	1.910820×10^{9}	0.906845
1.0	1.925136×10^{9}	0.913640

$\Sigma_{6\to5}$

t_{wdt}	$\overline{\text{FOM}}$	Ratio
0.1	5.809655×10^{6}	1.000000
0.2	5.418966×10^{6}	0.932752
0.3	5.825467×10^{6}	1.002722
0.4	5.357805×10^{6}	0.922224
0.5	5.633489×10^{6}	0.969677
0.6	5.634535×10^{6}	0.969857
0.7	5.875776×10^{6}	1.011381
0.8	5.424064×10^{6}	0.933629
0.9	5.457314×10^{6}	0.939352
1.0	5.893288×10^{6}	1.014396

$\Sigma_{7\to5}$

t_{wdt}	$\overline{\text{FOM}}$	Ratio
0.1	0.000000×10^{0}	0.000000
0.2	0.000000×10^{0}	0.000000
0.3	0.000000×10^{0}	0.000000
0.4	0.000000×10^{0}	0.000000
0.5	0.000000×10^{0}	0.000000
0.6	0.000000×10^{0}	0.000000
0.7	0.000000×10^{0}	0.000000
0.8	0.000000×10^{0}	0.000000
0.9	0.000000×10^{0}	0.000000
1.0	0.000000×10^{0}	0.000000

$\Sigma_{8\to5}$

t_{wdt}	$\overline{\text{FOM}}$	Ratio
0.1	0.000000×10^{0}	0.000000
0.2	0.000000×10^{0}	0.000000
0.3	0.000000×10^{0}	0.000000
0.4	0.000000×10^{0}	0.000000
0.5	0.000000×10^{0}	0.000000
0.6	0.000000×10^{0}	0.000000
0.7	0.000000×10^{0}	0.000000
0.8	0.000000×10^{0}	0.000000
0.9	0.000000×10^{0}	0.000000
1.0	0.000000×10^{0}	0.000000

$\Sigma_{9\to5}$

t_{wdt}	$\overline{\text{FOM}}$	Ratio
0.1	0.000000×10^{0}	0.000000
0.2	0.000000×10^{0}	0.000000
0.3	0.000000×10^{0}	0.000000
0.4	0.000000×10^{0}	0.000000
0.5	0.000000×10^{0}	0.000000
0.6	0.000000×10^{0}	0.000000
0.7	0.000000×10^{0}	0.000000
0.8	0.000000×10^{0}	0.000000
0.9	0.000000×10^{0}	0.000000
1.0	0.000000×10^{0}	0.000000

$\Sigma_{10\to5}$

t_{wdt}	$\overline{\text{FOM}}$	Ratio
0.1	0.000000×10^{0}	0.000000
0.2	0.000000×10^{0}	0.000000
0.3	0.000000×10^{0}	0.000000
0.4	0.000000×10^{0}	0.000000
0.5	0.000000×10^{0}	0.000000
0.6	0.000000×10^{0}	0.000000
0.7	0.000000×10^{0}	0.000000
0.8	0.000000×10^{0}	0.000000
0.9	0.000000×10^{0}	0.000000
1.0	0.000000×10^{0}	0.000000

$\Sigma_{11\to5}$

t_{wdt}	$\overline{\text{FOM}}$	Ratio
0.1	0.000000×10^{0}	0.000000
0.2	0.000000×10^{0}	0.000000
0.3	0.000000×10^{0}	0.000000
0.4	0.000000×10^{0}	0.000000
0.5	0.000000×10^{0}	0.000000
0.6	0.000000×10^{0}	0.000000
0.7	0.000000×10^{0}	0.000000
0.8	0.000000×10^{0}	0.000000
0.9	0.000000×10^{0}	0.000000
1.0	0.000000×10^{0}	0.000000

$\Sigma_{1\to6}$

t_{wdt}	$\overline{\text{FOM}}$	Ratio
0.1	0.000000×10^{0}	0.000000
0.2	0.000000×10^{0}	0.000000
0.3	0.000000×10^{0}	0.000000
0.4	0.000000×10^{0}	0.000000
0.5	0.000000×10^{0}	0.000000
0.6	0.000000×10^{0}	0.000000
0.7	0.000000×10^{0}	0.000000
0.8	0.000000×10^{0}	0.000000
0.9	0.000000×10^{0}	0.000000
1.0	0.000000×10^{0}	0.000000

$\Sigma_{2\to6}$

t_{wdt}	$\overline{\text{FOM}}$	Ratio
0.1	0.000000×10^{0}	0.000000
0.2	0.000000×10^{0}	0.000000
0.3	0.000000×10^{0}	0.000000
0.4	0.000000×10^{0}	0.000000
0.5	0.000000×10^{0}	0.000000
0.6	0.000000×10^{0}	0.000000
0.7	0.000000×10^{0}	0.000000
0.8	0.000000×10^{0}	0.000000
0.9	0.000000×10^{0}	0.000000
1.0	0.000000×10^{0}	0.000000

$\Sigma_{3\to6}$

t_{wdt}	$\overline{\text{FOM}}$	Ratio
0.1	0.000000×10^{0}	0.000000
0.2	0.000000×10^{0}	0.000000
0.3	0.000000×10^{0}	0.000000
0.4	0.000000×10^{0}	0.000000
0.5	0.000000×10^{0}	0.000000
0.6	0.000000×10^{0}	0.000000
0.7	0.000000×10^{0}	0.000000
0.8	0.000000×10^{0}	0.000000
0.9	0.000000×10^{0}	0.000000
1.0	0.000000×10^{0}	0.000000

$\Sigma_{4\to6}$

t_{wdt}	$\overline{\text{FOM}}$	Ratio
0.1	0.000000×10^{0}	0.000000
0.2	0.000000×10^{0}	0.000000
0.3	0.000000×10^{0}	0.000000
0.4	0.000000×10^{0}	0.000000
0.5	0.000000×10^{0}	0.000000
0.6	0.000000×10^{0}	0.000000
0.7	0.000000×10^{0}	0.000000
0.8	0.000000×10^{0}	0.000000
0.9	0.000000×10^{0}	0.000000
1.0	0.000000×10^{0}	0.000000

$\Sigma_{6\to6}$

t_{wdt}	$\overline{\text{FOM}}$	Ratio
0.1	4.663388×10^{1}	1.000000
0.2	4.673177×10^{1}	1.002099
0.3	4.531992×10^{1}	0.971824
0.4	4.465980×10^{1}	0.957669
0.5	4.608270×10^{1}	0.988181
0.6	4.780163×10^{1}	1.025041
0.7	4.703466×10^{1}	1.008594
0.8	4.471416×10^{1}	0.958834
0.9	4.477786×10^{1}	0.960200
1.0	5.001117×10^{1}	1.072421

$\Sigma_{6\to6}$

t_{wdt}	$\overline{\text{FOM}}$	Ratio
0.1	6.179493×10^{8}	1.000000
0.2	6.278734×10^{8}	1.016060
0.3	5.930937×10^{8}	0.959777
0.4	5.870792×10^{8}	0.950044
0.5	6.030585×10^{8}	0.975903
0.6	6.258569×10^{8}	1.012797
0.7	5.660424×10^{8}	0.916001
0.8	5.626295×10^{8}	0.910478
0.9	5.943561×10^{8}	0.961820
1.0	6.130523×10^{8}	0.992075

$\Sigma_{7\to6}$

t_{wdt}	$\overline{\text{FOM}}$	Ratio
0.1	2.254637×10^{6}	1.000000
0.2	2.233131×10^{6}	0.990461
0.3	2.091016×10^{6}	0.927429
0.4	2.218305×10^{6}	0.983886
0.5	2.187737×10^{6}	0.970328
0.6	2.263148×10^{6}	1.003775
0.7	2.187028×10^{6}	0.970013
0.8	2.177552×10^{6}	0.965810
0.9	2.190486×10^{6}	0.971547
1.0	2.318412×10^{6}	1.028286

$\Sigma_{8\to6}$

t_{wdt}	$\overline{\text{FOM}}$	Ratio
0.1	5.296726×10^{2}	1.000000
0.2	5.032829×10^{2}	0.950177
0.3	5.173327×10^{2}	0.976703
0.4	5.342590×10^{2}	1.008659
0.5	5.301566×10^{2}	1.000914
0.6	4.761283×10^{2}	0.898911
0.7	5.168753×10^{2}	0.975839
0.8	4.951345×10^{2}	0.934794
0.9	4.948002×10^{2}	0.934162
1.0	5.019859×10^{2}	0.947729

$\Sigma_{9\to6}$

t_{wdt}	$\overline{\text{FOM}}$	Ratio
0.1	0.000000×10^{0}	0.000000
0.2	0.000000×10^{0}	0.000000
0.3	0.000000×10^{0}	0.000000
0.4	0.000000×10^{0}	0.000000
0.5	0.000000×10^{0}	0.000000
0.6	0.000000×10^{0}	0.000000
0.7	0.000000×10^{0}	0.000000
0.8	0.000000×10^{0}	0.000000
0.9	0.000000×10^{0}	0.000000
1.0	0.000000×10^{0}	0.000000

$\Sigma_{10\to6}$

t_{wdt}	$\overline{\text{FOM}}$	Ratio
0.1	0.000000×10^{0}	0.000000
0.2	0.000000×10^{0}	0.000000
0.3	0.000000×10^{0}	0.000000
0.4	0.000000×10^{0}	0.000000
0.5	0.000000×10^{0}	0.000000
0.6	0.000000×10^{0}	0.000000
0.7	0.000000×10^{0}	0.000000
0.8	0.000000×10^{0}	0.000000
0.9	0.000000×10^{0}	0.000000
1.0	0.000000×10^{0}	0.000000

$\Sigma_{11\to6}$

t_{wdt}	$\overline{\text{FOM}}$	Ratio
0.1	0.000000×10^{0}	0.000000
0.2	0.000000×10^{0}	0.000000
0.3	0.000000×10^{0}	0.000000
0.4	0.000000×10^{0}	0.000000
0.5	0.000000×10^{0}	0.000000
0.6	0.000000×10^{0}	0.000000
0.7	0.000000×10^{0}	0.000000
0.8	0.000000×10^{0}	0.000000
0.9	0.000000×10^{0}	0.000000
1.0	0.000000×10^{0}	0.000000

$\Sigma_{1\to7}$

t_{wdt}	$\overline{\text{FOM}}$	Ratio
0.1	0.000000×10^{0}	0.000000
0.2	0.000000×10^{0}	0.000000
0.3	0.000000×10^{0}	0.000000
0.4	0.000000×10^{0}	0.000000
0.5	0.000000×10^{0}	0.000000
0.6	0.000000×10^{0}	0.000000
0.7	0.000000×10^{0}	0.000000
0.8	0.000000×10^{0}	0.000000
0.9	0.000000×10^{0}	0.000000
1.0	0.000000×10^{0}	0.000000

$\Sigma_{2\to7}$

t_{wdt}	$\overline{\text{FOM}}$	Ratio
0.1	0.000000×10^{0}	0.000000
0.2	0.000000×10^{0}	0.000000
0.3	0.000000×10^{0}	0.000000
0.4	0.000000×10^{0}	0.000000
0.5	0.000000×10^{0}	0.000000
0.6	0.000000×10^{0}	0.000000
0.7	0.000000×10^{0}	0.000000
0.8	0.000000×10^{0}	0.000000
0.9	0.000000×10^{0}	0.000000
1.0	0.000000×10^{0}	0.000000

$\Sigma_{3\to7}$

t_{wdt}	$\overline{\text{FOM}}$	Ratio
0.1	0.000000×10^{0}	0.000000
0.2	0.000000×10^{0}	0.000000
0.3	0.000000×10^{0}	0.000000
0.4	0.000000×10^{0}	0.000000
0.5	0.000000×10^{0}	0.000000
0.6	0.000000×10^{0}	0.000000
0.7	0.000000×10^{0}	0.000000
0.8	0.000000×10^{0}	0.000000
0.9	0.000000×10^{0}	0.000000
1.0	0.000000×10^{0}	0.000000

$\Sigma_{4\to7}$

t_{wdt}	$\overline{\text{FOM}}$	Ratio
0.1	0.000000×10^{0}	0.000000
0.2	0.000000×10^{0}	0.000000
0.3	0.000000×10^{0}	0.000000
0.4	0.000000×10^{0}	0.000000
0.5	0.000000×10^{0}	0.000000
0.6	0.000000×10^{0}	0.000000
0.7	0.000000×10^{0}	0.000000
0.8	0.000000×10^{0}	0.000000
0.9	0.000000×10^{0}	0.000000
1.0	0.000000×10^{0}	0.000000

$\Sigma_{6\to7}$

t_{wdt}	$\overline{\text{FOM}}$	Ratio
0.1	0.000000×10^{0}	0.000000
0.2	0.000000×10^{0}	0.000000
0.3	0.000000×10^{0}	0.000000
0.4	0.000000×10^{0}	0.000000
0.5	0.000000×10^{0}	0.000000
0.6	0.000000×10^{0}	0.000000
0.7	0.000000×10^{0}	0.000000
0.8	0.000000×10^{0}	0.000000
0.9	0.000000×10^{0}	0.000000
1.0	0.000000×10^{0}	0.000000

$\Sigma_{6\to7}$

t_{wdt}	$\overline{\text{FOM}}$	Ratio
0.1	6.284840×10^{3}	1.000000
0.2	6.489712×10^{3}	1.032598
0.3	6.084867×10^{3}	0.968182
0.4	5.959359×10^{3}	0.948212
0.5	6.506662×10^{3}	1.035295
0.6	6.596779×10^{3}	1.049633
0.7	6.002478×10^{3}	0.955073
0.8	6.156212×10^{3}	0.979534
0.9	5.911256×10^{3}	0.940558
1.0	6.216781×10^{3}	0.989171

$\Sigma_{7\to7}$

t_{wdt}	$\overline{\text{FOM}}$	Ratio
0.1	2.564454×10^{7}	1.000000
0.2	2.822263×10^{7}	1.100532
0.3	2.454385×10^{7}	0.957079
0.4	2.722732×10^{7}	1.061720
0.5	2.703728×10^{7}	1.054310
0.6	2.621164×10^{7}	1.022114
0.7	2.639073×10^{7}	1.029098
0.8	2.621284×10^{7}	1.022161
0.9	2.538075×10^{7}	0.989714
1.0	2.529530×10^{7}	0.986382

$\Sigma_{8\to7}$

t_{wdt}	$\overline{\text{FOM}}$	Ratio
0.1	3.928172×10^{5}	1.000000
0.2	4.246792×10^{5}	1.081111
0.3	4.067453×10^{5}	1.035457
0.4	4.200058×10^{5}	1.069214
0.5	4.122694×10^{5}	1.049520
0.6	4.086363×10^{5}	1.040271
0.7	4.099811×10^{5}	1.043694
0.8	4.000836×10^{5}	1.018498
0.9	3.759083×10^{5}	0.956955
1.0	4.028877×10^{5}	1.025637

$\Sigma_{9\to7}$

t_{wdt}	$\overline{\text{FOM}}$	Ratio
0.1	1.008565×10^{4}	1.000000
0.2	1.006397×10^{4}	0.997850
0.3	9.706334×10^{3}	0.962391
0.4	1.086260×10^{4}	1.077036
0.5	9.521993×10^{3}	0.944113
0.6	9.439352×10^{3}	0.935919
0.7	9.959517×10^{3}	0.987494
0.8	9.476622×10^{3}	0.939614
0.9	1.041477×10^{4}	1.032632
1.0	9.883803×10^{3}	0.979987

$\Sigma_{10\to7}$

t_{wdt}	$\overline{\text{FOM}}$	Ratio
0.1	4.367493×10^{3}	1.000000
0.2	4.412325×10^{3}	1.010265
0.3	4.086353×10^{3}	0.935629
0.4	4.033994×10^{3}	0.923641
0.5	4.419448×10^{3}	1.011896
0.6	4.495731×10^{3}	1.029362
0.7	4.395034×10^{3}	1.006306
0.8	4.363608×10^{3}	0.999110
0.9	4.319923×10^{3}	0.989108
1.0	4.458088×10^{3}	1.020743

$\Sigma_{11\to7}$

t_{wdt}	$\overline{\text{FOM}}$	Ratio
0.1	4.673141×10^{2}	1.000000
0.2	4.749493×10^{2}	1.016339
0.3	4.838791×10^{2}	1.035447
0.4	4.447622×10^{2}	0.951741
0.5	4.869820×10^{2}	1.042087
0.6	4.752545×10^{2}	1.016991
0.7	4.583026×10^{2}	0.980716
0.8	4.587925×10^{2}	0.981765
0.9	4.608184×10^{2}	0.986100
1.0	4.795647×10^{2}	1.026215

$\Sigma_{1\to8}$

t_{wdt}	$\overline{\text{FOM}}$	Ratio
0.1	0.000000×10^{0}	0.000000
0.2	0.000000×10^{0}	0.000000
0.3	0.000000×10^{0}	0.000000
0.4	0.000000×10^{0}	0.000000
0.5	0.000000×10^{0}	0.000000
0.6	0.000000×10^{0}	0.000000
0.7	0.000000×10^{0}	0.000000
0.8	0.000000×10^{0}	0.000000
0.9	0.000000×10^{0}	0.000000
1.0	0.000000×10^{0}	0.000000

$\Sigma_{2\to8}$

t_{wdt}	$\overline{\text{FOM}}$	Ratio
0.1	0.000000×10^{0}	0.000000
0.2	0.000000×10^{0}	0.000000
0.3	0.000000×10^{0}	0.000000
0.4	0.000000×10^{0}	0.000000
0.5	0.000000×10^{0}	0.000000
0.6	0.000000×10^{0}	0.000000
0.7	0.000000×10^{0}	0.000000
0.8	0.000000×10^{0}	0.000000
0.9	0.000000×10^{0}	0.000000
1.0	0.000000×10^{0}	0.000000

$\Sigma_{3\to8}$

t_{wdt}	$\overline{\text{FOM}}$	Ratio
0.1	0.000000×10^{0}	0.000000
0.2	0.000000×10^{0}	0.000000
0.3	0.000000×10^{0}	0.000000
0.4	0.000000×10^{0}	0.000000
0.5	0.000000×10^{0}	0.000000
0.6	0.000000×10^{0}	0.000000
0.7	0.000000×10^{0}	0.000000
0.8	0.000000×10^{0}	0.000000
0.9	0.000000×10^{0}	0.000000
1.0	0.000000×10^{0}	0.000000

$\Sigma_{4\to8}$

t_{wdt}	$\overline{\text{FOM}}$	Ratio
0.1	0.000000×10^{0}	0.000000
0.2	0.000000×10^{0}	0.000000
0.3	0.000000×10^{0}	0.000000
0.4	0.000000×10^{0}	0.000000
0.5	0.000000×10^{0}	0.000000
0.6	0.000000×10^{0}	0.000000
0.7	0.000000×10^{0}	0.000000
0.8	0.000000×10^{0}	0.000000
0.9	0.000000×10^{0}	0.000000
1.0	0.000000×10^{0}	0.000000

$\Sigma_{6\to8}$

t_{wdt}	$\overline{\text{FOM}}$	Ratio
0.1	0.000000×10^{0}	0.000000
0.2	0.000000×10^{0}	0.000000
0.3	0.000000×10^{0}	0.000000
0.4	0.000000×10^{0}	0.000000
0.5	0.000000×10^{0}	0.000000
0.6	0.000000×10^{0}	0.000000
0.7	0.000000×10^{0}	0.000000
0.8	0.000000×10^{0}	0.000000
0.9	0.000000×10^{0}	0.000000
1.0	0.000000×10^{0}	0.000000

$\Sigma_{6\to8}$

t_{wdt}	$\overline{\text{FOM}}$	Ratio
0.1	0.000000×10^{0}	0.000000
0.2	0.000000×10^{0}	0.000000
0.3	0.000000×10^{0}	0.000000
0.4	0.000000×10^{0}	0.000000
0.5	0.000000×10^{0}	0.000000
0.6	0.000000×10^{0}	0.000000
0.7	0.000000×10^{0}	0.000000
0.8	0.000000×10^{0}	0.000000
0.9	0.000000×10^{0}	0.000000
1.0	0.000000×10^{0}	0.000000

$\Sigma_{7\to8}$

t_{wdt}	$\overline{\text{FOM}}$	Ratio
0.1	3.624801×10^{4}	1.000000
0.2	3.573846×10^{4}	0.985943
0.3	3.357317×10^{4}	0.926207
0.4	3.633781×10^{4}	1.002478
0.5	3.367926×10^{4}	0.929134
0.6	3.623861×10^{4}	0.999741
0.7	3.604944×10^{4}	0.994522
0.8	3.555720×10^{4}	0.980942
0.9	3.833569×10^{4}	1.057595
1.0	4.075120×10^{4}	1.124233

$\Sigma_{8\to8}$

t_{wdt}	$\overline{\text{FOM}}$	Ratio
0.1	6.604787×10^{7}	1.000000
0.2	6.908472×10^{7}	1.045980
0.3	7.029599×10^{7}	1.064319
0.4	7.393059×10^{7}	1.119349
0.5	7.000481×10^{7}	1.059910
0.6	7.395961×10^{7}	1.119788
0.7	6.979038×10^{7}	1.056664
0.8	6.892649×10^{7}	1.043584
0.9	7.212280×10^{7}	1.091978
1.0	7.517225×10^{7}	1.138148

$\Sigma_{9\to8}$

t_{wdt}	$\overline{\text{FOM}}$	Ratio
0.1	2.370219×10^{5}	1.000000
0.2	2.461415×10^{5}	1.038476
0.3	2.312383×10^{5}	0.975599
0.4	2.482154×10^{5}	1.047226
0.5	2.382993×10^{5}	1.005390
0.6	2.402796×10^{5}	1.013744
0.7	2.334855×10^{5}	0.985080
0.8	2.300443×10^{5}	0.970562
0.9	2.419326×10^{5}	1.020719
1.0	2.521705×10^{5}	1.063913

$\Sigma_{10\to8}$

t_{wdt}	$\overline{\text{FOM}}$	Ratio
0.1	8.528104×10^{4}	1.000000
0.2	9.249724×10^{4}	1.084617
0.3	8.746691×10^{4}	1.025631
0.4	9.099322×10^{4}	1.066981
0.5	9.093714×10^{4}	1.066323
0.6	8.454517×10^{4}	0.991371
0.7	9.626479×10^{4}	1.128795
0.8	8.543830×10^{4}	1.001844
0.9	8.853355×10^{4}	1.038139
1.0	9.493499×10^{4}	1.113202

$\Sigma_{11\to8}$

t_{wdt}	$\overline{\text{FOM}}$	Ratio
0.1	1.888873×10^{4}	1.000000
0.2	1.961373×10^{4}	1.038383
0.3	1.968962×10^{4}	1.042401
0.4	1.940867×10^{4}	1.027527
0.5	2.083910×10^{4}	1.103256
0.6	1.943130×10^{4}	1.028725
0.7	1.953164×10^{4}	1.034037
0.8	1.945977×10^{4}	1.030232
0.9	2.015811×10^{4}	1.067203
1.0	2.006323×10^{4}	1.062180

$\Sigma_{1\to9}$

t_{wdt}	$\overline{\text{FOM}}$	Ratio
0.1	0.000000×10^{0}	0.000000
0.2	0.000000×10^{0}	0.000000
0.3	0.000000×10^{0}	0.000000
0.4	0.000000×10^{0}	0.000000
0.5	0.000000×10^{0}	0.000000
0.6	0.000000×10^{0}	0.000000
0.7	0.000000×10^{0}	0.000000
0.8	0.000000×10^{0}	0.000000
0.9	0.000000×10^{0}	0.000000
1.0	0.000000×10^{0}	0.000000

$\Sigma_{2\to9}$

t_{wdt}	$\overline{\text{FOM}}$	Ratio
0.1	0.000000×10^{0}	0.000000
0.2	0.000000×10^{0}	0.000000
0.3	0.000000×10^{0}	0.000000
0.4	0.000000×10^{0}	0.000000
0.5	0.000000×10^{0}	0.000000
0.6	0.000000×10^{0}	0.000000
0.7	0.000000×10^{0}	0.000000
0.8	0.000000×10^{0}	0.000000
0.9	0.000000×10^{0}	0.000000
1.0	0.000000×10^{0}	0.000000

$\Sigma_{3\to9}$

t_{wdt}	$\overline{\text{FOM}}$	Ratio
0.1	0.000000×10^{0}	0.000000
0.2	0.000000×10^{0}	0.000000
0.3	0.000000×10^{0}	0.000000
0.4	0.000000×10^{0}	0.000000
0.5	0.000000×10^{0}	0.000000
0.6	0.000000×10^{0}	0.000000
0.7	0.000000×10^{0}	0.000000
0.8	0.000000×10^{0}	0.000000
0.9	0.000000×10^{0}	0.000000
1.0	0.000000×10^{0}	0.000000

$\Sigma_{4\to9}$

t_{wdt}	$\overline{\text{FOM}}$	Ratio
0.1	0.000000×10^{0}	0.000000
0.2	0.000000×10^{0}	0.000000
0.3	0.000000×10^{0}	0.000000
0.4	0.000000×10^{0}	0.000000
0.5	0.000000×10^{0}	0.000000
0.6	0.000000×10^{0}	0.000000
0.7	0.000000×10^{0}	0.000000
0.8	0.000000×10^{0}	0.000000
0.9	0.000000×10^{0}	0.000000
1.0	0.000000×10^{0}	0.000000

$\Sigma_{6\to9}$

t_{wdt}	$\overline{\text{FOM}}$	Ratio
0.1	0.000000×10^{0}	0.000000
0.2	0.000000×10^{0}	0.000000
0.3	0.000000×10^{0}	0.000000
0.4	0.000000×10^{0}	0.000000
0.5	0.000000×10^{0}	0.000000
0.6	0.000000×10^{0}	0.000000
0.7	0.000000×10^{0}	0.000000
0.8	0.000000×10^{0}	0.000000
0.9	0.000000×10^{0}	0.000000
1.0	0.000000×10^{0}	0.000000

$\Sigma_{6\to9}$

t_{wdt}	$\overline{\text{FOM}}$	Ratio
0.1	0.000000×10^{0}	0.000000
0.2	0.000000×10^{0}	0.000000
0.3	0.000000×10^{0}	0.000000
0.4	0.000000×10^{0}	0.000000
0.5	0.000000×10^{0}	0.000000
0.6	0.000000×10^{0}	0.000000
0.7	0.000000×10^{0}	0.000000
0.8	0.000000×10^{0}	0.000000
0.9	0.000000×10^{0}	0.000000
1.0	0.000000×10^{0}	0.000000

$\Sigma_{7\to9}$

t_{wdt}	$\overline{\text{FOM}}$	Ratio
0.1	7.800747×10^{2}	1.000000
0.2	7.960933×10^{2}	1.020535
0.3	7.550821×10^{2}	0.967961
0.4	7.821837×10^{2}	1.002704
0.5	7.739794×10^{2}	0.992186
0.6	7.722892×10^{2}	0.990020
0.7	7.460471×10^{2}	0.956379
0.8	7.893194×10^{2}	1.011851
0.9	7.731645×10^{2}	0.991142
1.0	7.470403×10^{2}	0.957652

$\Sigma_{8\to9}$

t_{wdt}	$\overline{\text{FOM}}$	Ratio
0.1	1.720184×10^{5}	1.000000
0.2	1.598342×10^{5}	0.929169
0.3	1.556438×10^{5}	0.904809
0.4	1.462970×10^{5}	0.850473
0.5	1.580546×10^{5}	0.918823
0.6	1.621479×10^{5}	0.942619
0.7	1.608586×10^{5}	0.935124
0.8	1.482068×10^{5}	0.861575
0.9	1.545220×10^{5}	0.898288
1.0	1.665084×10^{5}	0.967969

$\Sigma_{9\to9}$

t_{wdt}	$\overline{\text{FOM}}$	Ratio
0.1	4.173106×10^{7}	1.000000
0.2	4.061579×10^{7}	0.973275
0.3	3.769576×10^{7}	0.903302
0.4	3.885440×10^{7}	0.931067
0.5	3.884879×10^{7}	0.930932
0.6	4.224812×10^{7}	1.012390
0.7	3.850030×10^{7}	0.922582
0.8	3.865356×10^{7}	0.926254
0.9	4.021949×10^{7}	0.963778
1.0	4.306924×10^{7}	1.032067

$\Sigma_{10\to9}$

t_{wdt}	$\overline{\text{FOM}}$	Ratio
0.1	1.549594×10^{5}	1.000000
0.2	1.562799×10^{5}	1.008522
0.3	1.496188×10^{5}	0.965535
0.4	1.480604×10^{5}	0.955478
0.5	1.555552×10^{5}	1.003845
0.6	1.558942×10^{5}	1.006032
0.7	1.520696×10^{5}	0.981351
0.8	1.523288×10^{5}	0.983023
0.9	1.605757×10^{5}	1.036244
1.0	1.630843×10^{5}	1.052432

$\Sigma_{11\to9}$

t_{wdt}	$\overline{\text{FOM}}$	Ratio
0.1	2.518567×10^{4}	1.000000
0.2	2.585920×10^{4}	1.026743
0.3	2.734494×10^{4}	1.085734
0.4	2.685702×10^{4}	1.066361
0.5	2.530842×10^{4}	1.004874
0.6	2.574334×10^{4}	1.022142
0.7	2.511917×10^{4}	0.997360
0.8	2.393741×10^{4}	0.950438
0.9	2.579552×10^{4}	1.024214
1.0	2.452881×10^{4}	0.973919

$\Sigma_{1\to10}$

t_{wdt}	$\overline{\text{FOM}}$	Ratio
0.1	0.000000×10^{0}	0.000000
0.2	0.000000×10^{0}	0.000000
0.3	0.000000×10^{0}	0.000000
0.4	0.000000×10^{0}	0.000000
0.5	0.000000×10^{0}	0.000000
0.6	0.000000×10^{0}	0.000000
0.7	0.000000×10^{0}	0.000000
0.8	0.000000×10^{0}	0.000000
0.9	0.000000×10^{0}	0.000000
1.0	0.000000×10^{0}	0.000000

$\Sigma_{2\to10}$

t_{wdt}	$\overline{\text{FOM}}$	Ratio
0.1	0.000000×10^{0}	0.000000
0.2	0.000000×10^{0}	0.000000
0.3	0.000000×10^{0}	0.000000
0.4	0.000000×10^{0}	0.000000
0.5	0.000000×10^{0}	0.000000
0.6	0.000000×10^{0}	0.000000
0.7	0.000000×10^{0}	0.000000
0.8	0.000000×10^{0}	0.000000
0.9	0.000000×10^{0}	0.000000
1.0	0.000000×10^{0}	0.000000

$\Sigma_{3\to10}$

t_{wdt}	$\overline{\text{FOM}}$	Ratio
0.1	0.000000×10^{0}	0.000000
0.2	0.000000×10^{0}	0.000000
0.3	0.000000×10^{0}	0.000000
0.4	0.000000×10^{0}	0.000000
0.5	0.000000×10^{0}	0.000000
0.6	0.000000×10^{0}	0.000000
0.7	0.000000×10^{0}	0.000000
0.8	0.000000×10^{0}	0.000000
0.9	0.000000×10^{0}	0.000000
1.0	0.000000×10^{0}	0.000000

$\Sigma_{4\to10}$

t_{wdt}	$\overline{\text{FOM}}$	Ratio
0.1	0.000000×10^{0}	0.000000
0.2	0.000000×10^{0}	0.000000
0.3	0.000000×10^{0}	0.000000
0.4	0.000000×10^{0}	0.000000
0.5	0.000000×10^{0}	0.000000
0.6	0.000000×10^{0}	0.000000
0.7	0.000000×10^{0}	0.000000
0.8	0.000000×10^{0}	0.000000
0.9	0.000000×10^{0}	0.000000
1.0	0.000000×10^{0}	0.000000

$\Sigma_{6\to10}$

t_{wdt}	$\overline{\text{FOM}}$	Ratio
0.1	0.000000×10^{0}	0.000000
0.2	0.000000×10^{0}	0.000000
0.3	0.000000×10^{0}	0.000000
0.4	0.000000×10^{0}	0.000000
0.5	0.000000×10^{0}	0.000000
0.6	0.000000×10^{0}	0.000000
0.7	0.000000×10^{0}	0.000000
0.8	0.000000×10^{0}	0.000000
0.9	0.000000×10^{0}	0.000000
1.0	0.000000×10^{0}	0.000000

$\Sigma_{6\to10}$

t_{wdt}	$\overline{\text{FOM}}$	Ratio
0.1	0.000000×10^{0}	0.000000
0.2	0.000000×10^{0}	0.000000
0.3	0.000000×10^{0}	0.000000
0.4	0.000000×10^{0}	0.000000
0.5	0.000000×10^{0}	0.000000
0.6	0.000000×10^{0}	0.000000
0.7	0.000000×10^{0}	0.000000
0.8	0.000000×10^{0}	0.000000
0.9	0.000000×10^{0}	0.000000
1.0	0.000000×10^{0}	0.000000

$\Sigma_{7\to10}$

t_{wdt}	$\overline{\text{FOM}}$	Ratio
0.1	0.000000×10^{0}	0.000000
0.2	2.541551×10^{-4}	0.000254
0.3	0.000000×10^{0}	0.000000
0.4	0.000000×10^{0}	0.000000
0.5	0.000000×10^{0}	0.000000
0.6	0.000000×10^{0}	0.000000
0.7	0.000000×10^{0}	0.000000
0.8	0.000000×10^{0}	0.000000
0.9	5.110467×10^{-4}	0.000511
1.0	0.000000×10^{0}	0.000000

$\Sigma_{8\to10}$

t_{wdt}	$\overline{\text{FOM}}$	Ratio
0.1	4.056444×10^{4}	1.000000
0.2	4.123366×10^{4}	1.016498
0.3	4.113303×10^{4}	1.014017
0.4	3.990449×10^{4}	0.983731
0.5	4.323667×10^{4}	1.065876
0.6	4.102492×10^{4}	1.011352
0.7	4.233098×10^{4}	1.043549
0.8	4.027418×10^{4}	0.992845
0.9	4.179091×10^{4}	1.030235
1.0	4.087831×10^{4}	1.007738

$\Sigma_{9\to10}$

t_{wdt}	$\overline{\text{FOM}}$	Ratio
0.1	1.162797×10^{5}	1.000000
0.2	1.130168×10^{5}	0.971939
0.3	1.182286×10^{5}	1.016760
0.4	1.085694×10^{5}	0.933691
0.5	1.159361×10^{5}	0.997046
0.6	1.126057×10^{5}	0.968404
0.7	1.233760×10^{5}	1.061028
0.8	1.113090×10^{5}	0.957252
0.9	1.110391×10^{5}	0.954931
1.0	1.207320×10^{5}	1.038290

$\Sigma_{10\to10}$

t_{wdt}	$\overline{\text{FOM}}$	Ratio
0.1	3.324662×10^{7}	1.000000
0.2	3.132910×10^{7}	0.942325
0.3	3.098730×10^{7}	0.932044
0.4	2.734922×10^{7}	0.822617
0.5	3.132156×10^{7}	0.942098
0.6	2.943307×10^{7}	0.885295
0.7	3.088198×10^{7}	0.928876
0.8	2.859264×10^{7}	0.860016
0.9	2.967680×10^{7}	0.892626
1.0	2.940634×10^{7}	0.884491

$\Sigma_{11\to10}$

t_{wdt}	$\overline{\text{FOM}}$	Ratio
0.1	4.906706×10^{4}	1.000000
0.2	4.948104×10^{4}	1.008437
0.3	5.393721×10^{4}	1.099255
0.4	4.904135×10^{4}	0.999476
0.5	5.398434×10^{4}	1.100216
0.6	5.094168×10^{4}	1.038205
0.7	5.259183×10^{4}	1.071836
0.8	4.828556×10^{4}	0.984073
0.9	5.104882×10^{4}	1.040389
1.0	5.082866×10^{4}	1.035902

$\Sigma_{1\to11}$

t_{wdt}	$\overline{\text{FOM}}$	Ratio
0.1	0.000000×10^{0}	0.000000
0.2	0.000000×10^{0}	0.000000
0.3	0.000000×10^{0}	0.000000
0.4	0.000000×10^{0}	0.000000
0.5	0.000000×10^{0}	0.000000
0.6	0.000000×10^{0}	0.000000
0.7	0.000000×10^{0}	0.000000
0.8	0.000000×10^{0}	0.000000
0.9	0.000000×10^{0}	0.000000
1.0	0.000000×10^{0}	0.000000

$\Sigma_{2\to11}$

t_{wdt}	$\overline{\text{FOM}}$	Ratio
0.1	0.000000×10^{0}	0.000000
0.2	0.000000×10^{0}	0.000000
0.3	0.000000×10^{0}	0.000000
0.4	0.000000×10^{0}	0.000000
0.5	0.000000×10^{0}	0.000000
0.6	0.000000×10^{0}	0.000000
0.7	0.000000×10^{0}	0.000000
0.8	0.000000×10^{0}	0.000000
0.9	0.000000×10^{0}	0.000000
1.0	0.000000×10^{0}	0.000000

$\Sigma_{3\to11}$

t_{wdt}	$\overline{\text{FOM}}$	Ratio
0.1	0.000000×10^{0}	0.000000
0.2	0.000000×10^{0}	0.000000
0.3	0.000000×10^{0}	0.000000
0.4	0.000000×10^{0}	0.000000
0.5	0.000000×10^{0}	0.000000
0.6	0.000000×10^{0}	0.000000
0.7	0.000000×10^{0}	0.000000
0.8	0.000000×10^{0}	0.000000
0.9	0.000000×10^{0}	0.000000
1.0	0.000000×10^{0}	0.000000

$\Sigma_{4\to11}$

t_{wdt}	$\overline{\text{FOM}}$	Ratio
0.1	0.000000×10^{0}	0.000000
0.2	0.000000×10^{0}	0.000000
0.3	0.000000×10^{0}	0.000000
0.4	0.000000×10^{0}	0.000000
0.5	0.000000×10^{0}	0.000000
0.6	0.000000×10^{0}	0.000000
0.7	0.000000×10^{0}	0.000000
0.8	0.000000×10^{0}	0.000000
0.9	0.000000×10^{0}	0.000000
1.0	0.000000×10^{0}	0.000000

$\Sigma_{6\to11}$

t_{wdt}	$\overline{\text{FOM}}$	Ratio
0.1	0.000000×10^{0}	0.000000
0.2	0.000000×10^{0}	0.000000
0.3	0.000000×10^{0}	0.000000
0.4	0.000000×10^{0}	0.000000
0.5	0.000000×10^{0}	0.000000
0.6	0.000000×10^{0}	0.000000
0.7	0.000000×10^{0}	0.000000
0.8	0.000000×10^{0}	0.000000
0.9	0.000000×10^{0}	0.000000
1.0	0.000000×10^{0}	0.000000

$\Sigma_{6\to11}$

t_{wdt}	$\overline{\text{FOM}}$	Ratio
0.1	0.000000×10^{0}	0.000000
0.2	0.000000×10^{0}	0.000000
0.3	0.000000×10^{0}	0.000000
0.4	0.000000×10^{0}	0.000000
0.5	0.000000×10^{0}	0.000000
0.6	0.000000×10^{0}	0.000000
0.7	0.000000×10^{0}	0.000000
0.8	0.000000×10^{0}	0.000000
0.9	0.000000×10^{0}	0.000000
1.0	0.000000×10^{0}	0.000000

$\Sigma_{7\to11}$

t_{wdt}	$\overline{\text{FOM}}$	Ratio
0.1	0.000000×10^{0}	0.000000
0.2	0.000000×10^{0}	0.000000
0.3	0.000000×10^{0}	0.000000
0.4	0.000000×10^{0}	0.000000
0.5	0.000000×10^{0}	0.000000
0.6	0.000000×10^{0}	0.000000
0.7	0.000000×10^{0}	0.000000
0.8	0.000000×10^{0}	0.000000
0.9	0.000000×10^{0}	0.000000
1.0	0.000000×10^{0}	0.000000

$\Sigma_{8\to11}$

t_{wdt}	$\overline{\text{FOM}}$	Ratio
0.1	5.457439×10^{3}	1.000000
0.2	6.117090×10^{3}	1.120872
0.3	5.771733×10^{3}	1.057590
0.4	5.980384×10^{3}	1.095822
0.5	6.186904×10^{3}	1.133664
0.6	6.010988×10^{3}	1.101430
0.7	6.359712×10^{3}	1.165329
0.8	5.837987×10^{3}	1.069730
0.9	5.904681×10^{3}	1.081951
1.0	6.637011×10^{3}	1.216140

$\Sigma_{9\to11}$

t_{wdt}	$\overline{\text{FOM}}$	Ratio
0.1	1.314684×10^{4}	1.000000
0.2	1.271546×10^{4}	0.967187
0.3	1.358137×10^{4}	1.033052
0.4	1.304614×10^{4}	0.992340
0.5	1.395270×10^{4}	1.061296
0.6	1.374074×10^{4}	1.045174
0.7	1.420596×10^{4}	1.080560
0.8	1.258387×10^{4}	0.957178
0.9	1.288483×10^{4}	0.980070
1.0	1.270420×10^{4}	0.966331

$\Sigma_{10\to11}$

t_{wdt}	$\overline{\text{FOM}}$	Ratio
0.1	3.753622×10^{4}	1.000000
0.2	3.691479×10^{4}	0.983444
0.3	3.815843×10^{4}	1.016576
0.4	3.545178×10^{4}	0.944468
0.5	3.829634×10^{4}	1.020250
0.6	3.680099×10^{4}	0.980413
0.7	3.735477×10^{4}	0.995166
0.8	3.793294×10^{4}	1.010569
0.9	3.654118×10^{4}	0.973491
1.0	3.771525×10^{4}	1.004769

$\Sigma_{11\to11}$

t_{wdt}	$\overline{\text{FOM}}$	Ratio
0.1	1.889146×10^{6}	1.000000
0.2	1.877980×10^{6}	0.994090
0.3	1.926872×10^{6}	1.019970
0.4	1.771631×10^{6}	0.937794
0.5	1.847542×10^{6}	0.977977
0.6	1.787648×10^{6}	0.946273
0.7	1.988811×10^{6}	1.052757
0.8	1.877231×10^{6}	0.993693
0.9	1.833813×10^{6}	0.970710
1.0	2.074412×10^{6}	1.098069